SYNTHESIS AND ELECTRONIC PROPERTIES OF TTFAQ BASED DONOR-ACCEPTOR MOLECULAR SYSTEMS

GUANG CHEN

Synthesis and Electronic Properties of TTFAQ Based Donor-Acceptor Molecular Systems

by

Guang Chen

A thesis submitted to the School of Graduate Studies

in partial fulfillment of the requirements for the degree of

Master of Science

Department of Chemistry

Memorial University of Newfoundland

December, 2006

St. John's, Newfoundland and Labrador, Canada

Your file Votre référence
ISBN: 978-0-494-31241-4
Our file Notre référence
ISBN: 978-0-494-31241-4

Abstract

Owing to their unique structural and redox properties, the anthraquinoid type of π-extended tetrathiafulvalene (referred to as TTFAQs) and their D-A functionalized derivatives have offered promising prospects in modern organic electronic and optic materials. This thesis primarily summarizes the research of a series of novel functionalized TTFAQ derivatives, including a series of novel dumbbell-shaped C_{60}-TTFAQ-C_{60} triad molecules and various donor/acceptor substituted TTFAQ systems. Electronic and optical properties of these compounds were studied by cyclic voltammetry (CV), UV-vis absorption, and fluorescence spectroscopy, and detailed oxidation state spectroscopic properties of the TTFAQ based donor/acceptor systems were characterized. These data contributed to establishing a clear structure-property relationship for these novel TTFAQ compounds, and was also informative to further investigation on their photophysical behavior and photovoltaic applications. In addition, some exploratory investigations on a TTFAQ-cored conjugated molecular switch and a one-pot synthetic strategy for rapidly preparing complex butadiynylene centered systems are reported.

Acknowledgements

I would like to express my sincere gratitude and deep appreciation to my supervisor, Dr. Yuming Zhao, for his guidance throughout my M.Sc. program, and assistance in the completion of this thesis.

Also I would like to thank my supervisor committee members, Drs S. V. Pansare and R. A. Poirier, for their suggestions on my research work. The appreciation is extended to Dr G. J. Bodwell, Dr P. E. Georghiou, entire organic group and the staff in the Chemistry Department for their generous help.

I would like to thank my group members, Ningzhang Zhou, Illias Mahmud and Min Shao, for their help during my research work.

I am grateful to the Natural Sciences and Engineering Research Council (NSERC) and Memorial University of Newfoundland (MUN) for financial support.

For spectroscopy services and discussions, I would like to give my thanks to Dr D. W. Thompson, Dr L. K. Thompson, Ms. L. Winsor, Ms. J. Colin and Ms. K. Zhang.

Deepest gratitude and appreciation are due to my parents and friends, for their encouragement, help and love.

Table of Contents

Chapter 1

Introduction

Chapter 2

Synthesis and Characterization of TTFAQ-C_{60} and TTFAQ Based D-A Molecules

Chapter 3

Other Work Related to Novel TTFAQ Derivatives

Chapter 4

Conclusion

List of Tables

List of Figures

List of Schemes

List of Abbreviations

AM1	Austin Model 1
APCI-MS	Atmospheric Pressure Chemical Ionization-Mass Spectrometry
aq.	Aqueous
C-S	Charge-separated
CV	Cyclic voltammetry
DBU	1,8-Diazabicyclo(5.4.0)undec-7-ene
DDQ	2,3-Dicyano-5,6-dichloro-parabenzoquinone
DFT	Density functional theory
DMAD	Dimethyl acetylenedicarboxylate
DMF	*N*,*N*-Dimethylformamide
Dmit	1,3-Dithiole-2-thione-4,5-dithiolate
DMS	Dimethyl sulfate
D-A	Donor-acceptor
eq.	Equivalent
exTTF	π-Extended tetrathiafulvalene
GC-MS	Gas Chromatography-Mass Spectrometry
HOMO	Highest occupied molecular orbital
HWE	Horner-Wadsworth-Emmons
LDA	Lithium diisopropylamide
LHMDS	Lithium hexamethyldisilazide

LUMO	Lowest unoccupied molecular orbital
MALDI-TOF MS	Matrix Assisted Laser Desorption Ionization- Time-of-Flight Mass Spectrometry
m.p.	Melting point
OPE	Oligo-*p*-phenyleneethynylene
OPV	Oligo-*p*-phenylenevinylene
quant.	Quantitative
rt.	Room temperature
satd.	Saturated
SCE	KCl saturated calomel electrode
TBAF	Tetra-*n*-butylammonium fluoride
TCNQ	Tetracyanoquinodimethane
TFA	Trifluoroacetic acid
THF	Tetrahydrofuran
TMS	Trimethylsilyl
TMSA	Trimethylsilylacetylene
TTF	Tetrathiafulvalene
TTFAQ	9,10-Bis(1,3-dithiol-2-ylidene)-9,10-dihydroanthracene

Chapter 1

Introduction

1.1 A Brief Overview of Tetrathiafulvalene and π-Extended Tetrathiafulvalene Derivatives

Tetrathiafulvalene (TTF, Figure 1.1) and its derivatives are well known for their excellent electron-donor and charge-transfer complexing abilities. As early as 1972, the first organic conductor $[TTF]^{+}Cl^{-}$ was reported.[1] In this charge-transfer salt, the π-donors (TTFs) stacked aligned with their central double bonds to effect sufficient interactions of molecular orbitals, which in turn gave rise to metallic electrical conductivity along the direction of stacking. This milestone discovery hence seeded the research in the areas of "organic metals" in the late 1970s and later heralded the advent of "molecular electronics". In the following year, another remarkable charge-transfer compound, TTF-TCNQ (Figure 1.1), was reported, which showed a considerably improved conductivity value of *ca.* 400 $\Omega\ cm^{-1}$ at room temperature.[2] In this complex, delocalized electrons responsible for conduction were generated by intermolecular charge transfer from TTF to a good organic electron acceptor, TCNQ.[3] Compared with other organic electron donors, TTF has relatively low oxidizing potentials and exceptional aromaticity-stabilized oxidation states (*i.e.* radical cation, and dication). As such, it can readily generate charge-transfer complexes with appropriate organic and/or inorganic electron acceptors as long as their electron affinities were greater than 2.5 eV.[3]

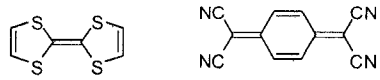

1 2

Figure 1.1. Molecular structures of an organic electron donor, tetrathiafulvalene **1** (TTF), and an electron acceptor counterpart, tetracyanoquinodimethane **2** (TCNQ), for charge-transfer complex.

In the following two decades after the discovery of TTF, many TTF derivatives, charge-transfer complexes and ion radical salts were synthesized, which possessed excellent metallic conductivity and even superconductivity.[4] Later, many π-extended TTF derivatives (referred to as exTTFs henceforth) were prepared in order to decrease the disfavored Coulombic repulsion through electron delocalization in the oxidized dicationic TTF structure.[4] The intermolecular interactions among the TTF moiety in the solid state, which play an important role in governing the conduction, will be considerably improved when the intra- and intermolecular Coulombic repulsions are reduced. However, since the planar π-conjugated molecules tend to form a columnar-fashioned solid-state π-stacking, these organic based conductive materials would display one-dimensional electronic structures and thus inevitably suffer from the Peierls instability.[4,5] (*i.e.* the metallic-insulator transition occurs at certain temperatures due to the localization of the charge density wave.[6]) To circumvent this drawback, various novel conjugated structures were designed and prepared via the strategies of increasing dimensionality and generating multicomponent systems.[7]

Interest in other TTF applications has been growing steadily. In the 1970s Wudl's group prepared the unsubstituted TTF as a cathodic material, which opened the door to TTF applications in molecular electronics.[4] In general, D-A systems present an important

way to control the bandgap between the highest occupied molecular orbital (HOMO) of the donor and the lowest unoccupied molecular orbital (LUMO) of the acceptor. D-A molecules with a small electronic bandgap can both easily donate (from their high-lying HOMO) and accept electrons (to their low-lying LUMO). Such electrochemically amphoteric properties are of great interest in the design of various functional organic electronic devices.[4] A large number of functionalized TTF derivatives and TTF based D-A systems, have been synthesized for applications as molecular switches,[8] molecular rectifiers,[9] and nonlinear optics.[10]

1.1.1 Structural Properties of TTF and its Derivatives

TTF and its derivatives are important sulfur-based heterocyclic compounds, while the π-extended TTF derivatives contain larger conjugated molecular frameworks than those of TTF. In annulated exTTF, (**3** – **5,** Figure 1.2) the extended conjugated systems are placed at the double bonds of the dithiole rings, while in exTTF bridged by conjugated units (see Figure 1.3) the dithiole rings are connected with delocalized π-paths such as vinylene (**6**),[11] acetylene (**7**),[12] thiophene (**8**),[13] acene (**9** – **12**)[4] and many other π structures. It is worth mentioning that the acene-linked exTTF (Figure 1.4), such as 9,10-bis(1,3-dithiol-2-ylidene)-9,10-dihydroanthracene (TTFAQ, **11a**), are one of the most important series in the current exTTF family.

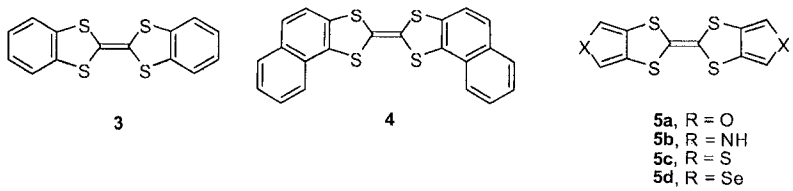

Figure 1.2 Examples of annulated exTTF.

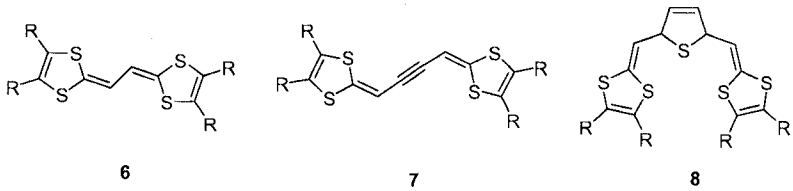

Figure 1.3 Structures of linear exTTF with conjugated units between the two dithiole rings.

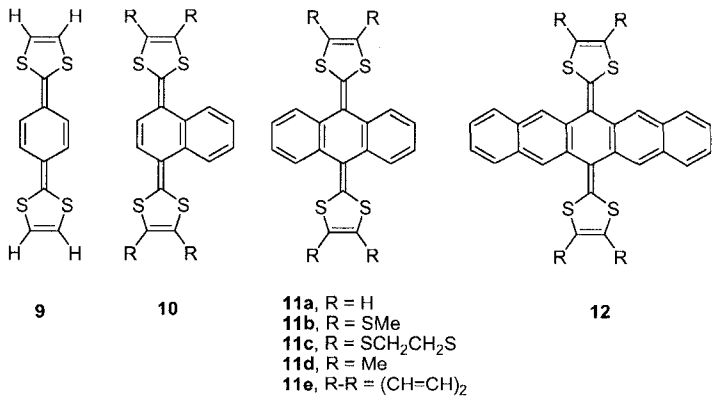

Figure 1.4 Structures of acene-linked exTTF.

TTF and exTTF are also important building blocks for various molecular electronic devices. They are particularly useful in constructing novel D-A systems, where the donor and acceptor can be connected via either saturated bonds as in a D-σ-A molecule (**13**), or π-conjugated linkers, as in a D-π-A molecule (**14**).[4]

(a) D-σ-A (b) D-π-A

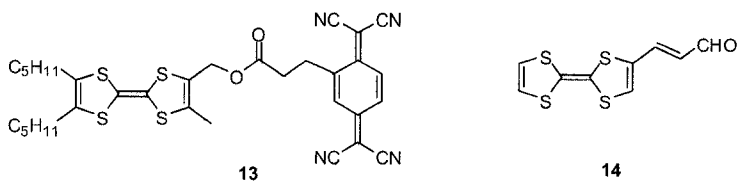

Figure 1.5 Two examples of TTF-based D-A dyads.

1.1.2 Electronic Properties of TTF and its Derivatives

Low oxidation potentials and the small HOMO-LUMO gap are prerequisites for efficient charge transfer processes. Therefore, two major goals in the design of new TTF derivatives have been focused on, *i.e.* achieving low oxidation potentials and reduced bandgaps. Generally a good electron donor has a high-lying HOMO associated with a high-lying LUMO. In a D-A system, however, the LUMO is located on the acceptor unit, which is low-lying in energy. Using the criterion outlined above, the covalent attachment of donor and acceptor units can create a hybrid D-A system that has an extremely narrow bandgap, which in turn should favor facile intramolecular charge transfer. In this section, a review of the existing literature will particularly concentrate on the oxidation potentials and bandgaps of various TTF derivatives as well as their relationship with different substituents on the dithiole rings, linkages, and acceptors. The bandgap can be experimentally measured in the forms of optical gap, based on the lowest energy absorption edge in the UV-vis spectrum, or electrochemical gap (E_g), calculated by E_{1ox}-E_{1red} (the difference between the first oxidation potential and the first reduction potential). Although the two measures tend to provide quite different values in many experimental

cases, they actually coincide with one another to a great extent in terms of the general trend of bandgap shift in studying various compound series. In this sense, both bandgaps were evaluated and compared in numerous TTF related research papers. These two methods were also adopted in this thesis work (Chapter 2).

Unsubstituted TTF can undergo two reversible one-electron oxidations to sequentially form a stable radical cation and a dication as shown in Scheme 1.1. Upon oxidation, the dithiole rings achieve 6π-electron aromaticity, which accounts for the high stability of the oxidized species. On the other hand, the dications are destablilized by intramolecular Coulombic repulsion between the two closely positioned cationic centers.[14] Despite the disfavored electrostatic repulsion, the redox potentials of TTF are still quite low (E°_{1ox} = 0.34 V, E°_{2ox} = 0.78 V vs Ag/AgCl in MeCN) and hence are easily accessible. Furthermore, the oxidation potentials can be finely tuned by modifying the substituents on the dithiole rings. In general, most substituents including alkylthio groups would act as electron-withdrawing groups and therefore increase the oxidation potentials of the entire molecule.[4] Methyl group is so far the only known electron-donating substituent that decreases the oxidation potentials of TTF (by 15 ~ 30 mV per methyl group introduced).[4]

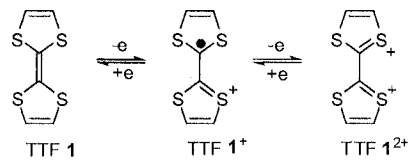

Scheme 1.1 Stepwise two-electron oxidations on unsubstituted TTF.

In annulated exTTF, the annulated rings can be considered as electron-withdrawing substituents increasing the oxidation potentials when compared with the unsubstituted

TTFs. For example, the first exTTF, dibenzo derivative **3** as shown in Figure 1.6, which was first synthesized in 1926 without recognizing its electron donor properties at that time,[15] showed an increase by *ca.* 250 mV in the oxidation potentials relative to unsubstituted TTF **1**.[16] Interestingly, one of the heterocycle-annulated TTF, bis pyrrolo-TTF **5b**, showed an oxidation potential lower than its parent unsubstituted TTF **1**.[4] Although reduced optical gaps were observed, none of the annulated exTTFs showed either electrochemical amphotericity or a significantly reduced bandgap narrower than 2 eV.[4]

3 5b

Figure 1.6 A dibenzo-TTF and a bispyrrolo-TTF.

In linearly conjugated oligo(ene) linked exTTFs, the extension of π-conjugation between the two dithiole rings changes their electrochemical properties. For example, the oxidation potentials of compound **15a** are greatly reduced (E^{o}_{1ox} = 0.20 V, E^{o}_{2ox} = 0.36 V vs Ag/AgCl in MeCN) and the difference between these two oxidation potentials is less than that of the reference TTF **1**. The decrease of ($E^{o}_{2ox} - E^{o}_{1ox}$) is ascribed to the stabilization of the dicationic species upon oxidation. Introduction of another double bond as shown in **15b** (Figure 1.7) has slightly affected the first oxidation potential E^{o}_{1ox}, however, resulting in a further decrease in E^{o}_{2ox}. Overall, a smaller ($E^{o}_{2ox} - E^{o}_{1ox}$) value of 6 mV was observed.[17] In addition, reduced optical bandgaps were observed in UV-Vis spectra, showing a redshift of the TTF bands from 368 nm to *ca.* 430 nm. Not

surprisingly, when the number of double bonds was increased to five (*e.g.* in the case of **16**), the ($E^{\circ}_{2ox} - E^{\circ}_{1ox}$) became close to zero and a simultaneous two-electron oxidation was observed. While the λ_{max} consistently redshifts as the spacer length increases, the first oxidation potential remains virtually unchanged once it arrives at a certain value. The convergence of first oxidation potential and the steady decrease of bandgap as the spacer's length increases suggest that the HOMO is mainly dictated by the dithiole rings and the LUMO is dependent mostly on the nature and effective conjugation length of the spacer.[6] Because the increase of spacer length is normally accompanied by a decrease in chemical stability, it is important to introduce strong electron-withdrawing substituents such as –COOMe and –CN to the dithiole rings in oligo(ene) bridged systems to attain satisfactorily stable exTTF derivatives.[6]

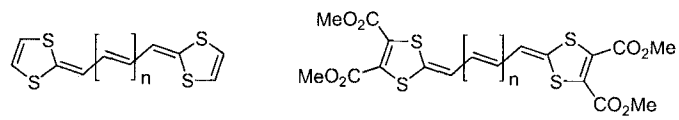

15a, n = 0
15b, n = 1

16

Figure 1.7 Conjugated oligo(ene) bridged exTTFs.

Because of the aforementioned instability arising from the vinylene linkage, an alternative way was designed to avoid such problems, that is, using more stable aromatic rings as spacers. The choice of aryl spacers might suffer from numerous problems. Besides the dimerization of 1,3,5-trisubstituted benzo-TTFs and the intramolecular cyclization of *ortho*-disubstituted benzo-TTFs, all benzo-TTFs bear high oxidation potentials due to the de-aromatization of the benzene ring into a quinoid form upon

oxidation.[6] Heterocyclic spacers such as furan, thiophene and pyrrole worked relatively better, because of their relatively weaker resonance energies (aromaticity). In the series of heterocycle-linked TTFs **17a-c** as shown in Figure 1.8, **17a** afforded much lower oxidation potentials as well as a smaller ($E^{\circ}_{2ox} - E^{\circ}_{1ox}$) than the reference TTF compound. However, further increase of the spacer length caused considerable interannular rotational disorder, thus resulting in a quick saturation of effective conjugation length.[6] The first oxidation potential reached its minimum in the case of $n = 0$. When $n = 1$ the ($E^{\circ}_{2ox} - E^{\circ}_{1ox}$) value reached its minimum and UV-vis λ_{max} reached its maximum. Such immediate saturation was not observed when a more planar spacer was applied such as in **18**, whose band gap was found at 1.80 eV.[6]

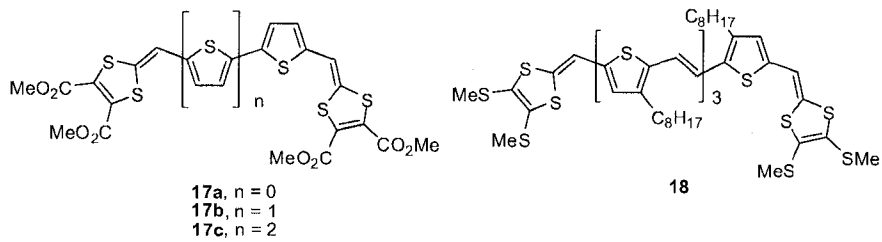

Figure 1.8 Heterocycle-linked TTF derivatives.

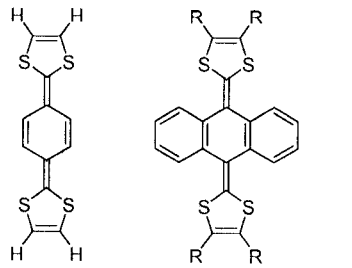

9

11a, R = H
11b, R = SMe
11c, R = SCH_2CH_2S
11d, R = Me
11e, R-R = $(CH{=}CH)_2$

Figure 1.9 The strongest TTF reducing reagent and TTFAQs.

In acene-linked exTTFs, a similar decreasing pattern of oxidation potentials was found. For example, in 1989 Yamashita's group reported the strongest TTF reducing reagent ever characterized, compound **9** (E°_{1ox} = –0.11 V, E°_{2ox} = –0.04 V vs SCE in MeCN).[18] Interestingly, it is the only TTF-acene that undergoes two distinctive, stepwise one-electron oxidations, which is of the same characteristic as TTF **1**. In addition, compound **9** appears as a red solid rather than the commonly observed yellow-orange color for the TTF parent molecule. The color change indicates a much reduced bandgap for **9**. When the acene linker was extended to naphthalene and higher aromatic structures, however, the two distinctive stepwise one-electron oxidations merged into one simultaneous two-electron oxidation process in electrochemical characterization. For example, Bryce demonstrated that TTFAQ **11a** underwent a two-electron oxidation to form the dication directly during the positive scan in a cyclic voltammetric (CV) experiment, showing a potential value of 0.44 eV vs SCE in CH_2Cl_2.[4] This behavior suggests a much higher stability of dication than the monocationic species, which can be explained by the changes of conformation and conjugation upon oxidation. In the neutral

TTFAQ, the molecule adopts a saddle-like conformation to minimize the steric repulsion between the peri hydrogen atoms of the acene unit and the sulfur atoms in dithiole rings. In the TTFAQ dication, the dithiole rings rotate by 90°, such that the anthracene core becomes planar and fully aromatic. The strong aromaticity gained in this way makes the oxidation potential of TTFAQ radical cation even lower than that of the neutral TTFAQ. As a consequence, the transient radical cation of TTFAQ becomes too unstable to be observed. The conformational change was supported by X-ray analysis of a neutral TTFAQ **11d** and its dication salts (see Figure 1.10).[19]

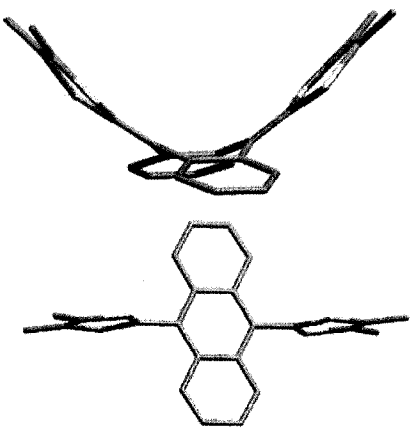

Figure 1.10 Single crystal structure of TTFAQ **11d** (top) and its dication $[\mathbf{11d}]^{2+}$ (bottom). The drawings are adopted from reference 4.

In the TTF based D-A molecules, a low bandgap can be more easily attained since the LUMOs depends on the nature of the acceptor units, and the nature of covalent linkage that bridges the donor and acceptor moieties. The first TTF-fused D-A molecule **19** was made in 1993 by Watson *et al.* using benzoquinone as the acceptor counterpart.[20] It was claimed that a low electrochemical band gap of *ca.* 0.8 eV was achieved, although later

experiments suggested a more reliable value at 1.52 eV. A few years later, triad **20** was prepared. The electrochemical bandgap (E_g) was characterized as 0.87 eV. A moderate intramolecular charge-transfer band was also observed in the NIR absorption spectrum in the region of 800 - 900 nm.[4]

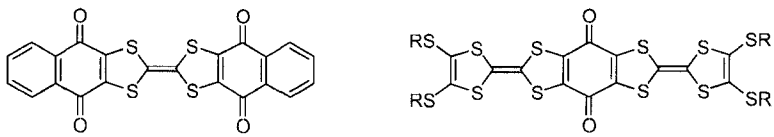

Figure 1.11 Examples of TTF-fused D-A molecules.

Compared with the TTF-A type molecules, the motif of TTF-π-A rendered corresponding molecules decreasing electrochemical bandgaps with the extending π-linker. The lowest E_g (1.0 eV) in this system was achieved in **21c** (see Figure 1.12) in which a thiobarbituric unit was incorporated as the electron acceptor.[4] In many cases, increase of the spacer length results in consistent blueshift of the longest wavelength absorption (*i.e.* increase of optical bandgap), whereas the electrochemical bandgap shows a reducing trend.[4]

TTFAQ has also been used in D-π-A systems. Because the first reduction potentials of TTFAQ derivatives **24** and **25** were somehow decreased in comparison to their TTF analogues **22** and **23**, no improvement in bandgap has been achieved (*ca.* 1.5 eV). On the other hand, its higher thermal stability seems promising for device applications.[4]

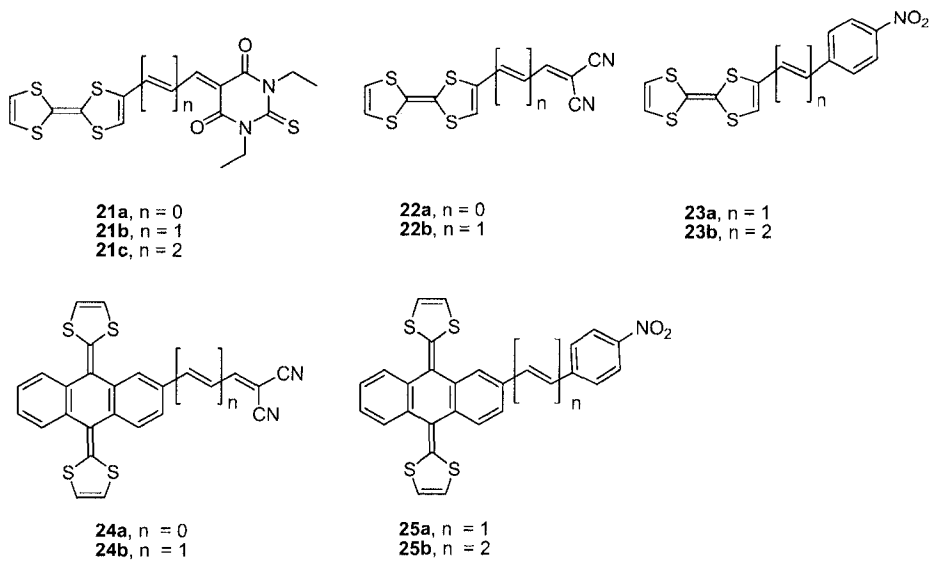

Figure 1.12 Examples of molecules with TTF-π-A motif.

In the TTF-σ-A systems, efforts were focused on the choice of acceptors since the increase of saturated linkages has no significant effect on bandgap. Many acceptors, such as viologen,[21] phthalocyanine,[22] porphyrin[23] have been tested and the resulting electrochemical bandgaps were found to be not less than 0.9 eV. The connection of stronger acceptors to TTF is synthetically very demanding, due to formation of charge-transfer complexes, caged radical ion pairs, and side reactions of the radical ion.[4] However, TCNQ and fluorenone have been successfully connected to the TTF moiety mostly via quinone precursors. Notably at -100 °C pure **13** was obtained (Scheme 1.2) with a bandgap value as low as 0.17 eV.[4]

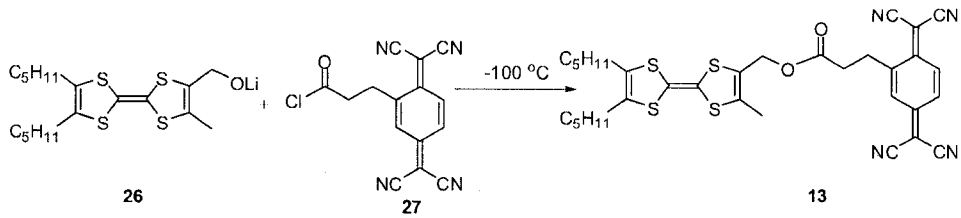

Scheme 1.2 Synthesis of the first TTF-σ-TCNQ derivative.

In TTF based D-A systems involving buckminsterfullerene (C_{60}), bandgap values of 1 – 1.2 eV were attained.[4] These values reflect well the moderate acceptor nature of C_{60}, along with the saturated linkage created via the general C_{60} functionalization methodologies, for example, Prato's protocol,[44,45] Bingel reactions[40] or Diels-Alder reactions.[42] Although in the C_{60}-TTF system weak charge transfer interactions in the ground state were observed, photoexcitation of C_{60} resulted in more pronounced charge transfer from TTF to C_{60} associated with strong quenching effect of the TTF emission spectrum. The electron transfer rate decreases dramatically as the linkage length increases.

1.1.3 Synthetic Methods for TTF and its Derivatives

Thanks to the great efforts by numerous synthetic groups over the past decades, a wealth of synthetic methods are currently available for construction of various TTF based structures. Synthetic methods for TTF have been reviewed by Fanghaenel and co-workers in 1987 along with the synthetic routes to the two most important TTF precursors, thione and dithiolium salt (Schemes 1.3 and 1.4).[4,24] The following section describes the synthetic protocols relavent to preparing the target molecules in this project.

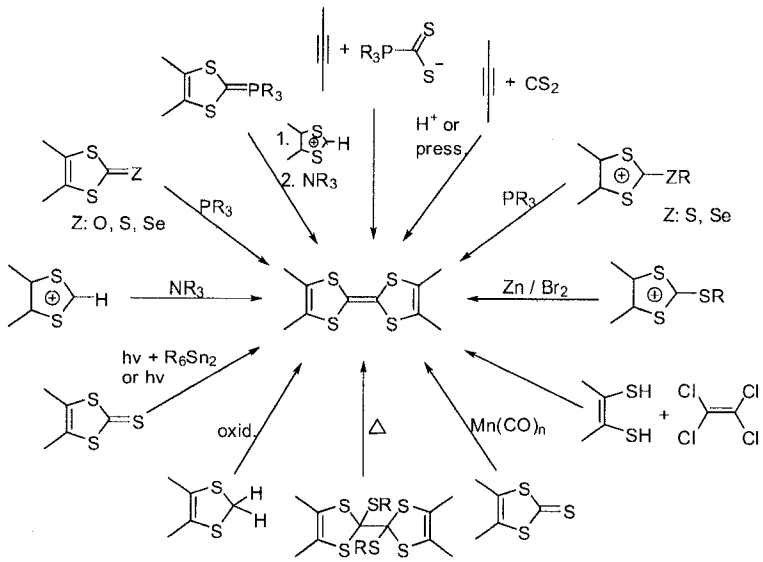

Scheme 1.3 Synthetic methods for preparing the TTF skeleton (adopted from reference 4).

(a)

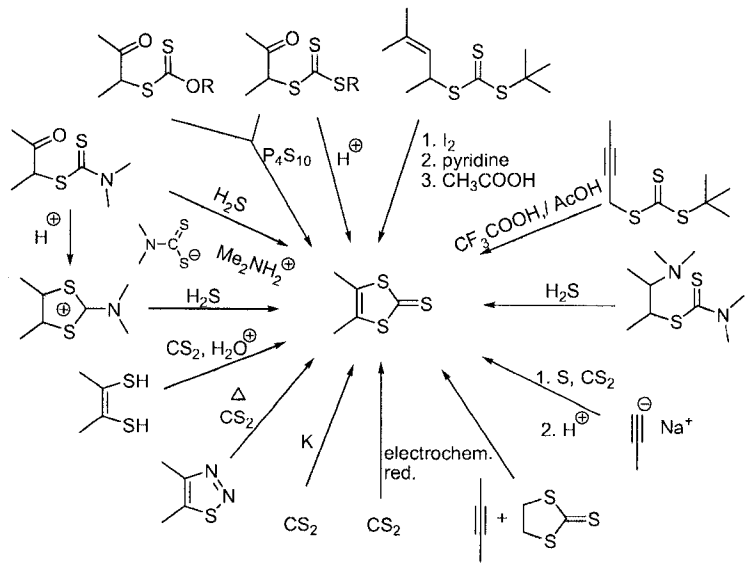

(b)

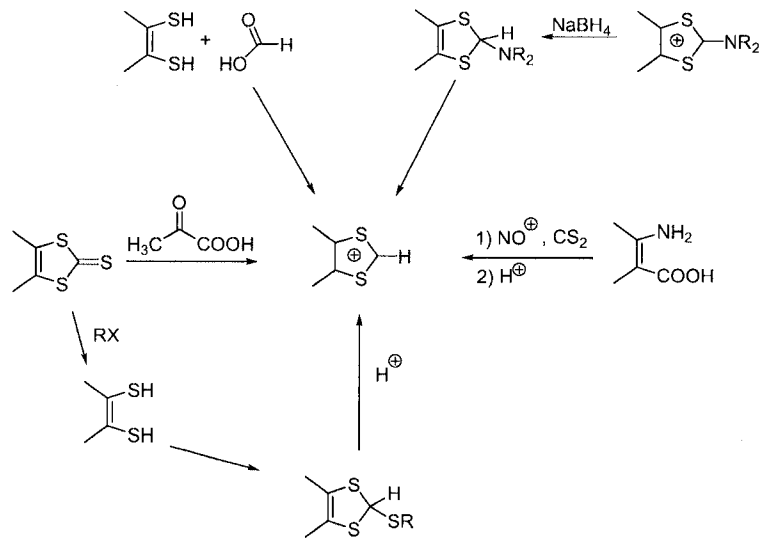

Scheme 1.4 Synthetic methods for dithione and dithiolium salt (adopted from reference 4).

The three most popular methods so far for construction of TTF as summarized in Scheme 1.5 include: (a) phosphite promoted coupling of dithiole-2-thiones **28**, (b) base-catalyzed coupling of dithiolium salts **29**, and (c) Wittig reaction between reagent **30** or its

phosphonate derivative **31** and a dithiolium salt in the presence of a strong base. In general, methods (a) and (b) are more suitable for preparing symmetrical TTFs, while method (c) is particularly efficient in synthesizing asymmetrical TTFs. It is worth noting that the coupling of different substituted 1,3-dithiole-2-thiones and 1,3-dithiole-2-ones in neat triethyl phosphate can give the asymmetrical product in good yields (as shown Scheme 1.6).[25]

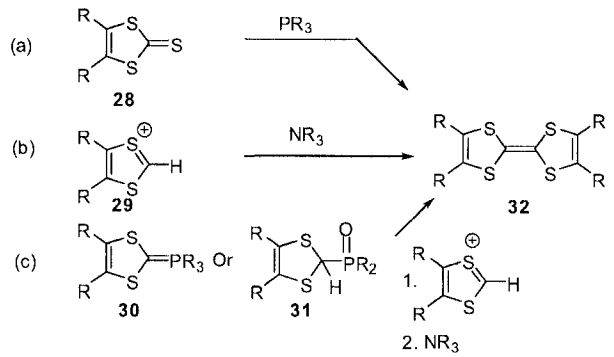

Scheme 1.5 Three important synthetic routes to TTF.

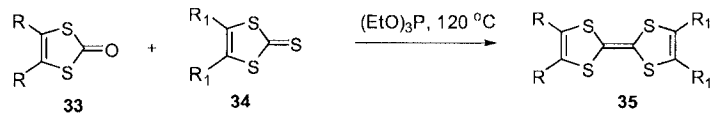

Scheme 1.6 Asymmetrical coupling in neat triethyl phosphate.

Thione **28** can be prepared on a large scale from the readily available CS_2 and alkali metals such as K or Na (Scheme 1.7). This method was mainly developed by Hoyer's group in 1979.[26] Reduction of CS_2 with K or Na will produce 1,3-dithiole-2-thione-4,5-dithiolate (dimercaptoisotrithione, dmit), the proposed mechanism of which is described in Scheme 1.8.[27] The resulting dithiolate was separated from K_2CS_3 as the

tetraethylammonium salts of its zinc chelate. The following reaction with suitable electrophilic agent (RX) will afford desired substituted thione products. The possible electrophiles for such reactions include alkyl halides, vinyl halides, propargyl bromides, acyl chlorides, and so forth.[27]

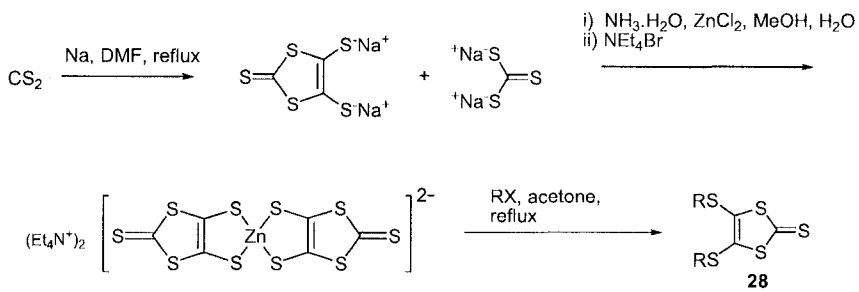

Scheme 1.7 Preparation of thione **28** by reduction of CS_2 with Na.

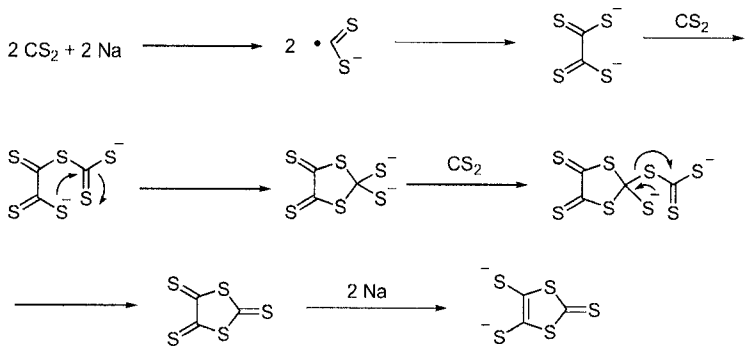

Scheme 1.8 Mechanism of the reduction of CS_2 with Na (adopted from reference 27).

The dithiolium salts **29** can be prepared from thione **28** via an addition-reduction-elimination sequence (Scheme 1.9). Although the alkylation of the thione is favored by aromatization of the dithiole ring, methyl iodide is not reactive enough to effect such a reaction. The preferable choices of alkylating reagents are methyl fluorosulfate, methyl

tirfluorosulfonate, triethyloxonium tetrafluoroborate and others. Thione **28** reacts with dimethyl sulfate at 100 °C smoothly and gives the corresponding dithiolium tetrafluoroborate upon addition of a strong acid, hydrofluoroboric acid (HBF_4) (Scheme 1.10).[11] Subsequent reduction with $NaBH_4$ and hydride elimination in acidic condition furnish the desired product **29**.

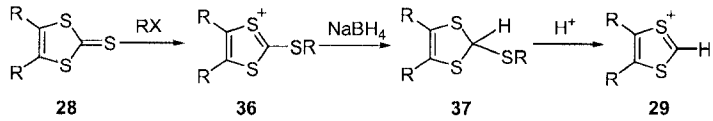

28 **36** **37** **29**

Scheme 1.9 Synthesis of dithiolium salts **29**.

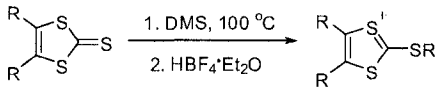

28 **36**

Scheme 1.10 Methylation of thione **28** by dimethyl sulfate.

Further reaction of dithiolium salt **29** with either phosphine or phosphate yields the Wittig reagent **30** or phosphonate **31** (Scheme 1.5) as precursors for the Horner-Wadsworth-Emmons reaction. In highly diluted conditions the reaction of the 4,5-bis(alkylthio)-1,3-dithiole-2-thione with a trialkyl phosphates yielded a phosphonate as the major product along with trace coupling product of tetrathiafulvalene.[27,28]

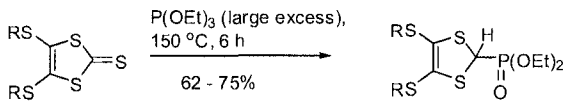

38 **39**

R = $-C_{10}H_{21}$, $-CH_2CH_2-$

Scheme 1.11 Direct preparation of phosphonate **39** from thione **38**.

The reaction of an electrophilic alkyne, such as dimethyl acetylenedicarboxylate (DMAD), with a 1,3-dipole, the adduct of Bu_3P and CS_2, affords the ylide intermediate **42**, which can be directly dimerized into TTF product **32**. However, the direct transformation from **42** to TTF suffers from a very low yield. To avert this problem, ylide intermediate **42** is usually trapped by addition of HBF_4 to form a stable phosphonium salt **40**,[29] which has been proven to be a good precursor for olefination of various carbonyl groups.

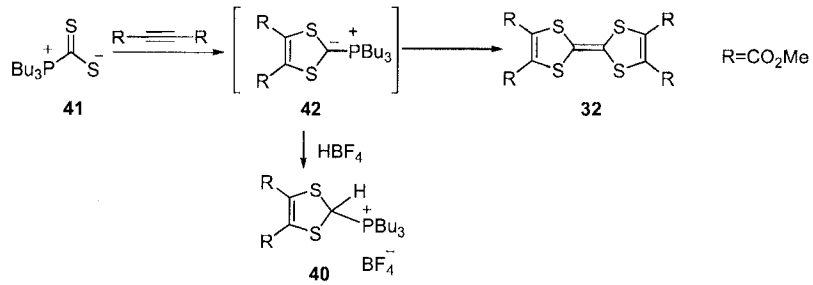

Scheme 1.12 Synthesis of phosphonium salt **40** by 1,3-dipolar cycloaddition.

Once TTF is formed, it can be further functionalized through a number of well-established methodologies. An important route is the lithiation of TTF with a strong lithium base such as LDA at -78 °C, followed by reactions with various available electrophiles (Scheme 1.13).[30] The various products shown in the scheme are useful for further synthetic elaboration. The aldehyde TTF derivatives are especially suitable for preparing π-extended systems via Wittig reactions, while the alcohol and acid derivatized TTFs can be readily linked to other functional groups via esterification reactions. When there is an electron donating substituent (*e.g.* Me) attached to one of the dithiole rings, the acidity of the adjacent proton on the very same dithiole ring decreases. This allows lithiation to occur preferentially on the other dithiole ring. In contrast, an electron

withdrawing group will direct the lithiation to the same dithiole ring. Such directing effects by substituents make this methodology very useful in regioselectively preparing multisubstituted TTFs.[30]

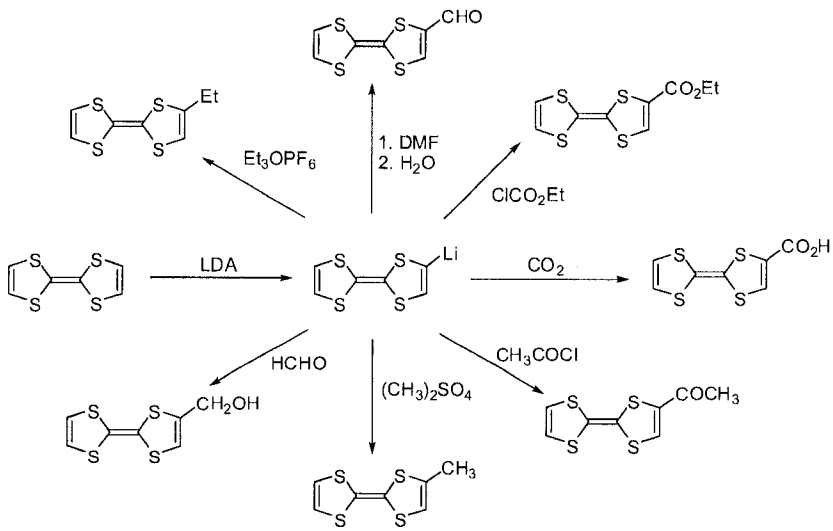

Scheme 1.13 Lithiation of TTF and further reactions with different electrophiles (adopted from reference 41).

Another important methodology for TTF functionalization is based on the use of a β-cyanoethyl protecting group. The β-cyanoethyl group can be introduced via the reaction of dmit (1,3-dithiole-2-thione-4,5-dithiolate) with 3-bromopropionitrile.[27] The removal of the β-cyanoethyl group occurs smoothly in the presence of a base such as MeONa.[31] The resulting thiolate reacts with suitable electrophiles to yield various TTF derivatives (Scheme 1.14).[4] In addition, monodeprotection of a bis-protected precursor can be easily achieved by using one eq. of $CsOH{\cdot}H_2O$ in $MeOH/CHCl_3$. The resulting cesium thiolate is stable and precipitates out of the reaction mixture.[31]

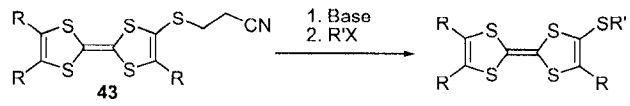

Scheme 1.14 Deprotection of β-cyanoethyl group and further reaction with an electrophile.

While Wittig olefination is an important way to generate exTTF, especially for the ones with large π-conjugated structures between the two dithiole rings, the Diels-Alder reactions, on the other hand, have been widely used in preparing various annulated structures (Scheme 1.15).[29] The highly reactive diene intermediate **45** was generated *in situ* to stereoselectively react with a dienophile. However, the relatively high temperature for the diene generation may cause problems in the cases where thermal stability of the product is an issue.

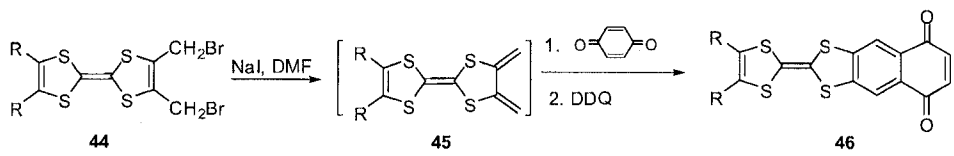

Scheme 1.15 Synthesis of an annulated TTF via the Diels-Alder reaction.

1.2 A Brief Overview of Buckminsterfullerene (C_{60})

In 1985 Kroto, Smalley and Curl together discovered a new type of carbon allotrope, Buckminster fullerene C_{60}.[32] Five years later, Kratschmer and co-workers developed a technique to prepare C_{60} in macroscopic quantity based on resistive heating of graphite,[33] which allowed for the rapid development of C_{60} chemistry. Now a Japanese company produces fullerene by burning toluene on a 40 ton/yr scale.[32]

1.2.1 Structure and Properties of C_{60}

[60]Fullerene (C_{60}) is the smallest stable fullerene with an icosahedral (I_h) symmetry. Its molecular structure contains 12 pentagons and 20 hexagons arranged on a spherical surface in the same way as a soccer ball. The bonds between two hexagons (6-6 bond) are shorter than those between one hexagon and one pentagon (5-6 bond). Thus all the double bonds locate at the junction of two hexagons to achieve the lowest strain energy. Unlike planar aromatics, the sp^2 carbons on fullerene are pyramidalized in geometry. The strain energy resulting from deviation from planarity therefore accounts for the unique reactivity on the C_{60} cage.

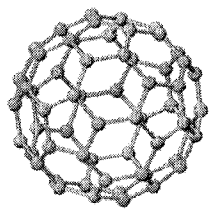

Figure 1.13 Stick-and-ball model of buckminsterfullerene C_{60}.

C_{60} has been used as an important building block in many molecular systems, resulting in interesting properties such as photovoltaic responses,[34] nonlinear optical properties,[35] and biological activities.[36] Investigation of the electron D-A systems containing C_{60} as an electron acceptor have been exceedingly fruitful due to the properties of C_{60}. C_{60} possesses a unique 3-D electron delocalization pattern which results in a very small reorganization energy (λ) that facilitates rapid electron transfer reactions.[37] C_{60} can reversibly accept up to six electrons by stepwise one-electron reductions.[38] C_{60} is a good

chromophore for photo-induced electron transfer. Excitation of C_{60} over a wide range of wavelengths in the solar spectrum results in the formation of an energetic singlet excited state $^1C_{60}$* which undergoes rapid and efficient intersystem crossing to yield $^3C_{60}$*. In the D-A system, such as the TTF-C_{60} type dyad, excitation of C_{60} results in fast electron transfer from the donor group to $^3C_{60}$* if the charge-separation (C-S) state is thermodynamically downhill. In the presence of an external electric field, the C-S state will further lead to the transport of bipolar charges through the bulk of organic materials to eventually produce photoinduced electric current. These constitute the essential steps to convert light to electric energy in an organic photovoltaic cells. In early studies of C_{60} based organic solar cells, pristine C_{60} and various conducting polymers were blended in order to enhance the efficiency of photoinduced electron transfer as well as charge transport. One shortcoming of directly using pristine C_{60} in organic composite materials is the poor solubility and compatibility of C_{60} with the conducting polymer matrix. However, this difficulty can be partially overcome by introducing solubilizing appendages on the C_{60} cage.

1.2.2. Covalent Functionalization Methods for C_{60}

The propensity to release the strain energy caused by pyramidalized sp^2 carbons make C_{60} itself reactive towards nucleophilic attacks, radical additions, and electrocyclic reactions, in which one or more saturated tetrahedral sp^3 carbon centers are formed on its surface. In the nucleophilic addition, the products are generated by 1,2-addition to 6-6 bonds. 1,4-Addition is disfavored since the formation of a 5-6 double bond is more energetically demanding. The reaction of 1,2-addition usually proceeds at room

temperature. Thus, a relatively clean reaction outcome is usually expected. Apart from phosphorous and amine based nucleophiles, various carbon nucleophiles have also been explored. In general, carbon nucleophiles used for C_{60} addition can be divided into two classes: (i) Grignard reagents and organolithium compounds (Scheme 1.16), and (ii) α-halo esters and α-halo ketones (Scheme 1.17). For the first class of nucleophiles, the addition reactions on C_{60} generate a relatively stable fulleride anion, which directly leads to substituted fullerenes **47** by simple protonation. Notably, the addition of an alkynylide anion to C_{60} can give the maximal orbital overlap between fullerene and conjugated substituent group via peri-conjugation, where only one sp^3 carbon forms the linkage.[39]

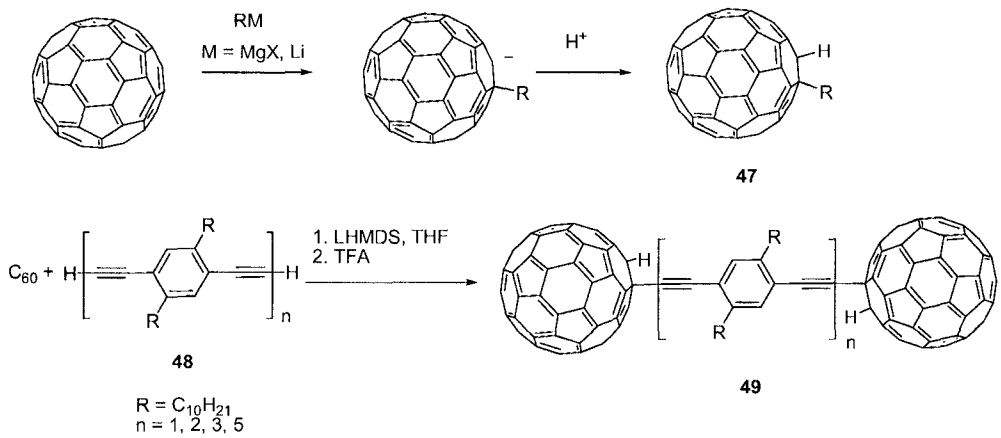

Scheme 1.16 Examples of nucleophilic additions on C_{60} with carbon nucleophiles.

The second type of carbon nucleophiles commonly used in synthesis of C_{60} derivatives are normally generated by deprotonation of an α-halo ester with a base. The addition of such a nucleophile to C_{60}, followed by an intramolecular displacement of the halogen group, affords methanofullerene **50** as the product (Bingel reaction).[40] As a

modification, the halo ester can be generated *in situ*, such as in the preparation of compound **52**.[41] Through these reactions, various groups can be attached to C_{60} via a cyclopropane linkage.

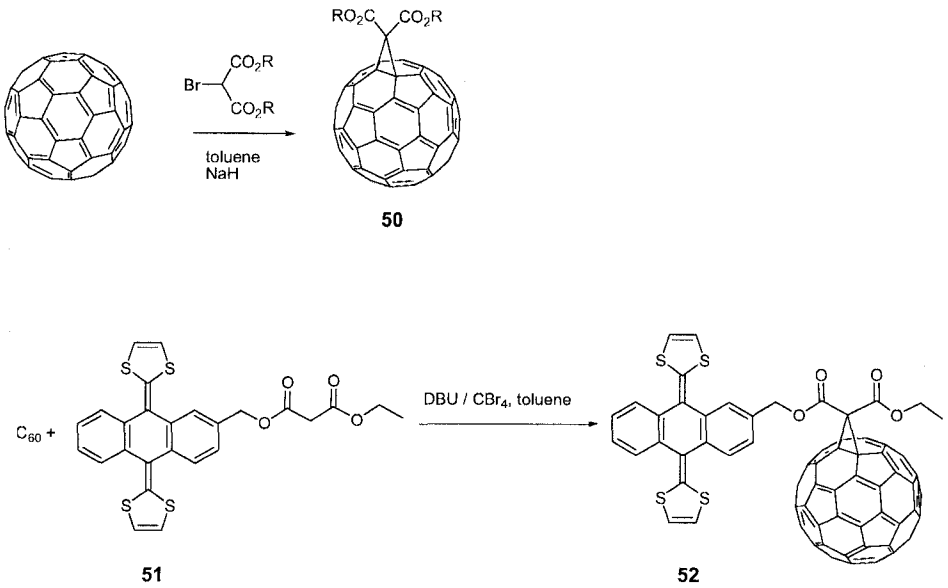

Scheme 1.17 Functionalization of C_{60} with the Bingel cyclopropanation.

In cycloadditon functionalization of C_{60}, [4 + 2] and [3 + 2] cycloadditions are the most popular approaches. Both types of reaction require relatively high temperatures to achieve satisfactory yields. In [4 + 2] cycloadditions, cycloadduct formation is strongly dependent on the reactivity of the diene counterpart. For example, the reaction of anthracene and C_{60} was found to be reversible (Scheme 1.18).[33] Therefore, temperature control is critical in these reactions. In some cases, reactive dienes were used to achieve efficient functionalization of C_{60}. Such dienes could be generated *in situ*, for instance,

thermal ring opening of benzocyclobutenes or 1,4-elimination of dihalides, and would rapidly react with the dienophile C_{60} to form a cyclohexene linkage. An example of making a TTF-C_{60} type D-A dyad using this method is shown in Scheme 1.18.[42]

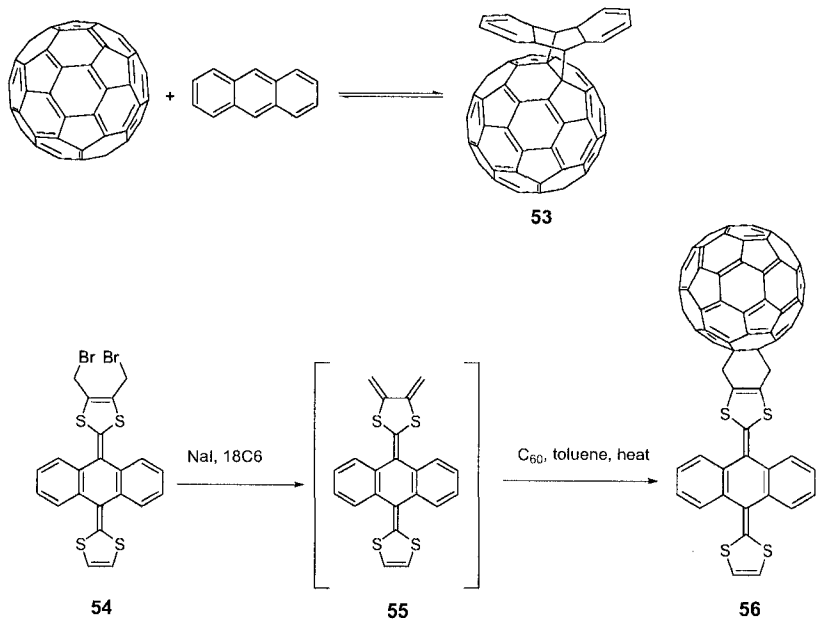

Scheme 1.18 Functionalization of C_{60} with [4 + 2] Cycloadditions.

In [3 + 2] cycloadditions, C_{60} acts as a 1,3-dipolarophile. A series of frequently used 1,3-dipoles in C_{60} functionalization are diazo compounds including diazomethanes, diazoacetates, and diazoamides. The reaction between a diazo compound and C_{60} was first explored by Wudl's group.[33] The addition product afforded, pyrazoline **57**, could be either separated, or further subjected to N_2 extrusion to afford methano-bridged fullerene derivatives. The products of diazo functionalization of C_{60} were not singular but a mixture of stereoisomers, such as compounds **58**, **59**, and **60** shown in the top reaction of Scheme 1.19. However, the 1,2-bridged isomer **58** is the most thermodynamically stable and thus

obtained as the major product under thermodynamically controlled conditions.[33] The synthesis of a TTF-C_{60} dyad **63** with the simple D-A motif is demonstrated in Scheme 1.19.[43]

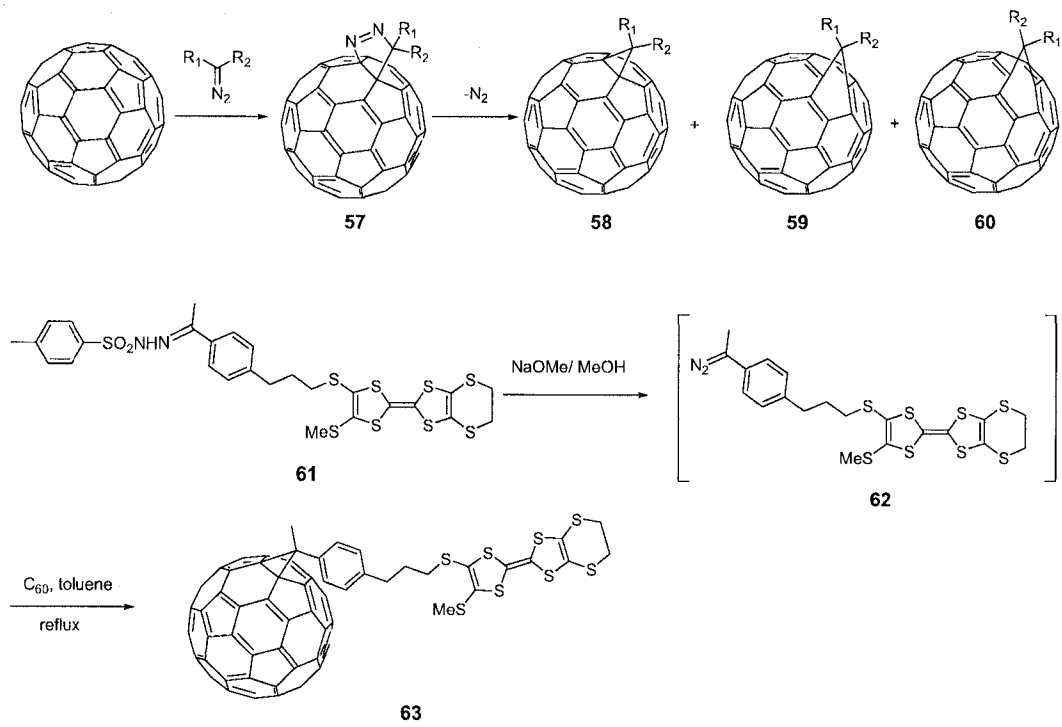

Scheme 1.19 Reactions of diazo compounds with C_{60}.

Another type of very reactive 1,3-dipole is the azomethine ylides **64** (Scheme 1.20), which are usually generated *in situ* from condensations of aldehydes or ketones with substituted glycines. The major product of the reaction between an azomethine ylide and C_{60} (often referred to as the Prato reaction) is fulleropyrrolidine **65**.[44, 45] For example, in the one-pot synthesis of a pyrrolidine linked TTF-C_{60} derivative **69**, TTF-carbaldehyde **66** and sarcosine were mixed together with C_{60} in refluxing toluene. Condensation between **66** and sarcosine followed by decarboxylation afforded azomethine yildes **68** *in situ*,

which immediately reacted with fullerene to give the pyrrolidinefullerene **69**.[46]

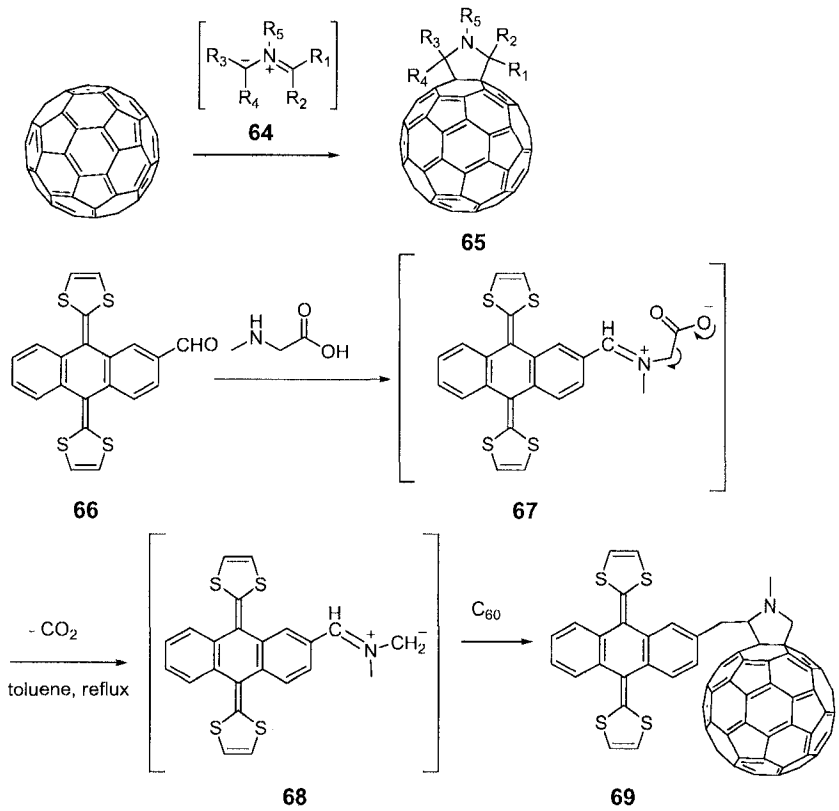

Scheme 1.20 Functionalization of C_{60} via the Prato reaction.

1.3 Recent Advances in Molecular Ensembles Containing TTFAQ and C_{60}

In 1997, Martín and co-workers prepared the first TTFAQ-C_{60} derivative **70a-c** (Figure 1.14), where the TTFAQ and C_{60} were connected via a pyrrolidine bridge by 1,3-dipolar cycloadditions (Prato's protocol).[47] A wealth of TTFAQ-C_{60} molecular assembles have been prepared by this methodology.

The electrochemical properties of these compounds were studied primarily by cyclic voltammetry in various solvents. Generally, the cyclic voltammograms of these molecular ensembles show four quasi-reversible reduction waves corresponding to the

sequential reductions on C_{60} and a two-electron oxidation wave characteristic of TTFAQ. The electrochemical bandgaps of these compounds are generally within the range of 1.1 – 1.5 eV, which are too high for significant charge transfer to take place in the ground state. These results, not surprisingly, are congruous with those observed in the UV-vis spectra, that is, no noticeable charge-transfer bands were seen in the UV-vis and near IR spectrum. However, upon excitation, a rapid electron transfer occurs as the major pathway of photodeactivation, which was reflected by the strong quenching effect in the fluorescent emission of TTFAQ moiety. Further investigations by time-resolved fluorescence and transient absorption measurements have revealed that the detailed photophysical dynamics for numerous C_{60}-containing TTFAQ ensemble molecules indeed involve electron transfer processes. Photophysical property measurements such as fluorescence quantum yields, fluorescence lifetimes, and the lifetimes of the charge separation states were particularly informative in establishing reasonable photoexcitation/deactivation mechanisms for these compounds.

1.3.1 TTFAQ-C_{60} Dyads

In 2000, Martín and co-workers reported the synthesis of compounds **71a-b**, where the TTFAQ and C_{60} were connected via cycloaddition of a diazo precursor with C_{60}.[47] These compounds showed low bandgaps (1.12 eV for **71a**, and 1.19 eV for **71b**), and the lifetimes of the charge-separated (C-S) states were several hundreds of nanoseconds in deoxygenated PhCN, much higher than the lifetimes (several nanoseconds) of analogous TTF-C_{60} dyads. The experimental results suggest that the gain of aromaticity and planarity of the TTFAQ core is a critical factor favoring the formation of C-S states.

In 1999, Herranz and Martín synthesized TTFAQ-C_{60} dyads **72** using the Diels-Alder reaction.[48] This compound showed a remarkable anodic shift in the oxidation potential (0.31 eV) and cathodic shift of the first reduction potential (0.12 eV) in comparison to the TTFAQ and C_{60} parents, which were rationalized on the basis of the electronic interactions between the TTFAQ and C_{60} units. However, what remained puzzling in this study was that an enhanced electron interaction between the donor and acceptor hindered the charge transfer process, since these shifts in potentials furnished a much larger bandgap (1.47 eV) compared with other TTFAQ-C_{60} dyads. Most likely, the increase of first oxidation potential in **72** could be ascribed to the change of the TTFAQ moiety to an annulated structure. Another TTFAQ-C_{60} series of **73a-c** constructed by Diels-Alder reactions were later reported in 2002 by Martín's group.[49] These compounds showed comparable first reduction potentials to that of **72** and slightly increased first oxidation potentials compared with TTFAQ parent. The bandgaps are *ca.* 1.2 eV and the lifetimes of the C-S states are *ca.* 200 ns in PhCN. Interestingly, a retro-Diels-Alder reaction of **72** took place as the reaction temperature was further elevated. Such reversible interconversion was considered to be useful in the design of TTFAQ-based fluorescing switches.

In 2003, Guldi *et al* compared the photophysical properties of two series of structural analogues of TTFAQ-C_{60} dyads; one was the fulleropyrrolidines prepared by the 1,3-dipolar cycloaddition, and the other was the Diels-Alder cycloadducts. Interestingly, these compounds (**70a**, **72** and **74**) showed similar lifetimes of photoinduced C-S states. As suggested by the authors, the delocalization of positive charge (hole) across the entire TTFAQ donor unit was a determining factor to the rates of charge separation and

recombination in the photophysical and photochemical processes; as a result, the linkage structure between C_{60} and TTFAQ had little impact on the lifetimes of the radical pair species.[42]

In 2004, Guldi and co-workers introduced oligo-*p*-phenylenevinylene (OPV) groups between the TTFAQ and C_{60} as shown in molecular wire **75**.[50] It was suggested that the small energy difference of HOMOs between C_{60} and the OPV bridge would allow facile electron injections from the bridge to C_{60}. In the meantime, the full conjugation between OPV bridge and TTFAQ furnished strong electron coupling. As a consequence, it was reasonable to assume a fast charge separation would be favored in this system. Moreover, because of the long distance separation between the donor and acceptor units, a slow charge recombination would be expected. Significantly, the lifetime of C-S species of **73** was observed to be 10 times longer than that of the TTFAQ-C_{60} **70a**. Two years later, oligo-*p*-phenyleneethynylene (OPE) bridges were applied by Guldi *et al.* into a similar TTFAQ-π-C_{60} triad series, as shown in compounds **76a-c**.[51] Because theoretical calculations on the topological and electronic structures of **76c** at DFT (density functional theory) and semiperical AM1 (Austin Model 1) levels showed that the benzene moiety of TTFAQ was not in the same plane as the phenyl ring adjacent to the pyrrolidine ring, it was believed that the electronic coupling between the donor and acceptor units was disrupted. In addition, the slightly reduced HOMO value of OPE than OPV was supposed to further diminish possible interactions between OPE and C_{60}. These examples shed light into the structure dependence of the wire-like behavior, and demonstrate the favorable effect caused by the introduction of conjugated spacers between donor and acceptor groups. Nonetheless, it is worthy of commenting here that an intrinsic drawback in such

pyrrolidine linked C_{60}-π-TTAFQ systems as **75** and **76** is the severe interruption of conjugation between C_{60} and the bridge by the saturated pyrrolidine linker, no matter how extensively conjugated the π-bridge is. This issue has not been adequately addressed, and to what degree this saturated linker group on C_{60} would influence the electronic coupling remains unclear.

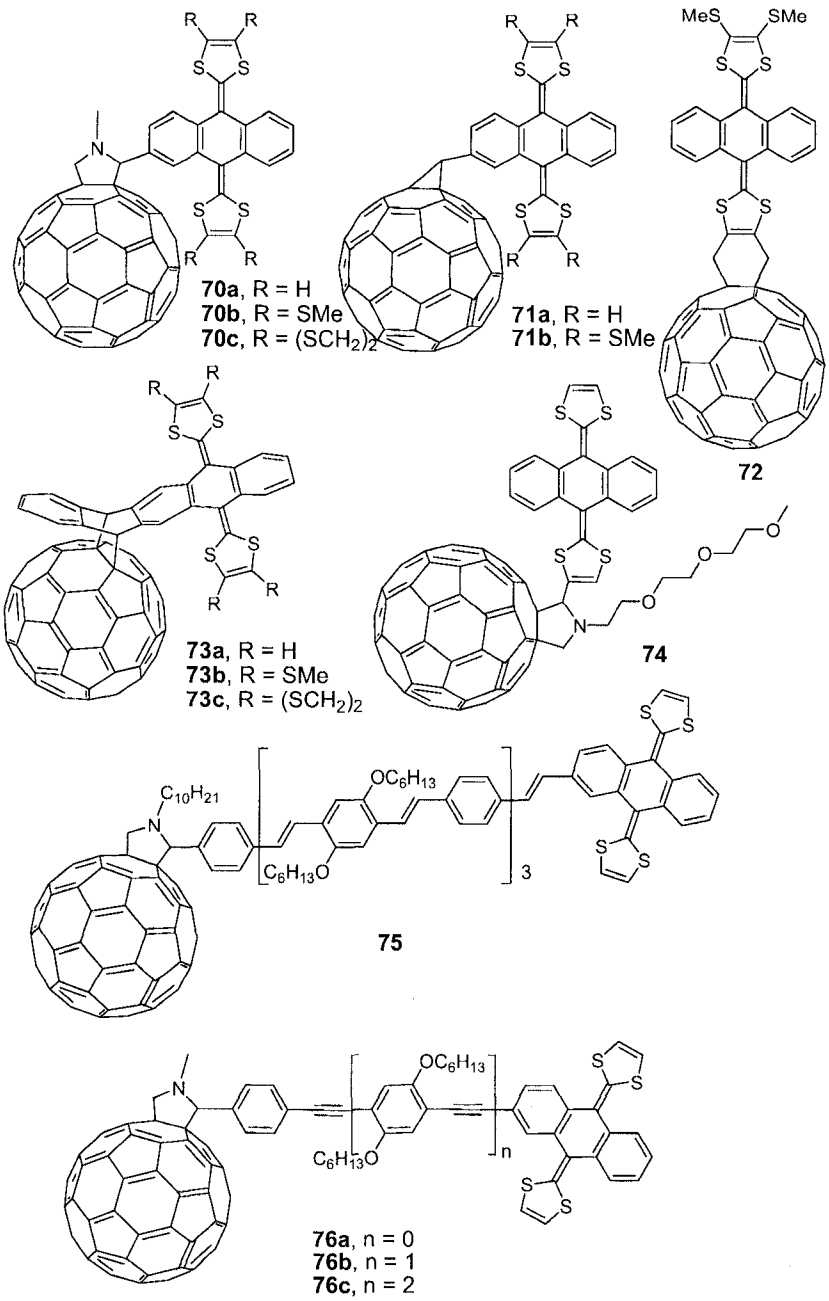

Figure 1.14 Examples of TTFAQ-C_{60} dyads.

1.3.2 C_{60}-TTFAQ-C_{60} Triads

The C_{60}-TTFAQ-C_{60} type triads are more intriguing molecular ensembles than the TTFAQ-C_{60} dyads, while the synthesis of which is certainly more laborious and

challenging. Because of the synthetic difficulties, only a handful of examples are available in the current literature. In 2003, Guldi *et al.* reported a series of TTFAQ-C_{60} ensembles synthesized by the Bingel reaction, including the C_{60}-TTFAQ-C_{60} triads **77a-d**.[41] Based on the CV data, **77c** had a bandgap of 1.27 eV, which was moderate among the TTFAQ-C_{60} systems. Unfortunately, no other data was given in that report with respect to the electronic properties of these triads.

In 2005, another series of TTFAQ-C_{60}-TTFAQ triads, **78a-d**, were synthesized by Guldi *et al.*[52] These compounds had rather small bandgaps ranging from 1.16 to 1.22 eV. Notably, the presence of the second C_{60} has doubled the lifetimes of the C-S species in comparison to their analogous dyads. This result strongly indicates that the second C_{60} group plays a significant role in the process of photoinduced charge transfer. The exact role of the second C_{60}, however, is still not clearly understood, while intensive investigations on this issue are currently being elaborated by our group and others.

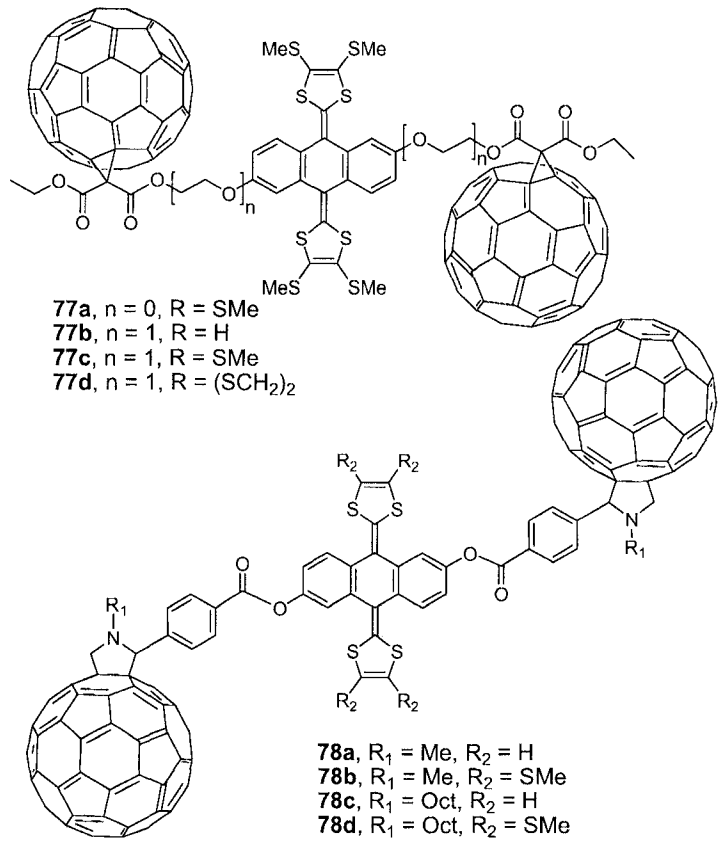

Figure 1.15 Examples of TTFAQ-C_{60}-TTFAQ triads.

1.3.3 Other Multiple C_{60}/TTFAQ Polyads

Besides the dumbbell shaped TTFAQ-C_{60}-TTFAQ triads, other molecular architectures containing multiple C_{60} and TTFAQ units have also been synthesized over the past years, in spite of the great synthetic challenges of making such large molecular systems. Several examples are given in Figure 1.16. Among them, compounds **79a-c**[41] and **80a-b**[53] have two donor and one acceptor units linked to one another. The presence of the second donor group was found neither to interact with the other donor, nor to cause alternative electron transfer pathway. However, when the three components were linearly linked such as in **81a-b**[54] and **82a-b**,[55] the electron transfer occurred first between C_{60} and

the adjacent donor to form a short-distance C-S state, which was followed by migration of the positive charge to the remote donor group, forming a second long-distance C-S state. Because the relay of charge transfers further distanced the separated charges within the molecule, recombination rate was significantly reduced. This led to significantly prolonged lifetimes for the final C-S states into the μs regime.

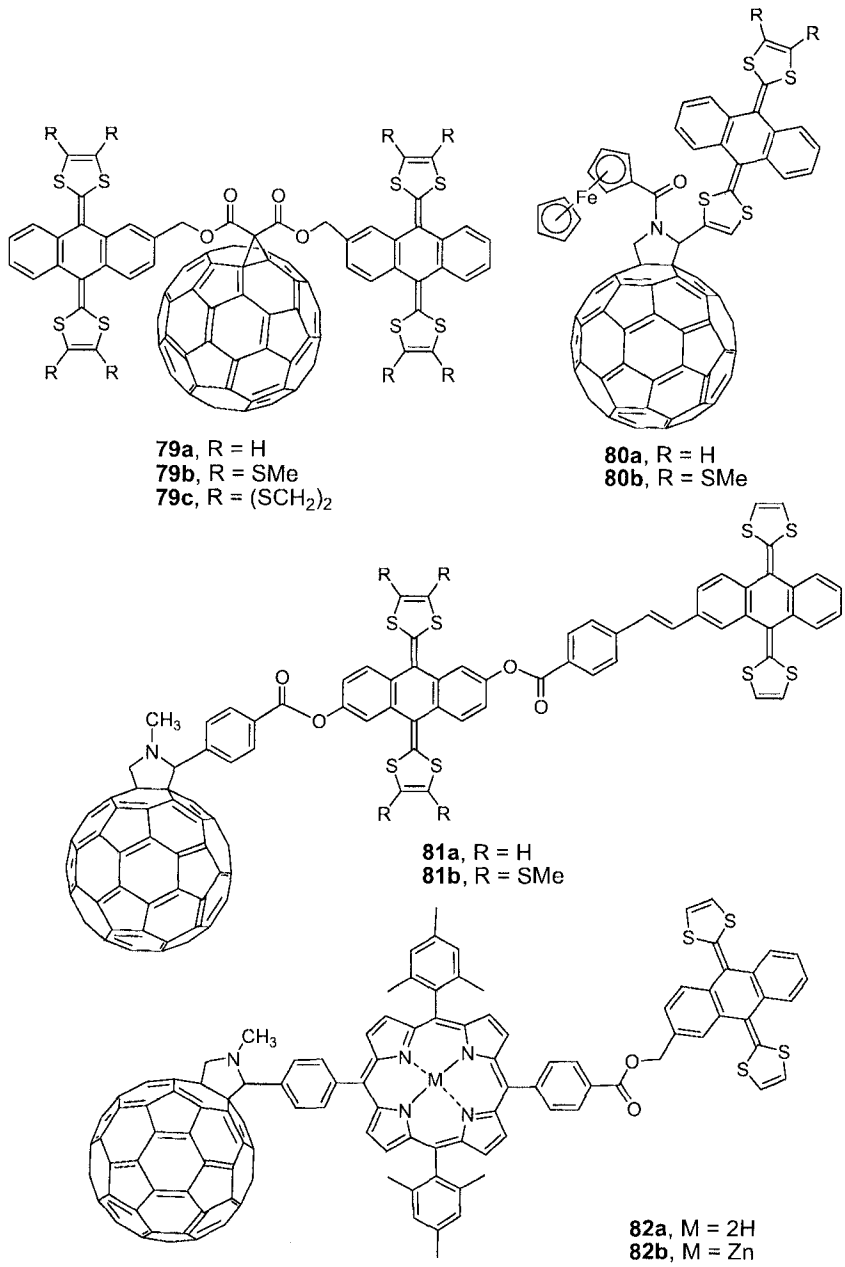

Figure 1.16 Other recently synthesized multiple TTFAQ/C_{60} ensembles.

1.4 Aim and Outline of this Thesis

The first goal was to synthesize a new series of C_{60}-TTFAQ-C_{60} triads in which the electroactive units are connected with a highly conjugated structure. As such, the

electronic interaction between TTFAQ and C_{60} can be further enhanced compared with those triads with non-conjugated bridges in the literature. Besides the planned synthetic work, the electronic properties of these compounds were investigated by UV-vis, fluorescence and cyclic voltammetry. The targeted C_{60}-TTFAQ-C_{60} compound may be useful for applications in organic optoeletronics.

A series of TTFAQ based donor-acceptor molecules were prepared, and their electronic and electrochemical properties were studied, aiming at an understanding of the structure-property relationship in such systems, particularly, the ground state properties for both neutral and oxidation states of these compounds. Understanding such properties will greatly benefit further photophysical characterization on these molecules using laser flash photolysis experiments. The steady state absorption properties of these molecules were investigated. Chemical oxidations were carried out on these compounds, and the absorption properties of the resulting oxidized species were discussed.

In the last section of this thesis, relevant work on the synthesis of a new TTFAQ based molecular switch and a preliminary exploration on a one-pot homo/cross coupling synthesis of complex butadiynylene core π-conjugated systems were discussed.

Chapter 2

Synthesis and Characterization of C_{60}-TTFAQ-C_{60} and TTFAQ Based D-A Molecules

2.1 Introduction

As mentioned in the first chapter, 2,6-diethynylated TTFAQs are a class of novel electron donor building blocks that could render unprecedented electronic, redox, and photophysical properties. The first part of this chapter focuses on the synthesis of a series of dumbbell-shaped C_{60}-TTFAQ-C_{60} triads. Compound **83** as shown in Scheme 2.1 was selected as the first target in the synthetic work. The retrosynthetic strategy towards this fairly large molecule is outlined in Scheme 2.1. The central TTFAQ core could be synthesized via the Horner-Wadsworth-Emmons (HWE) reaction between 2,6-diethynylated anthraquinone **84** and phosphonate **85**. Two π-spacing groups could be then attached to the TTFAQ unit via the Sonogashira coupling between arylacetylene iodide **86** and corresponding diethynylated TTFAQ. The final step will involve the attachment of two C_{60} cages to a bis(terminal alkyne) via an *in situ* alkynylation protocol. The later part of this chapter describes the synthesis of a series of TTFAQ based donor-acceptor (D-A) molecular systems using Sonagashira coupling reactions. Electronic and spectroscopic properties for these novel TTFAQ based molecular systems were investigated by various spectroscopic and electrochemical methods, which are introduced in the later sections of this chapter.

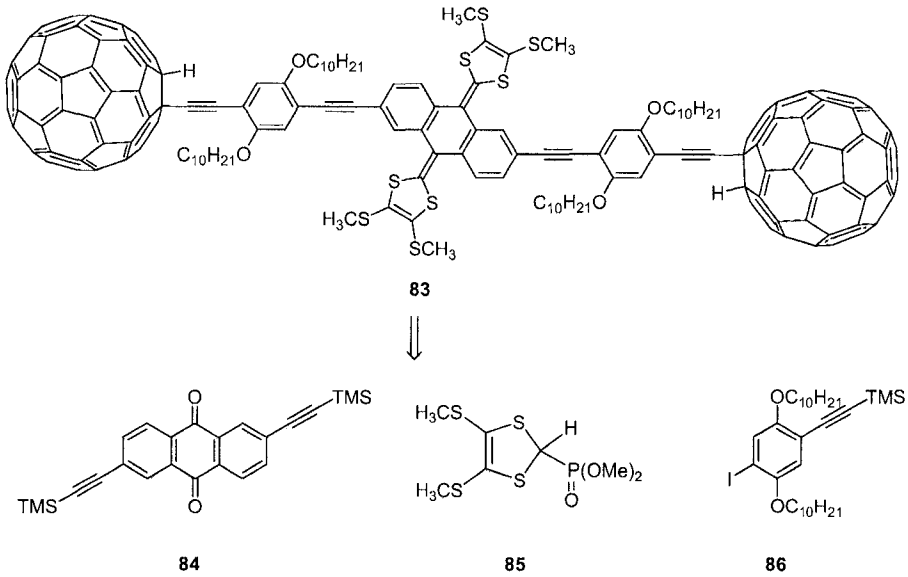

Scheme 2.1 Retrosynthetic strategy for C_{60}-TTFAQ-C_{60} **83**.

2.2 Results and Discussions

2.2.1 Synthesis of C_{60}-TTFAQ-C_{60} triads 83

2.2.1.1 Synthesis of 2,6-Diethynylated Anthraquinone 84

The synthesis of an essential building block for triad **83**, the TTFAQ core, began with the preparation of 2,6-diethynylated anthraquinone **84**. Compound **84** was prepared following a known route from the literature and the details are outlined in Scheme 2.2.[56,57] In the synthesis, a Sandermeyer reaction was first carried out on 2,6-diaminoanthraquinone **87** to afford dibromide **88** in 49% yield. Two points are worth some comments for this Sandermeyer reaction. First, the reaction temperature was found to be critical to the outcome of the reaction. While high temperatures tended to result in accelerated reaction rates, rather complex mixtures of various products were obtained under such conditions affording low yields of the desired product. Low temperatures, on the other hand, could significantly decelerate the reaction. Taking these into consideration,

the reaction thus needs to be performed at an optimized temperature so as to achieve both satisfactory speed and yield. Second, purification of the product was problematic. The solubilities of dibromide **88** and concomitant byproducts were poor in common solvents such as CH_2Cl_2, toluene, and benzene. The poor solubility made it difficult and tedious to purify **88** in a large quantity on a silica column. In order to get pure **88**, a column chromatographic separation was undertaken at first to mainly remove an unidentified byproduct that appeared as one spot above **88** on the TLC plate.[58] The crude product after the column separation was then subjected to recrystallization from toluene or benzene under N_2 protection. Even though exhaustive efforts have been invested in this step, the purity of the product could not be improved significantly. Nevertheless, it was fortunate that the impurities neither affected the subsequent coupling reaction nor caused any problems in the purification of **84**.

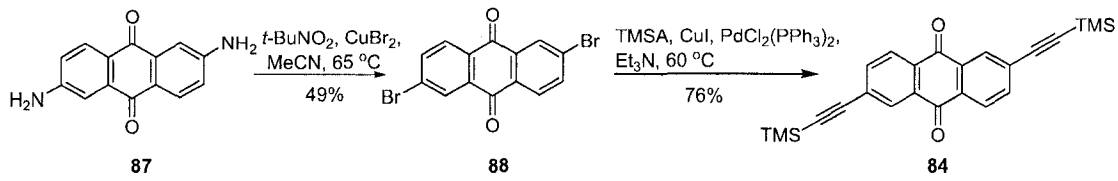

Scheme 2.2 Synthesis of 2,6-bis(trimethylsilyl ethynyl) anthraquinone **84**.

In the subsequent reaction, crude dibromide **88** was subjected to a Sonagashira coupling reaction with trimethylsilylacetylene (TMSA) to afford 2,6-bis(trimethylsilyl-ethynyl)anthraquinone **84**. At first, DBU/toluene was used as the base and the solvent, in consideration of better solubility of starting material **88** in aromatic solvents. However, a number of attempts using this condition consistently gave a similar low yield around 25%.

Therefore, the reaction condition was altered by using pure Et_3N as both the base and solvent, since there had been numerous successful examples of using Et_3N to achieve reasonable yields for bromide-involved Sonogashira coupling reactions. Indeed, the yield was dramatically improved to 76% under these conditions. Moreover, chromatographic purification was not necessary for this reaction, because most of the product precipitated out as a nice crystalline solid from CH_2Cl_2 when the reaction mixture was cooled with an ice bath.

2.2.1.2 Synthesis of *S*-Decyl Phosphonate 85a and *S*-Methyl Phosphonate 85b

Subsequent to the synthesis of **84**, the complementary starting materials for the next HWE reaction, phosphonates **85a-b**, were prepared following the procedures established by Bryce and co-workers with slight modifications.[11,59] In the beginning, an *S*-decyl phosphonate **85a** was chosen because the long *n*-decyl side chain was expected to impart good solubility to the final product which would contain two C_{60} cages. The synthetic details of compound **85a** are outlined in Scheme 2.3. First, reaction of Na with CS_2 followed by Zn chelation gave zinc dithiolate salt **89**. Surprisingly, although it was cautioned in the literature that the dithiolate was unstable and the reaction required a slow addition over several hours and stirring overnight in an ice bath,[27,60] an excellent yield (88%) of the dithiolate complex **89** was achieved in the synthesis following the procedure by Steimecke.[26] The mechanism of the reduction of CS_2 by Na involves a radical reaction as described in Section 1.1.3, and the reaction took place smoothly in refluxing DMF. The dithiolate intermediate formed was stabilized by chelation with Zn^{2+}, and the product **89** precipitated out as a stable red-color tetraethylammonium salt.

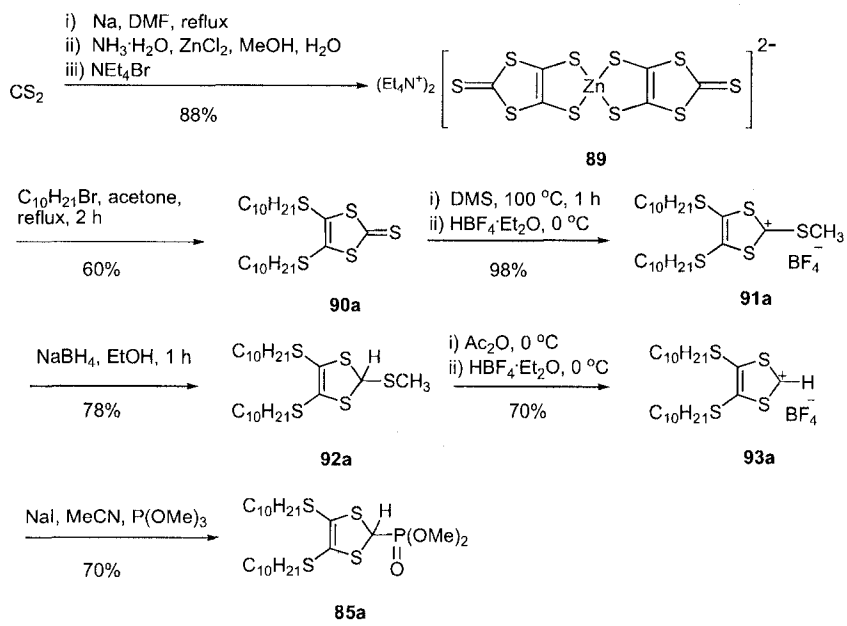

Scheme 2.3 Synthesis of *S*-decyl phosphonate **85a**.

Compound **89** was then refluxed in acetone to liberate free dithiolate from complexation, which immediately reacted with an alkylating reagent $C_{10}H_{21}Br$ to afford thione **90a**. Thione **90a** was obtained as a crystalline solid by addition of MeCN to the concentrated solution of reaction mixture in an ice bath.[61] This was an unexpected result because thione **90a** possessed good solubility in acetone or MeCN due to the solubilizing *n*-decyl chains attachment. Moreover, while other polar solvents such as methanol, ethanol, and H_2O were added to the reaction mixture, the mixture became cloudy but no crystalline product was formed.

The initial attempts to carry on the synthesis towards compounds **91a-93a** and eventually product **85a** were not successful due to the high solubility and instability of the salts **91a** and **93a** which made purification via recrystallization extremely difficult. To avert these drawbacks, we then diverted to the preparation of *S*-methyl phosphonate **85b**,

which turned out to be much easier to be prepared in relatively large quantity. The recent efforts on the preparation of **85a** have resulted in good yields and high purity under much more carefully controlled conditions.

Thione **90a** was alkylated with dimethyl sulfate (DMS) at 100 °C. Higher temperature (120 °C) or longer reaction time (3 h) resulted in a complex mixture of products. After addition of HBF_4, the mixture was placed in a fridge and product **91a** precipitated out as a yellow salt. A crystallization temperature below 0 °C was essential for high yield in this step because the product is soluble in diethyl ether to some degree at room temperature. Salt **91a** is sensitive to moisture; therefore, the filtration must be performed as quickly as possible.

The next step was reduction of salt **91a** to thiol **92a** by $NaBH_4$. The newly formed thiol **92a** was a liquid, but solidified after it was stored in a fridge overnight. Applying an excess amount of $NaBH_4$ or prolonged reaction time (1 day) did not cause any problem with the reaction. Thiol **92a** was reasonably stable and could be stored in a fridge for more than 2 months without significant decomposition.

Reacting **92a** with Ac_2O, followed by addition of HBF_4, yielded salt **93a** as a pale yellow precipitate. This salt, like **91a**, was moisture sensitive. So a swift filtration step was necessitated. Because **91a** dissolved well in diethyl ether (the solvent for recrystallization) at room temperature, freezing condition was applied to ensure satisfactory precipitation, and cooled diethyl ether was used for rinsing.

The conversion of salt **93a** to its phosphonate derivative **95a** was conducted by treatment with NaI and sequential addition of $P(OMe)_3$. In most cases, phosphonate **95a** obtained after general workup was pure enough for further reaction. Otherwise, it could

be further purified via a short silica plug using EtOAc/hexane as the eluent. Newly formed phosphonate **95a** was a liquid but solidified at freezing temperatures. This compound could be stored in a fridge more than half a year without significant decomposition.

At this point, it is worth commenting on some interesting observations during the attempted recrystallization of salt **91a** following the procedure reported in Ref. 59. When a polar solvent, methanol or ethanol, was added, salt **91a** slowly dissolved. TLC of the solution showed a new spot formed, with the same Rf value as that of **92a**, along with the disappearance of **91a**, which used to appear as a spot on the baseline. This indicated some unwanted reaction(s) took place. Evaporation of the solution afforded **91a**, which suggested the transformation was reversible. Treatment of the solution with $NaBH_4$ resulted in a liquid with the same appearance as **92a**. However, further reaction of this liquid with Ac_2O and HBF_4 afforded an unidentified white salt (insoluble in diethyl ether) instead of **93a**. No firm conclusion could be drawn at the present time with the current experimental evidence. However, further mechanistic study is warranted.

Using the same synthetic strategy as **85a**, *S*-methyl phosphonate **85b** was prepared as illustrated in Scheme 2.4. First, treatment of dithiolate **89** with MeI in refluxing acetone afforded *S*-methyl thione **90b**, which was purified by recrystallization from MeOH under N_2 protection. Addition of MeCN to the reaction mixture did not induce precipitation. The following alkylation of thinoe **90b** was achieved by heating **90b** in neat DMS. The resulting salt **91b** precipitated out from the reaction mixture upon the addition of diethyl ether. Reduction of **91b** by $NaBH_4$ yielded **92b** as a crystalline solid after general workup, which was smoothly converted to phosphonate **85b** under the same

conditions as the preparation of *S*-decyl phosphonate **85a**. Notably, the two salts **91b** and **93b** were much more stable than their decyl analogues.

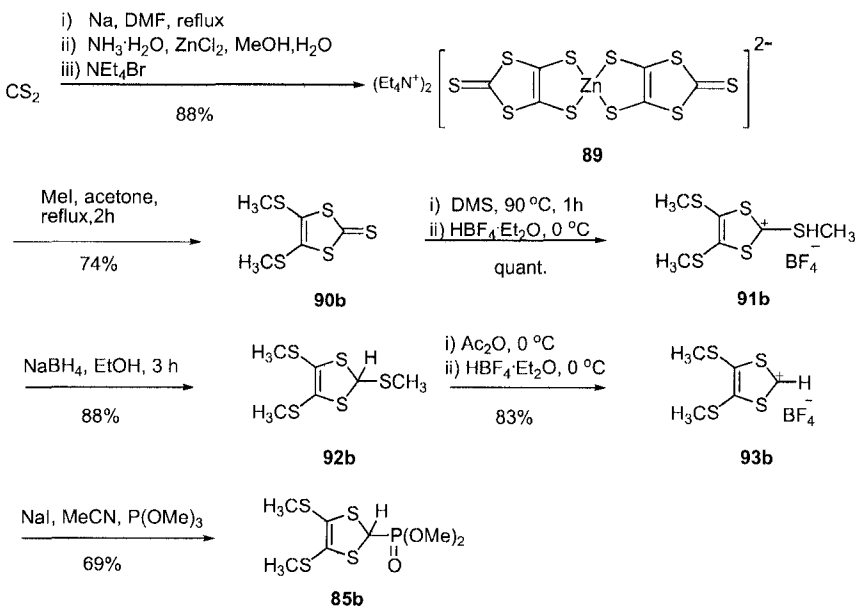

Scheme 2.4 Synthesis of S-methyl phosphonate **85b**.

2.2.1.3 Synthesis of TTFAQ 94

The preparation of TTAFQ **94** was accomplished using an HWE reaction between anthraquinone **84** and phosphonate **85b** in the presence of *n*-BuLi as the base (Scheme 2.5).[59,62] Interestingly, in the first several attempts, a mono olefination product **95** was persistently obtained in 23% yield along with product **94** in 54% yield. Later on, when a new batch of base was used, the yield of **94** was dramatically increased up to 88%, while the yield of **95** was significantly reduced. The formation of **95** in the early synthetic experiments was ascribed to an uncalibrated base concentration then in use. The newly formed **94** was orange in color and quickly turned into reddish orange under exposure to

air. Dissolving the reddish orange **94** in CH_2Cl_2 followed by evaporation of the solvent gave orange color back for the resulting **94**. Single crystals of **94** suitable for X-ray analysis were grown by slow diffusion of MeOH into its CH_2Cl_2 solution followed by moderate evaporation at low temperatures.

Compound **95** was a stable reddish crystalline solid. In contrast, pure compound **94** slowly decomposed under air, and compound **95** was found in the residue. Similar decompositions were also found in its phenyleneethynylene derivatives. This type of transformation has not been previously reported. However, unique reactivity of TTF was reported by Wudl[63] where TTF and *o*-chloranil formed the cycloadduct **D** (shown in Scheme 2.6). Reduction of **D** gave TTF by reduction. Similar chemistry may be occurring in the TTFAQ **95** system described above.

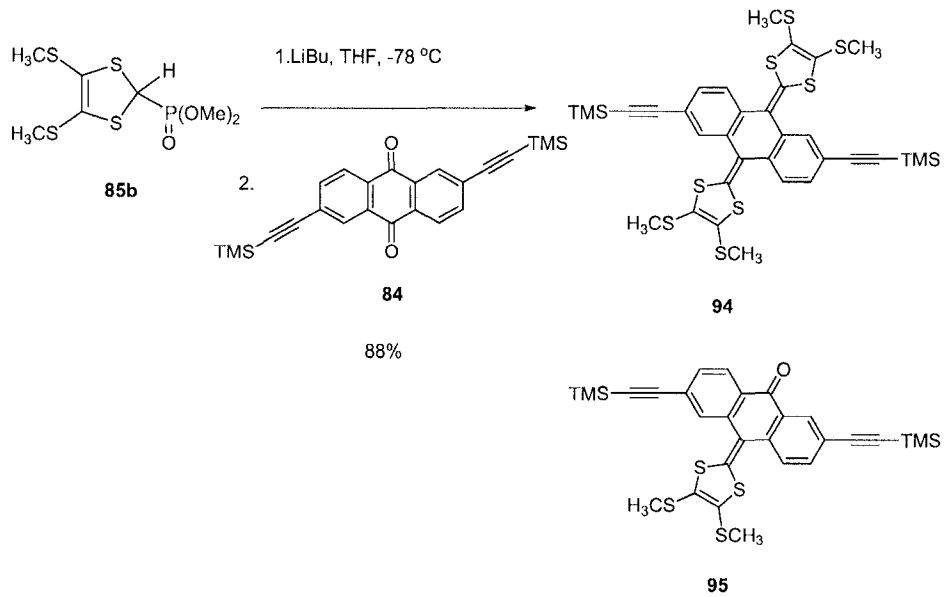

Scheme 2.5 Synthetic route for TTFAQ **94**.

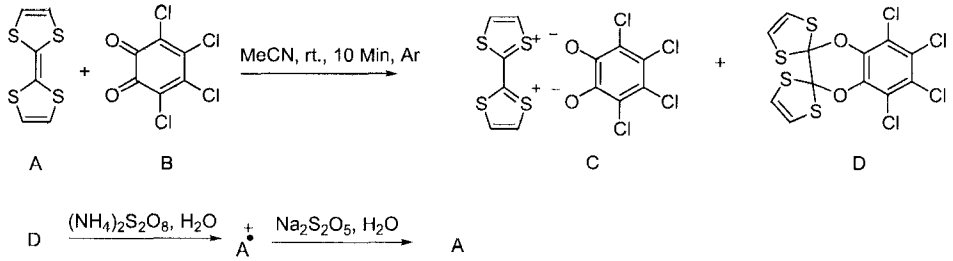

Scheme 2.6 A cycloaddition reaction between TTF and *o*-chloranil.

Very likely O_2 plays an important role in the conversion of **94** to **95**. TTFAQ can be photoexcited to ^{1}TTFAQ* by absorbing at certain wavelengths of visible light. ^{1}TTFAQ* can undergo intersystem crossing to afford ^{3}TTFAQ*, which may sensitize the ground state O_2 via energy transfer to yield more reactive singlet $^1O_2^*$. The energetic $^1O_2^*$ in principle should be capable of oxidizing the reductive double bond on TTFAQ to form a [2 + 2] cycloaddition intermediate, which could convert to **95** via a four-membered ring opening reaction (see Scheme 2.7). Another possible mechanism for the cycloaddition intermediate could be a single electron transfer to form $[TTFAQ]^{+\bullet}$ under air followed by cycloaddition of the radical cation with O_2.[64] Overall, the thermodynamic stabilities of the ketone and thione products make the decomposition pathway thermodynamically downhill.

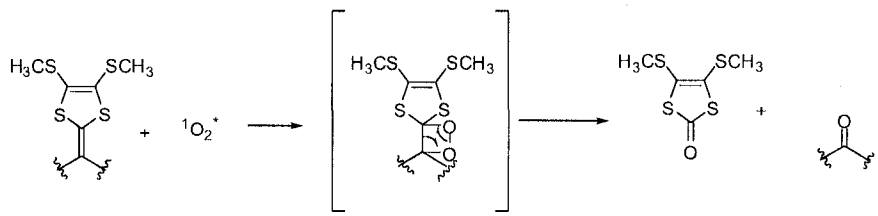

Scheme 2.7 Proposed mechanism for decomposition of TTFAQ.

2.2.1.4 Synthesis of Arylacetylene Iodide 86

In order to improve the solubility of the C_{60}-TTFAQ-C_{60} triad, a solubility-assisting conjugated unit, bis(decyloxy)arylacetylene, was planned to be incorporated in the conjugated backbone of the molecule. An essential building block for such a molecular structure is the aryacetylene iodide **86**, the synthesis of which was according to known procedures[65] and is described in Scheme 2.8. Alkylation of hydroquinone, followed by iodination and Sonagashira coupling, easily furnished the desired compound **86** in satisfactory yield.

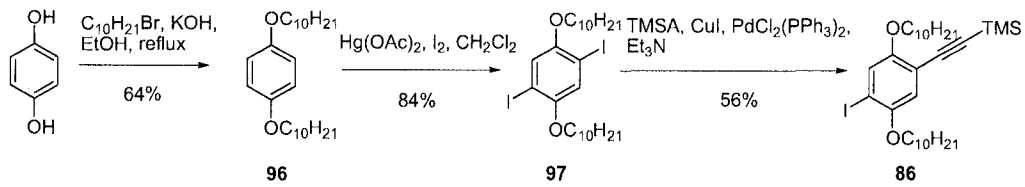

Scheme 2.8 Synthesis of arylacetylene iodide **86**

2.2.1.5 Synthesis of C_{60}-TTFAQ-C_{60} 83

With all necessary precursors available, the synthesis of dumbbell-shaped C_{60}-TTFAQ-C_{60} triads could be completed. Bis(trimethylsilyl) protected TTFAQ **94** was first desilylated by K_2CO_3 or TBAF to give terminal dialkyne **98** (Scheme 2.9). Although in most cases the deprotection went on smoothly on a small (tens of milligrams) scale, a low yield of 20% was obtained when the deprotection reaction was scaled up to the gram scale using K_2CO_3. Since the only notable difference was the quantity, and the deprotection with TBAF on the gram scale was successful, it was reasoned that the instability or unknown reactivity of the terminal alkyne product in the presence of K_2CO_3 was

responsible for the reduced yield. Cooling of a hot concentrated CH_2Cl_2/hexane solution of **98** yielded a crystalline product, which showed different appearance than its TMS protected precursor **94**.

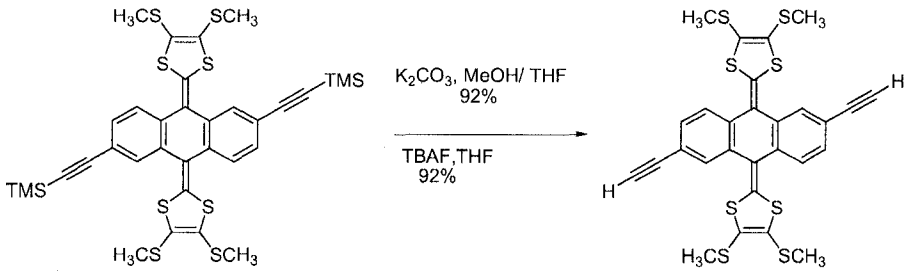

94 **98**

Scheme 2.9 Deprotection of TTFAQ **94**.

From dialkyne **98**, it should have been very straightforward to synthesize the desired bis(fullerenyl)-endcapped product, the C_{60}-TTFAQ-C_{60} triad. Our initial attempt was focused on connecting two C_{60} cages directly to the TTFAQ core via an *in situ* alkynlation as shown in Scheme 2.10. But this reaction was not successful. The mixture of C_{60} and **98** in THF was sonicated for 4 h in order to form a good suspension of C_{60} and **98** (C_{60} has very limited solubility in THF). Then a strong base, lithium hexamethyldisylizide (LHMDS), was added to generate the alkynylide anion *in situ*, which is a good nucleophile to attack the C_{60} cage. After 0.5 h, the reaction was quenched by TFA. General workup followed by chromatographic separation did not give any desired product bisfullerene **97**. Surprisingly, besides the recovery of **98**, a significant amount of **94** was isolated from the reaction mixture. The molecular structure of recovered **94** was confirmed by MALDI-TOF MS and ^{1}H-NMR spectroscopy. An

investigation was undertaken to identify the reasons for the observations described above. First, the solution of **98** was sonicated for 1 h, and TLC analysis showed no new product was formed at this stage. At this stage, LHMDS was added slowly to the reaction solution. After stirring for 0.5 h, TLC analysis showed roughly half of the amount of **98** had been converted into **94**. Notably, no mono-silylated product was observed. The failure of converting **98** to triad **99** can be tentatively ascribed to the extremely low solubility of **99** that retards the desired reaction as well as the competitive side reaction of silylation of **98** with LHMDS which yielded **94**. Further attempts to synthesize triad **99** were abandoned and later synthetic efforts were directed at the more soluble target compound **83**.

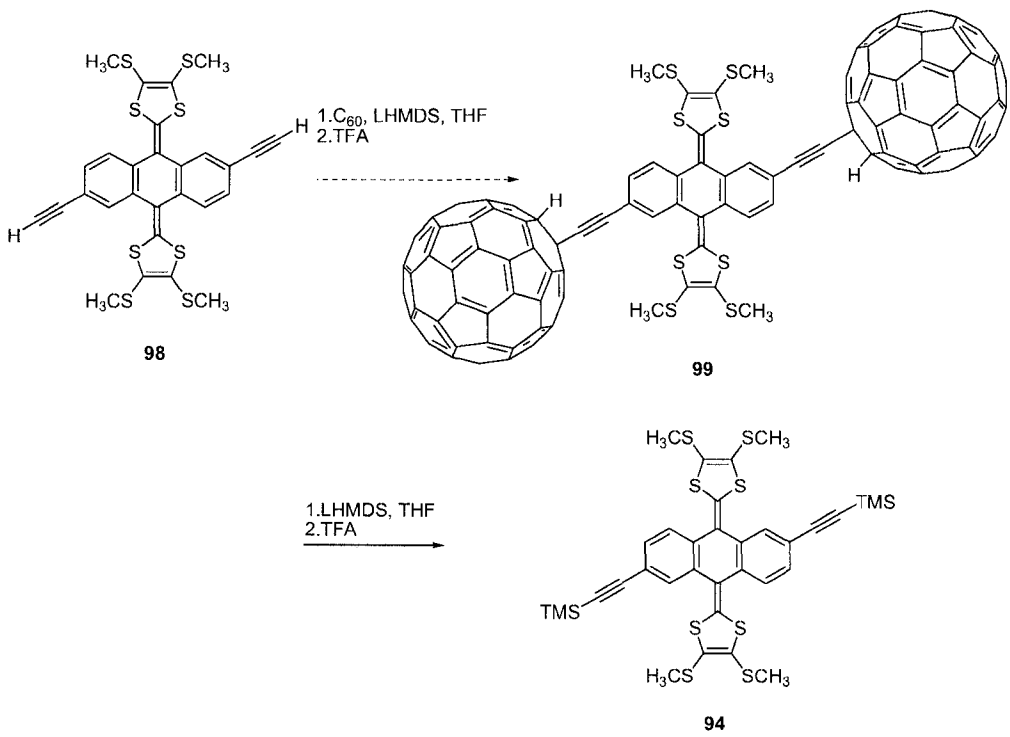

Scheme 2.10 Attempted synthesis of C_{60}-TTFAQ triad **99**.

The new synthetic target **83** (Scheme 2.1) requires one additional Sonogashira

coupling. As shown in Scheme 2.11, Sonagashira reaction of **98** and **86** furnished compound **100** in 50% yield, as well as the unanticipated TTFAQ dimer **101** in 20% yield. Although decompositions of **100** and **101** to their TTFAQ precursor (see Scheme 2.7) were observed at room temperature under an air atmosphere, they were seen to be more stable. The coupling reaction was performed under a number of different conditions, however, the yield of **101** was not improved, with the yield ratio of **101** to **98** remained relatively constant. This observation seeded the idea of constructing the butadiynylene structure via a one-pot Sonagashira reaction. Details of experiments and theoretical kinetics modeling will be discussed in Section 3.2.

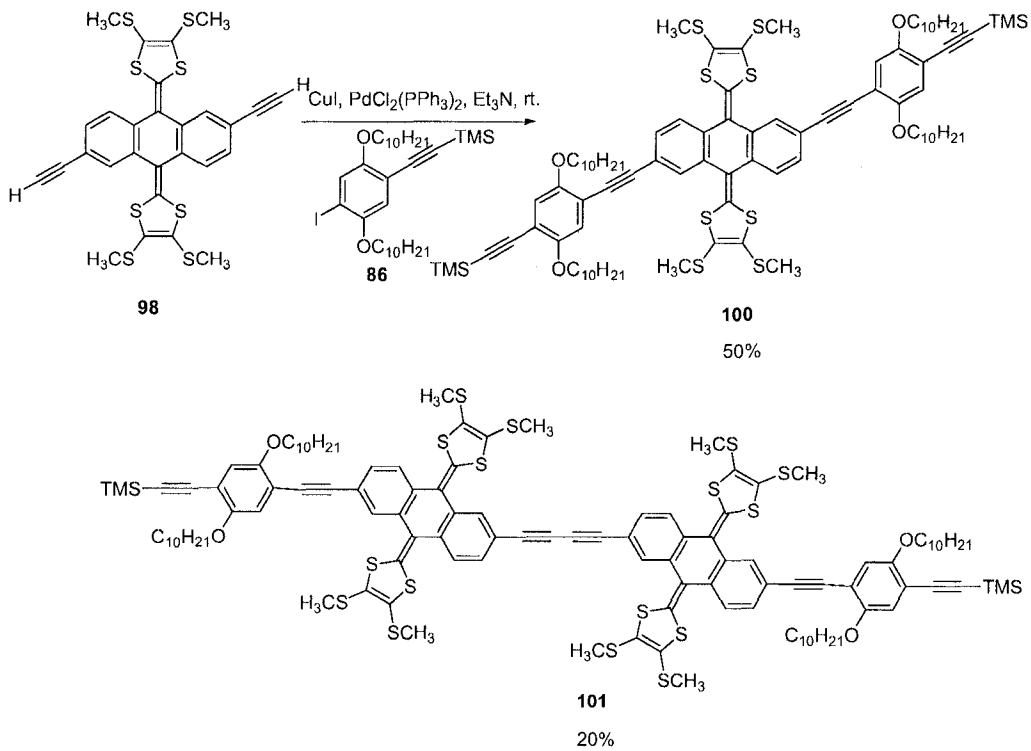

Scheme 2.11 Sonagashira reaction between TTFAQ **98** and arylethynyleneiodide **86**.

The acquisition of both **100** and **101** provided two useful precursors to bis(fullerenyl) dumbbell-shaped molecules. The deprotection of **100** was easily performed with K_2CO_3 and further reaction with C_{60} via the *in situ* ethynylation protocol successfully gave the bis(fullerenyl) triad **83** in 25% yield (Scheme 2.12). The yield was moderate in comparison to other known fullerene ethynylation reactions probably due to the multifunctionalization of C_{60} and the instability of product under the acidic condition during workup. The crude product obtained after workup completely decomposed within 12 h, if silica column purification was not immediately performed. The column purified product was much more stable and was stored in the freezer for more than half a year albeit with mild degradation. The major decomposed product was separated and MALDI-TOF MS analysis suggested that one heterocyclic ring in the TTFAQ moiety was replaced by an oxygen atom, which was in line with the previously proposed TTFAQ decomposition mechanism (see Scheme 2.7). Since the $^3C_{60}$* base excited state is known to generate $^1O_2$*, it was not surprising that the crude reaction mixture accelerated the decomposition of the bis(fullereneyl)-TTFAQ product.

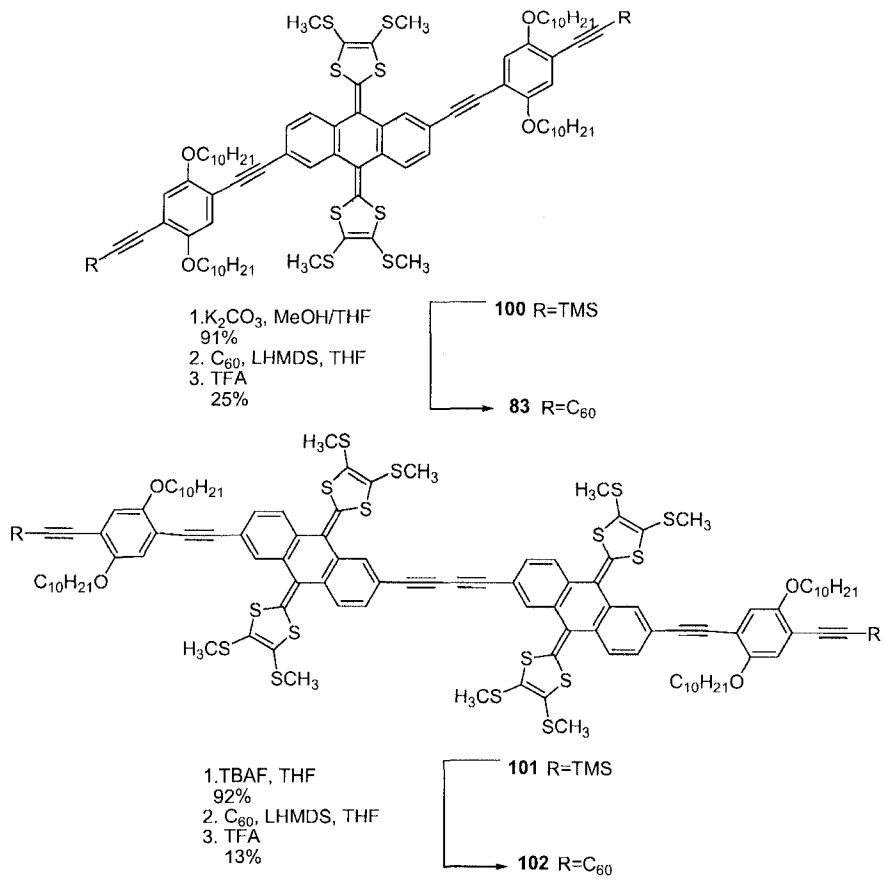

Scheme 2.12 Synthesis of C_{60}-TTFAQ-C_{60} triad **83** and C_{60}-TTFAQ-TTFAQ-C_{60} tetrad **102**.

The tetrad **102** was prepared following the route given in Scheme 2.12. Removal of TMS groups was accomplished with TBAF instead of K_2CO_3, due to the hypothesized instability of TTFAQ towards K_2CO_3. The resulting terminal dialkyne was attached to C_{60} subsequently in the presence of LHMDS, affording **102** in a yield of 13%. The low yield of **102** was not surprisingly given the much larger TTFAQ-dimer core involved. The small yield of **102** precluded the acquisition of meaningful ^{13}C-NMR spectrum. However, ^{1}H-NMR and MALDI-TOF MS of **102** are consistent with the proposed structure.

2.2.1.6 Electronic and Electrochemical Properties

The unique 2,6-bis(ethynylated)-TTFAQ core together with the rich π-electron delocalization on C_{60} should render the relevant TTFAQ derivatives appealing electronic and redox properties that may be eventually useful in the design of molecular nanodevices. Therefore, the electronic properties of compound **94**, **95**, **100**, **101**, and **83** were investigated by UV-vis and fluorescence spectroscopy, and detailed redox behavior for each of them was examined by cyclic voltammetry (CV).[66]

In the UV-Vis spectra (as shown in Figure 2.1), the longest maximum absorption wavelength (λ_{max}) that corresponds to the electronic transition from HOMO to LUMO was observed to redshift slightly among compounds **83**, **94**, **100**, and **101**, a trend in line with the increasing conjugation length along the dialkyne-anthrancene direction. This indicates that conjugation length actually dominates the HOMO-LUMO gap in these compounds. A dramatic redshift can be seen in compound **95**, whose conjugation length was similar to **94**. Obviously, in this case, the electron push-and-pull effect caused by the ketone (electron acceptor) and the dithiole ring (electron donor) comes into play. The shape of the absorption curve of dimer **101** was almost identical to that of **100** in the low-energy region of the spectrum, suggesting no significant electronic interactions between the two TTFAQ cores. A weak absorption band centered at 701 nm in the spectrum of compound **83** was also observable, which is the characteristic absorption commonly seen for functionalized C_{60} derivatives.

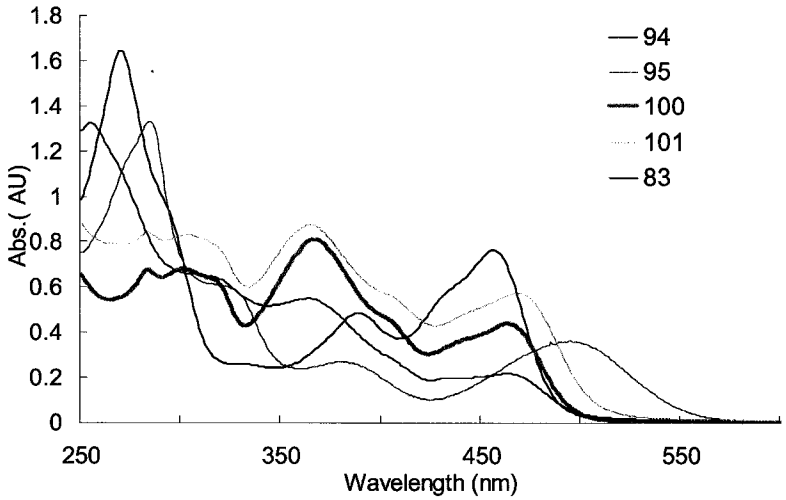

Figure 2.1 UV-vis spectra of compounds **94**, **95**, **100**, **101**, and **83**.

Electronic emission behavior of compounds **83**, **94**, **95**, **100**, and **101** was investigated by fluorescence spectroscopy in degassed $CHCl_3$ solutions at an excitation wavelength of 380 nm. In Figure 2.2, a redshift pattern for the longest maximum emission wavelength similar to that of the UV-vis spectra can be observed. Notably, dimer **101** behaves differently from **100** in the high-energy emission region by splitting the emission band around 450 nm. In stark contrast to the others, the emission in C_{60}-TTFAQ-C_{60} triad **83** was considerably quenched. The quenching was presumably due to rapid intramolecular photoinduced electron/energy transfer after vertical photoexcitation. In addition, a relative weak emission band at 709 nm was discernible, which was assigned to the well known 0*-0 transition of triplet C_{60}*, indicating a significant intersystem crossing (ISC) process on the C_{60} cage. This emission wavelength is nearly identical to the C_{60} band in the absorption spectrum of triad **83**, which signifies a very small reorganization energy (λ) of the functionalized C_{60} group.

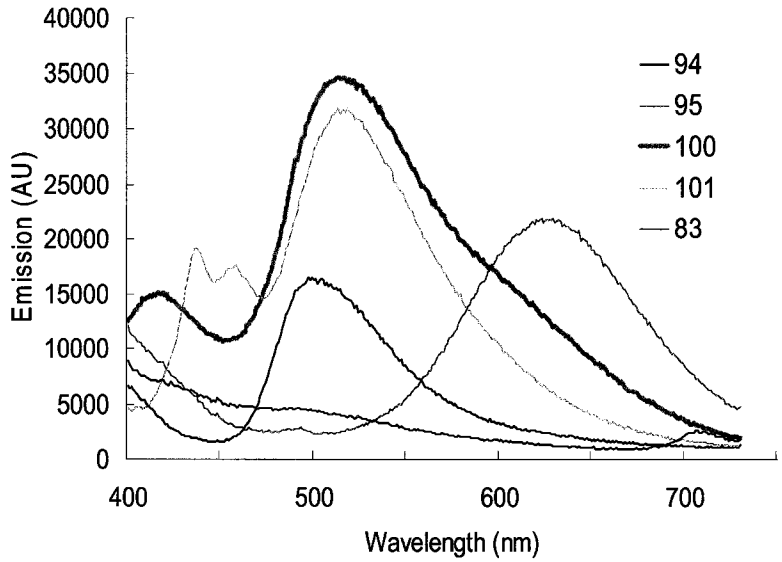

Figure 2.2 Fluorescence spectra of compounds **94**, **95**, **100**, **101**, and **83**. Spectra measured in degassed $CHCl_3$, excitation wavelength at 380 nm.

Besides the interesting electronic properties, the above TTFAQ derivatives were also expected to show a wealth of electrochemical properties due to the remarkable redox properties of the TTFAQ unit. Prior to this work, the effects of various electroactive groups on TTFAQ through 2,6-diethynylene conjugation were not known. In order to better understand their electrochemical properties, cyclic voltammetric experiments were carried out on compounds **83**, **94**, **95**, **100**, and **101**. In the cyclic voltammograms, all these compounds showed amphoteric redox behavior and detailed data are given in Table 2.1 (also see selected CVs in appendix). In the positive potential region, compound **94**, **100**, **101** and **83** exhibit a similar reversible or quasi-reversible oxidation wave pair in the region of 0.44-0.54 V, which is assigned to the simultaneous two-electron oxidation process of the TTFAQ unit. The large shift of the first oxidation potential in **83**, compared with those in **94**, **100** and **101**, suggests that there are detectable electronic interactions

between C_{60} and the TTFAQ unit. The high $E_{1/2ox}$ value of **95** corresponds to its weaker electron donor ability than other TTFAQ derivatives as one dithiole ring was replaced by an electron withdrawing C=O group. In the negative potential region, compounds **94** and **100** show noticeable irreversible reduction potentials; however, their origins cannot be clearly assigned. For compound **83**, the two C_{60} fragments give rise to four reduction waves. That no peak splitting was observed on these reduction waves clearly indicates no significant electronic communication between the two C_{60} fragments in this dumbbell-shaped triad. This observation is in accord with the electrochemical data of other reported C_{60}-oligomer-C_{60} systems.

Table 2.1 Results of cyclic voltammetric experiments for **94**, **95**, **100**, **101** and **83**.[a]

Entry	$E_{1/2ox}$(V)	$E_{1/2red1}$(V)	$E_{1/2red2}$(V)	$E_{1/2red3}$(V)	$E_{1/2red4}$(V)
94[c]	+0.44	-1.84[b]			
95[c]	+0.98	-1.21	-1.48	-1.93[b]	
100[c]	+0.45	-1.79[b]			
101[c]	+0.46	-1.64[c]			
83[d]	+0.54	-0.6[b]	-0.92	-1.32	-1.92

[a]Cyclic voltammograms were recorded in Bu_4NBF_4 (0.1 M) solution as the supporting electrolyte. Glassy carbon as the working electrode and platinum wire as the counter electrode. Potentials are given in volts versus a Ag/AgCl reference electrode. Scan rate: 100 $mV \cdot S^{-1}$. For chemically reversible process, half wave potentials ($E_{1/2}$) are caculated as averages of oxidation and reduction peak potentials.

[b]For irreversible processes, oxidation or reduction peak potentials are reported as $E_{1/2}$.

[c]Solvent: CH_2Cl_2/MeCN (4:1)

[d]Solvent: *o*-dichlorobenzene/CH_2Cl_2 (4:1)

[e]Not clearly observed.

The HOMO-LUMO gaps of the compounds were characterized with both electrochemical and optical absorption analyses. The data are summarized in Table 2.2. In most cases, the optical bandgaps are larger than the electrochemical bandgaps with the exception of compound **95**. Notably, a narrow electrochemical gap of 1.14 eV was characterized for compound **83**. Such a small badgap could render this molecule useful in such fields as organic semiconducting and optoelectronic devices.

Table 2.2 Summary of HOMO-LUMO gaps for compounds **94**, **95**, **100**, **101** and **83**.

Entry	Abs. λ_{max} (nm)	Em. λ_{max} (nm)	$E_g(1)$ (eV)	$E_g(2)$ (eV)
94	456, 388, 294 (sh)	501	2.53	2.28
95	495, 382, 324(sh)	629	2.19	2.19
100	465, 367, 301	517, 420	2.48	2.24
101	468, 408(sh), 364	517, 458, 437	2.43	2.1
83	701, 469, 435, 367, 311(sh)	709, 492	1.74	1.14

[a]Optical bandgap calculated by the absorption wavelength at the cross point of a tangential line passing through the turning point of the lowest energy absorption peak and the *x*-axis of the UV-vis spectrum.

[b]Bandgap calculated based on CV results. $E_g(2) = E_{1/2ox} - E_{1/2red1}$.

2.2.2 Synthesis and Characterization of TTFAQ Base D-A Systems

2.2.2.1 Synthesis and Cyclic Voltammetric Properties of TTFAQ Base D-A Molecules

Diethynylated TTFAQ **98** also serves a versatile building block for the construction of a series of TTFAQ based D-A systems. Such novel D-A systems could be useful in probing relevant substituent effects on the electronic and redox properties of the central TTFAQ unit, and eventually they would allow clear structure-property relationship to be established.

With the terminal dialkyne groups in **98**, further derivatization with various D/A groups can be readily performed via the Sonogashira coupling reaction. In this work, a series of *para*-electron withdrawing group substituted phenyl rings were employed in synthesizing various TTFAQ based D-A systems. Scheme 2.13 outlines the general Sonogashira protocol for the synthesis of compounds **103a-d**. Notable in these coupling reactions is that no homocoupled dimers was observed, in contrast to their

phenyleneethynylene analogue (Scheme 2.12) discussed previously. The results suggest that more rapidly occurred cross-coupling in these reactions effectively competes with the homo-coupling side reaction when electron-withdrawing groups are present in the aryl halides. The high yield in **103c** might result from the excellent iodo leaving group. In contrast, 4-bromobenzaldehyde, although having a strong electron withdrawing aldehyde group at the *para*-position to Br, did not react with TTFAQ under the same reaction conditions.

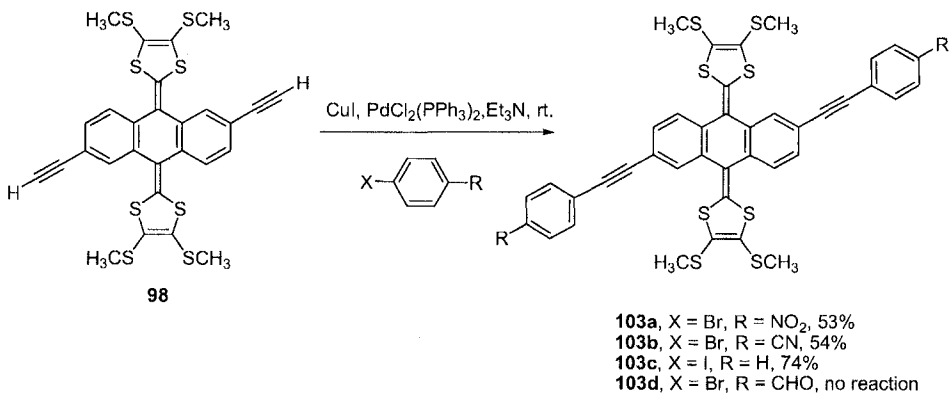

Scheme 2.13 Synthesis of TTFAQ base D-A molecules **103a-d** by the Sonagashira reaction.

The electrochemical redox properties of compound **103a-c** were characterized by cyclic voltammetry experiments. As shown in Table 2.3, all three compound exhibit reversible or quasi-reversible oxidation waves in the positive potential region of 0.49-0.56 V, which were assigned as the simultaneous two-electron oxidation processes occurring on the TTFAQ units. In contrast to **103b** and **103c** which showed two irreversible reduction processes in the high negative potential region, **103a** displayed an extra quasi-reversible reduction wave around –0.96 V, which was due to the presence of the two nitro groups.

The lowest electrochemical gap in this series was achieved in **103a** at 1.62 eV, which was in line with the strongest electron acceptor ability of the nitro group among the other substituents.

Table 2.3 Results of cyclic voltammetry for compounds **103a-c**.[a]

Entry	$E_{1/2ox}$	$E_{1/2red1}$	$E_{1/2red2}$	$E_{1/2red3}$	E_g[d] (eV)
103a	+0.56	-0.96	-1.56[c]	-1.93[b]	1.62
103b	+0.50	-1.68[b]	-1.81[b]		2.18
103c	+0.49	-1.81[b]	-1.96[b]		2.30

[a]Cyclic voltammograms were recorded in Bu_4NBF_4 (0.1 M) solution as the supporting electrolyte. Glassy carbon as the working electrode and platinum wire as the counter electrode. Potentials are given in volts versus a Ag/AgCl reference electrode. Scan rate: 100 $mV \cdot S^{-1}$. Solvent: CH_2Cl_2/MeCN 4:1. For chemical reversible process, half wave potentials ($E_{1/2}$) are calculated as averages of oxidation and reduction peak potentials.

[b]For irreversible processes, oxidation or reduction peak potentials are reported as $E_{1/2}$.

[c]Not clearly observed.

[d]Bandgap calculated based on CV results. $E_g(2) = E_{1/2ox} - E_{1/2red1}$.

2.2.2.2 X-ray Crystal Structure of TTFAQ 94

Crystals of **94** with quality suitable for single crystal X-ray diffraction analysis were obtained by slow diffusion of MeOH into a $CHCl_3$ solution at 4 °C over a period of several weeks. The ORTEP plots of **94** are given in Figure 2.3. In the crystal structure, each unit cell contains two molecules of **94**, both of which adopt a saddle-shaped molecular conformation as shown in Figure 2.1. Although significant disorder occurred at the terminal silyl groups, the TTFAQ central framework showed well-refined crystal structural data, which provides insightful information about the ethynylated TTFAQ unit in the solid state. The anthraquinone moiety is observed to be bent downwards about the C_7–C_9 axis, bearing a dihedral angle of *ca.* 146°, while the two dithiole rings bend upwards with a dihedral angle of *ca.* 114°. Moreover, each dithiole ring deviates from planarity by folding themselves inward by *ca.* 12° about the S–S axis. Overall, the crystal structure of **94** shows a consistent conformation of TTFAQ core with other similar TTFAQ structures reported in the literature.[19]

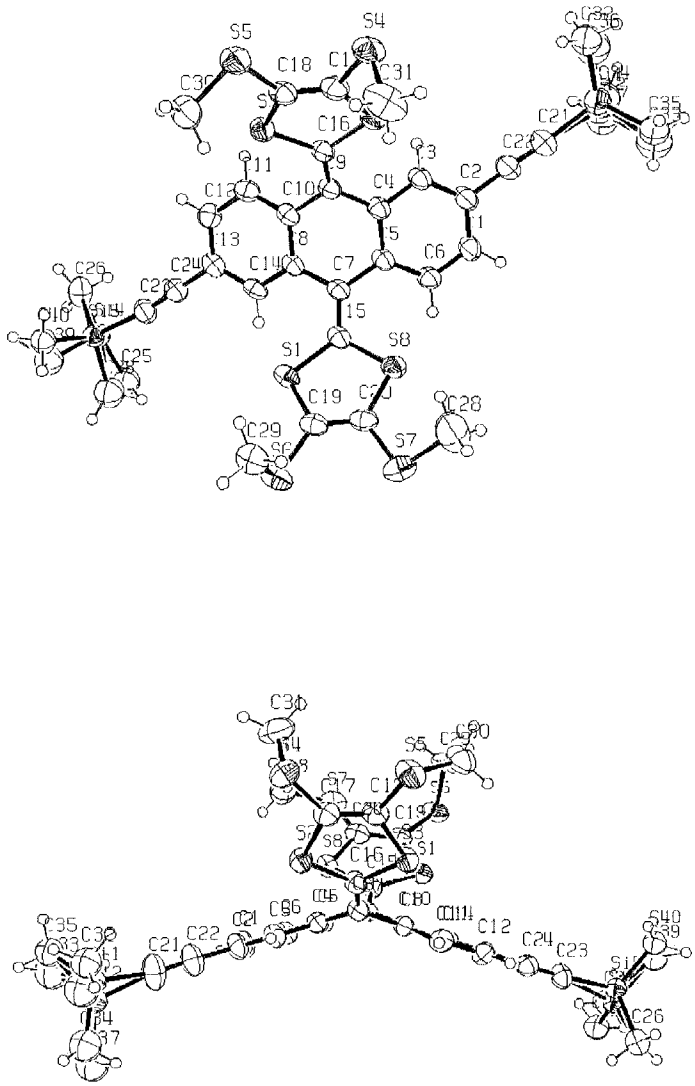

Figure 2.3 Single crystal structure of **94**: (top) Front view, (bottom) side view. Selected bond length (Å): C3-C4, 1.397(6); C4-C9, 1.464(6); C9-C16, 1.362(6); C16-S2, 1.759(4); S2-C17, 1.759(5); C17-C18, 1.333(7); C17-S4, 1.752(5). Selected bond angle (°): C9-C16-S2, 123.9(4); S3-C16-S2, 112.1(2); C16-S2-C17, 96.2(2); S2-C17-S4, 116.4(3); C18-C17-S2, 117.0(4); S2-C17-S4, 116.4(3); C17-S4-C31, 100.6(3).

2.2.2.3 Oxidative Titration of TTFAQ Based D-A Systems

The combination of π-electron accepting groups such as nitro and cyano to TTFAQ through conjugation was expected to exert significant influence on the electronic and spectroscopic properties of the central TTFAQ unit. Most likely, the ground state of the D-A systems would feature interesting intramolecular charge transfer characteristics; as a result, the electronic absorption properties of the molecules may be considerably altered in comparison to the unsubstituted TTFAQ parent structure. Indeed, as shown in Figure 2.4, the ground state TTFAQ **94** displays three maxima in the absorption band; the peaks at 456 and 389 nm were assigned to the electronic transition occurring at the dithiole rings, while the one at 268 nm was consistent with the absorption of the anthracene moiety. The elongation of conjugated structure in the alkyne-anthracene direction in compound **103a** and **103c** led to redshifts of the anthracene absorption band as well as dithiole ring absorptions. The absorption pattern of compound **103c** was similar to that of **84**. However, with strong electron withdrawing groups attached, compound **103a** showed very different absorption properties. Besides a broad dithiole ring absorption band from 370 to 470 nm, compound **103a** showed a long absorption tail extending to 570 nm.

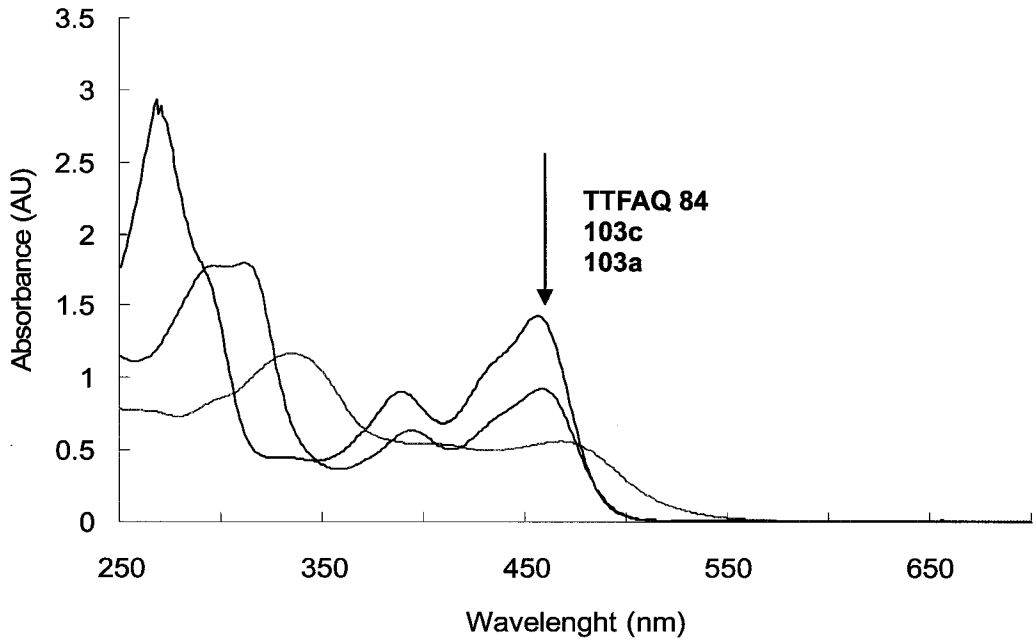

Figure 2.4 Steady state absorption spectra of TTFAQ derivatives **84**, **103a** and **103c**.

Another interesting property envisioned for these TTFAQ derivatives was their electrochemical spectroscopic behavior, in which the UV-Vis absorption would be dramatically changed in response to the oxidation states of the molecules. Revealing such properties will allow the detailed redox processes occurring in a particular D-A system to be well understood. Also determination of electronic absorptions of the oxidative species will benefit the assignment of various excited species in the future transient absorption spectroscopic study. Upon this consideration, a series of oxidative titration experiments was carried out to investigate the properties of the redox mechanisms for the TTFAQ-based molecules.[67] The chemical oxidant used was diacetoxyiodobenzene, with triflic acid being the counter ion.[68] One mole of oxidant would take 2 moles of electrons from the TTAFQ D-A molecules. As a consequence, it oxidizes the TTFAQ moiety into a

dicationic state (see Eq. 2.1).

$$PhI(AcO)_2 + 2CF_3SO_3H + TTFAQ \rightarrow TTFAQ^{2+}(CF_3SO_3^-)_2 + PhI + 2AcOH \quad (eq\ 2.1)$$

In the experiments, electronic absorption spectroscopic behavior of each of the D-A compounds was monitored by a UV-Vis spectrometer in the process of progressively titrating an oxidant solution into the solution of respective D-A compound at room temperature. Figures 2.5 and 2.6 show the absorption spectra of compound **94** (the parent unsubstituted TTFAQ) upon gradual chemical oxidation. The solvent used was spectroscopic grade $CHCl_3$. As we can see in Figure 2.5, the addition of oxidant led to steady decrease in the intensity of all three major absorption bands (268 nm assigned to non-planar anthracene; 456 and 389 nm assigned to neutral dithiole rings), as well as gradual increase in the intensity of two newly formed absorption bands (294 nm assigned to planar anthracene; 415 nm assigned to oxidized dithiole rings). Notably, the dicationic species formed on addition of 1 eq. of oxidant displayed a long absorption tail ended at *ca.* 570 nm. The isosbestic points indicated the oxidation was clean.

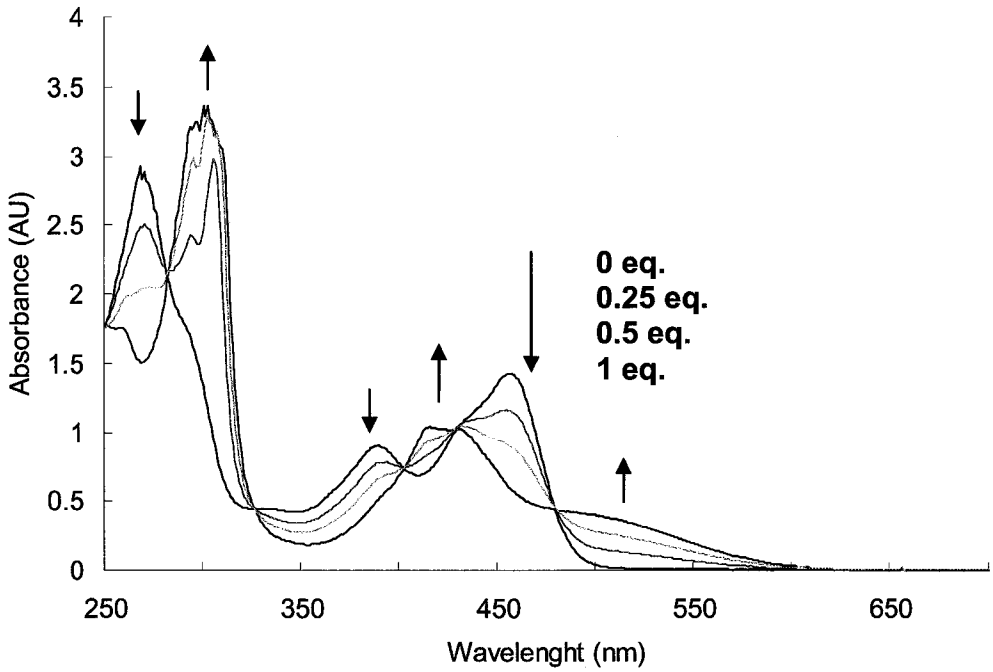

Figure 2.5 Selected UV-vis spectra of TTFAQ **94** upon addition with various equivalents of oxidant.

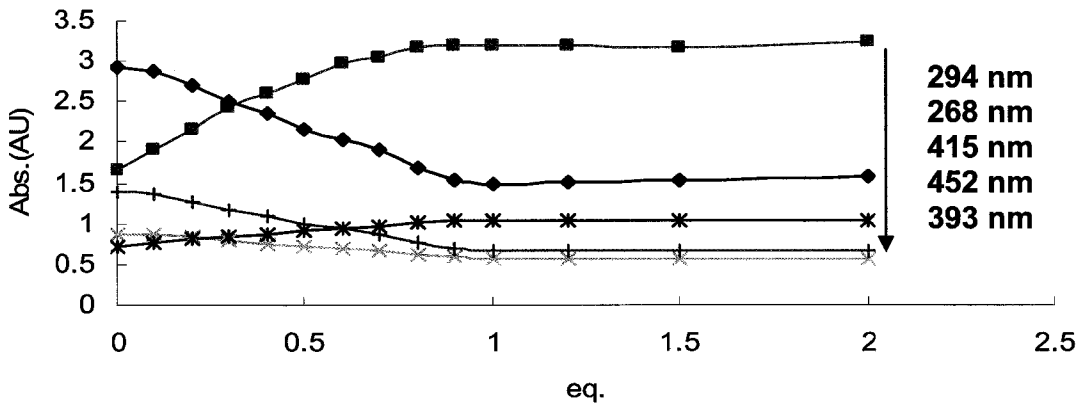

Figure 2.6 Trends of absorbance variation of TTFAQ **94** at certain wavelengthes upon oxidation.

Following a similar procedure, we performed the oxidative titration of **103a** and the UV-vis data are given in Figures 2.7 and 2.8. Upon oxidation, the intensity decrease in the neutral dithiole ring absorptions (471 nm and 405 nm) was accompanied by the intensity increase in the oxidized dithiole ring absorption band (433 nm). However, further addition of oxidant beyond 0.25 eq resulted in unexpected precipitation, and meaningful UV-Vis characterization turned out to be impossible. It was reasoned that the presence of nitro groups increased the polarity of the ionic oxidative species and thus decreased their solubility in nonpolar $CHCl_3$. If such were the case, the oxidized species should be more soluble in more polar solvent systems according to the "like-dissolves-like" paradigm.

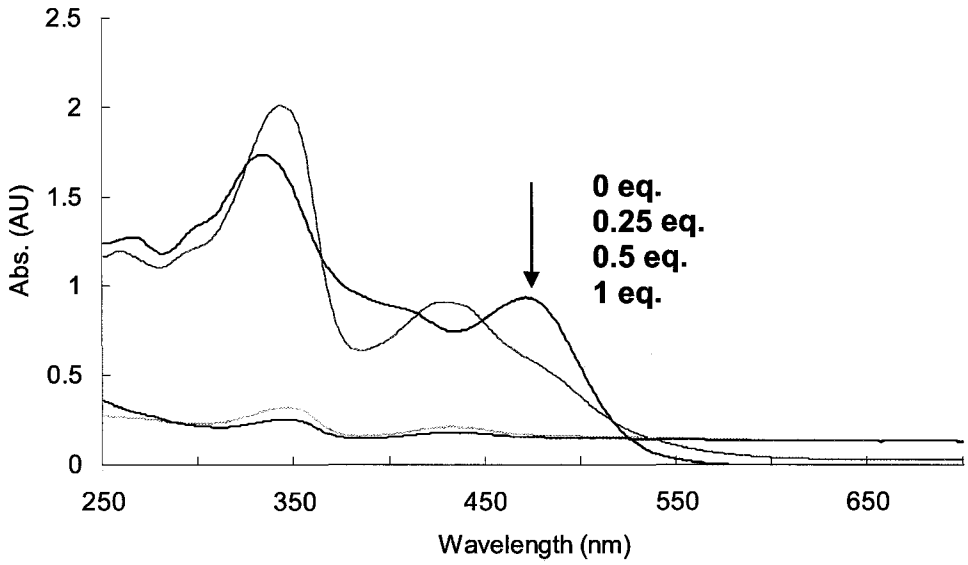

Figure 2.7 Selected UV-vis spectra of **103a** upon oxidation in $CHCl_3$.

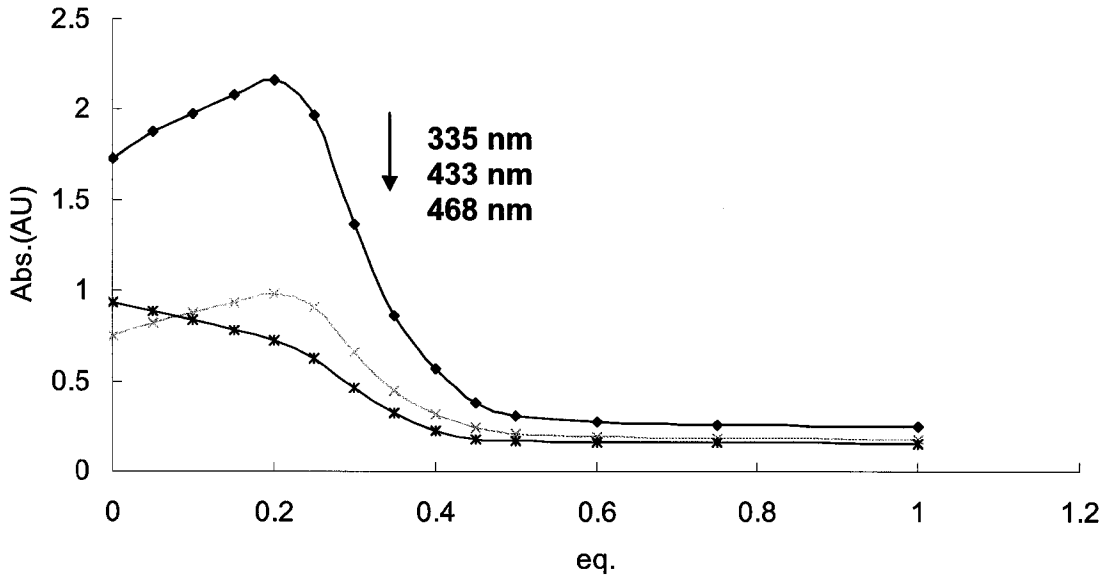

Figure 2.8 Trends of absorbance variation of **103a** at certain wavelength upon oxidation in $CHCl_3$.

Another oxidative titration of **103a** in 1:1 MeCN:$CHCl_3$ was attempted, because MeCN was supposed to be a good solvent for ionic salts. The change of solvent polarity caused a slight blueshift (by *ca.* 4 nm) in the absorption bands of the neutral molecule relative to the spectrum in $CHCl_3$. As shown in Figures 2.9 and 2.10, upon chemical oxidation a decrease in 468 nm (neutral dithiole ring absorption) and increases in 331 nm (anthracene) and 428 nm (dication) were clearly seen. The long absorption tail extending to 570 nm was characteristic of the dication species. The magnitude of intensity increase in the long absorption tail upon oxidation was much smaller than that of the TTFAQ **94**. Based on the observations that the neutral molecule of **103a** has an absorption tail in the same region as its dication species, and the absorption shape of neutral **103a** is similar to a hybrid of the absorptions of neutral and oxidized TTFAQ **94**, it is believed the existence of

electron withdrawing nitro group has a significant effect on the electron distribution of the neutral molecule, which may induce ground-state charge transfer. It was also notable that the intensity of absorption bands was saturated on addition 0.6 eq. of oxidant rather than 1.0 eq., the origin of which was unknown.

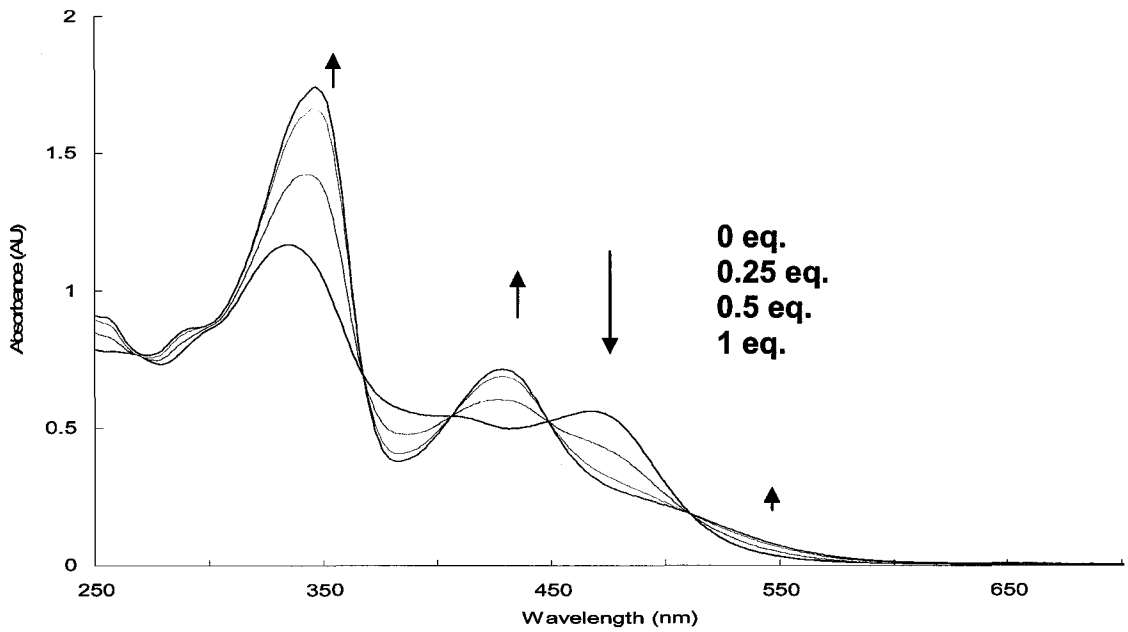

Figure 2.9 Selected UV-vis spectra of **103a** upon oxidation in 1:1 $CHCl_3$:MeCN.

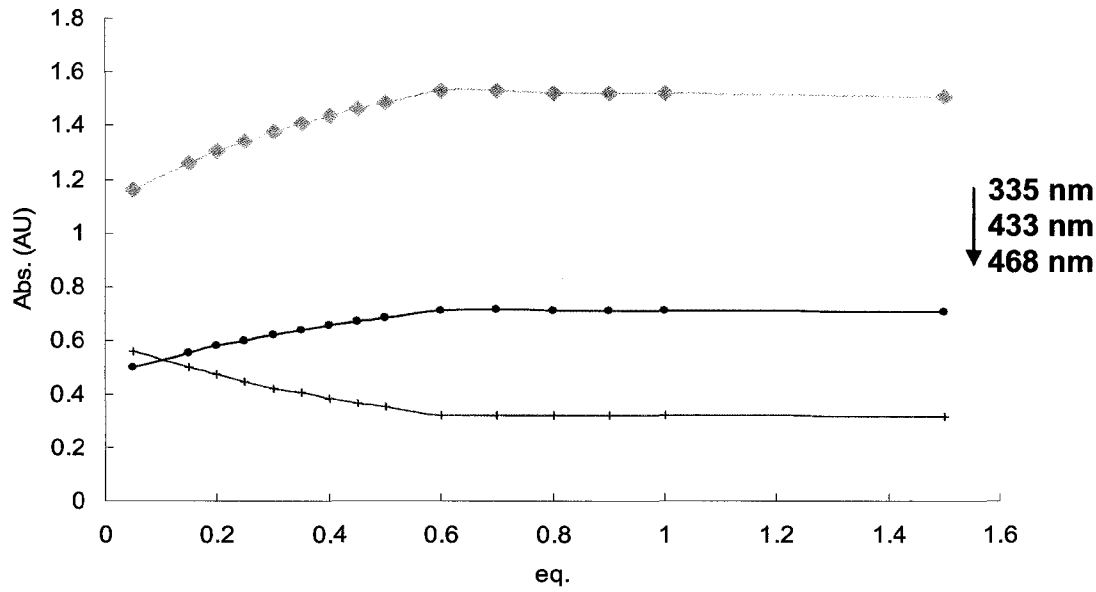

Figure 2.10 Absorptions alternation trends of **103a** at certain wavelengthes upon oxidation in 1:1 $CHCl_3$: MeCN.

The same experiment on **103c** was performed, which possesses a much longer conjugation path than TTFAQ **94** but no electron withdrawing group attached. From Figures 2.11 and 2.12 it can be seen that the absorption behavior of **103c** upon oxidation was almost identical to that of TTFAQ **94**. Decrease of absorption intensities at 311 nm, 391 nm, and 458 nm was accompanied by increase at 331 nm and 437 nm. Also a long absorption tail was formed upon oxidation, the intensity increase of which was similar to compound **94.**

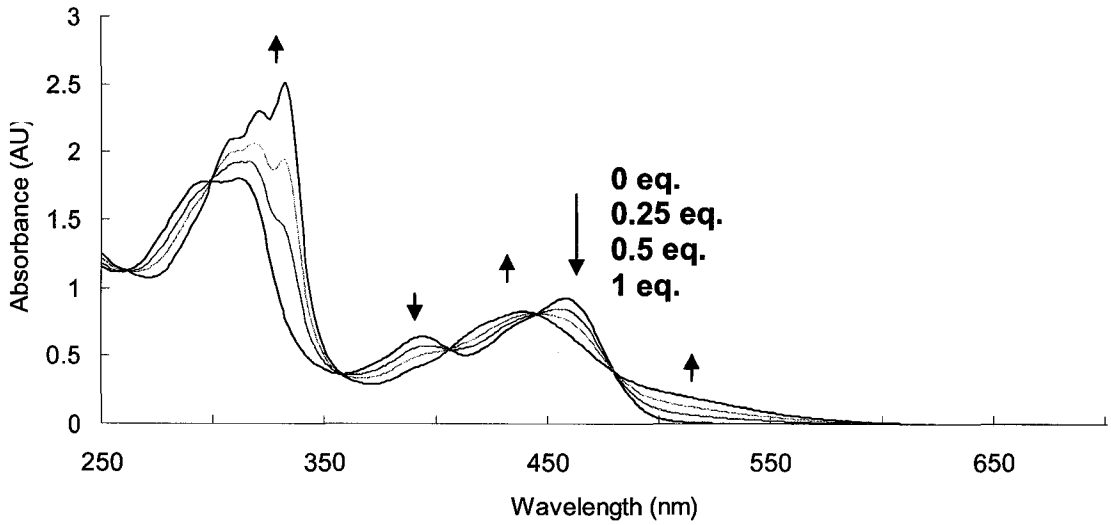

Figure 2.11 Selected UV-vis spectra of **103c** upon oxidation in 1:1 $CHCl_3$:MeCN.

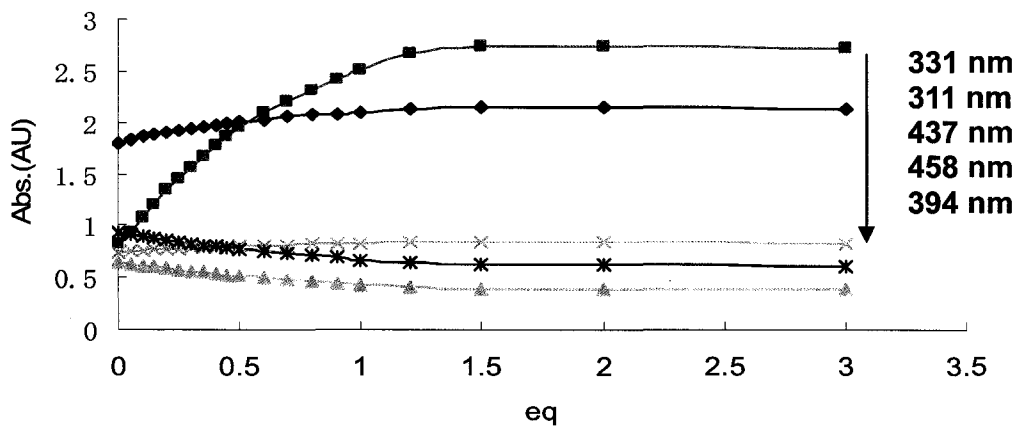

Figure 2.12 Absorptions alternation trends of **103c** at certain wavelengthes upon oxidation in 1:1 $CHCl_3$: MeCN.

The comparison of the shapes of the absorption profiles of TTFAQ **94**, **103a** and **103c** in oxidized forms did not reveal much information (Figure 2.13). Redshift of the

absorptions of planar anthracene and oxidized dithiole ring was in agreement with the assumption that the hole was delocalized within the whole molecule rather than merely on the dithiole rings. The long absorption tail in the low energy region was characteristic of the oxidized species.

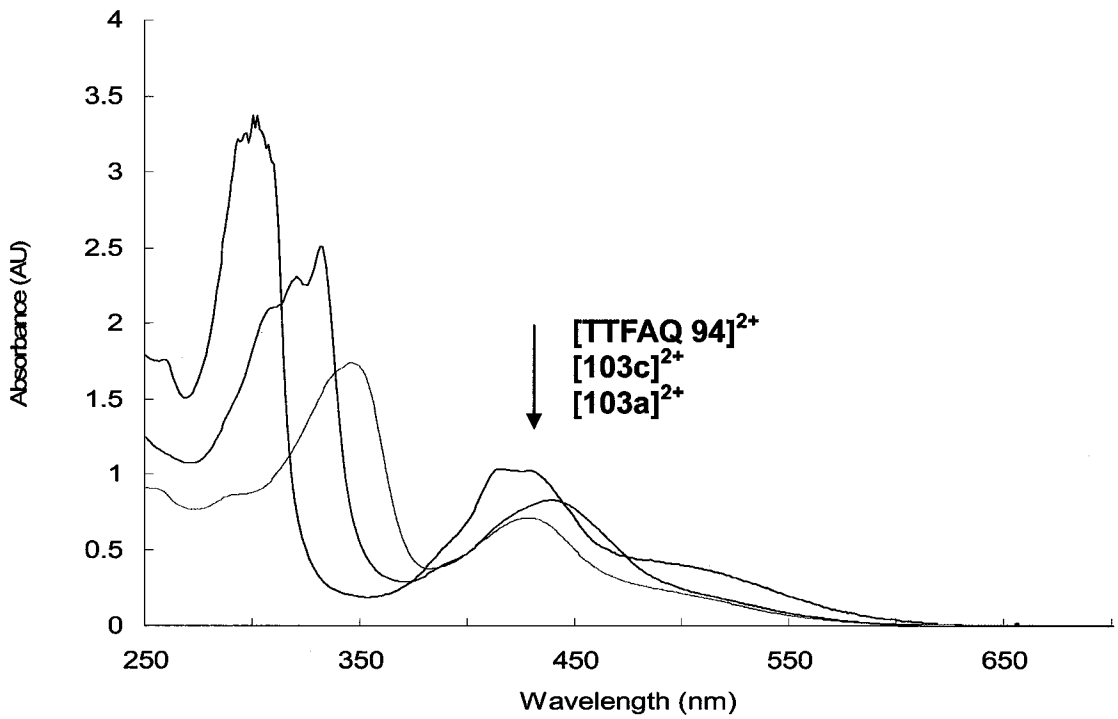

Figure 2.13 Steady state absorption spectra of **94**, **103a**, and **103c** in their dicationic forms.

2.3 Experimental

General Procedures

All reactions were carried out under a nitrogen atmosphere unless otherwise noted. All chemicals were of reagent grade. Solvents THF and Et_3N were dried over appropriate drying agents and used after distillation. Flash column chromatography was performed

using 240-400 mesh silica gel. ^{1}H NMR and ^{13}C NMR spectra were measured on the Bruker Advance 500 MHz instrument in $CDCl_3$ using tetramethylsilane as the internal standard. Mass spectra were recorded on a MALDI-TOF spectrometer using dithranol as the matrix or obtained from Atmospheric Pressure Chemical Ionization-Mass Spectrometry (APCI-MS). Melting points were measured from an uncorrected Fisher-Johns hot stage apparatus.

C_{60}-TTFAQ-C_{60} triad (83)

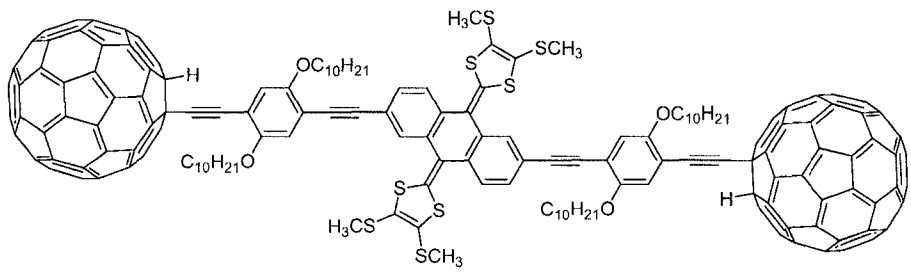

83

TTFAQ phenylethynylene derivative **100** (40 mg, 0.025 mmol) was desilylated by K_2CO_3 in MeOH/THF. After general workup, it was chromatographied with 30% CH_2Cl_2 in hexane to give the deprotected product (33 mg, 0.023 mmol, 91% yield), which was carefully dried under vacuum overnight.

The deprotected product (31 mg, 0.022 mmol) and C_{60} (72 mg, 0.099 mmol) were added to an oven-dried round-bottom flask, and the content was placed under vacuum for 1 h to remove moisture. Afterwards the flask was further flame-dried for 10 min under vacuum and purged with pure N_2 three times. Dried THF (60 ml) was added through a syringe. The mixture was sonicated for 3.5 h to suspend the C_{60} in the THF. LIHMDS (0.50 mL, 0.50 mmol) was added over 10 min. The brown-green mixture turned to a greenish black color with increasing addition of the base. 40 min after the base was added,

TFA was added (0.10 ml, 13 mmol) to quench the reaction, forming a red-brown solution with visible black-brown sediments. After 5 min standing, the mixture was filtered with a short $MgSO_4$ plug. The residue was washed with THF. The combined filtrate was evaporated *in vacuo*. To the resulting residue, consisting of a black-brown solid and pale brown oil, 2 mL of CS_2 was added. The solution was separated from the oil and evaporated *in vacuo*. To the residue was added 2 mL of $CHCl_3$. Then the solution was separated and evaporated. The residue was dissolved in 2 mL of CS_2 and directly loaded on a silica column. It was first eluted with 20:1 hexane/CS_2 (20 mL) to remove trace amount of unreacted fullerene. Then with an eluent of 5:3:1 $CHCl_3$/hexane/CS_2 (90 mL) crude product was eluted out of the column. The crude product was subjected to a second chromatographic purification using 2:1:1 $CHCl_3$/hexane/CS_2 as the eluent (40 mL) to afford triad **83** (15 mg, 0.0052 mmol, 25% yield) as a dark brown solid. IR (KBr) 2923, 2852, 1625, 1384 cm^{-1}; ^1H NMR (500 MHz, $CDCl_3$) δ 7.76 (d, J = 1.5 Hz, 2H), 7.59 (d, J = 7.5 Hz, 2H), 7.53 (dd, J = 1.0 Hz, J = 8.0 Hz, 2H), 7.30 (s, 2H), 7.19 (s, 2H), 7.18 (s, 2H), 4.21-4.15 (m, 8H), 2.44 (s, 12H), 1.98-1.93 (m, 8H), 1.71-1.59 (m, 8H), 1.48-1.20 (m, 48H), 0.89-0.81 (m, 12H); ^{13}C NMR (125 MHz, $CDCl_3$) δ 154.8, 154.0, 151.8, 151.7, 147.9, 147.6, 146.9, 146.7, 146.5, 146.4, 146.3, 146.1, 146.0, 145.9, 145.8, 145.7, 145.6, 145.0, 144.8, 143.5, 142.89, 142.86, 142.4, 142.34, 142.28, 142.2, 142.0, 141.9, 140.7, 140.6, 136.4, 135.4, 134.9, 134.6, 133.7, 129.9, 128.4, 127.0, 126.3, 125.8, 122.9, 121.8, 117.3, 117.0, 115.0, 113.3, 99.8, 97.9, 95.7, 87.4, *80.8* (impurity from CS_2), 69.9, 69.8, 62.2, 55.8, 30.0, 29.93, 29.89, 29.87, 29.84, 29.80, 29.60, 29.56, 29.5, 26.9, 26.5, 23.1, 19.6, 19.5, 19.3, 14.5, 14.3; MALDI-TOF MS (dithranol) *m/z* (%) calcd for $C_{204}H_{108}O_4S_8$ 2876.60, found 2875.42 (100) $[M]^+$, 2696.03 (29).

2,6-Bis(trimethylsilylethynyl)anthraquinone (84)

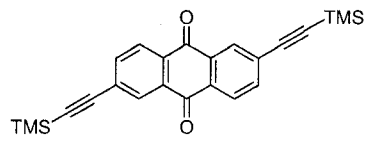

84

To a mixture of dibromo compound **88** (1.30 g, 3.54 mmol) and $PdCl_2(PPh_3)_3$ (0.22 g, 0.32 mmol) was added Et_3N (50 mL) under the protection of N_2. CuI (0.19 g, 0.98 mmol) was then added. The mixture was heated to 50 °C and then TMSA (2.3 mL, 16 mmol) was added. The mixture was stirred overnight at 50 °C. After removal of solvents under vacuum, the residue was dissolved in CH_2Cl_2 and washed with aq. NH_4Cl and H_2O. The organic layer was then dried over $MgSO_4$. The solution was then concentrated and cooled with an ice bath. Vacuum filtration afforded a residue, which was washed with CH_2Cl_2 to afford **84** a yellow solid (0.68 g, 1.7 mmol, 48% yield). More product **84** (0.24 g, 0.59 mmol, 17% yield) could be obtained by further concentration and recrystallization of the filtrate. The final filtrate was evaporated and chromatographied by 9:1 hexane/CH_2Cl_2 to afford a pale yellow solid **84** (0.16 g, 0.39 mmol, 11% yield). The overall yield was 76%. M.p. 257-258 °C; IR 3324, 3100, 2959, 2901, 2154, 1670, 1589, 1309, 1250 cm^{-1}; ^1H NMR (500 MHz, $CDCl_3$) δ 8.37 (d, J = 1.0 Hz, 2H), 8.26 (d, J = 7.5Hz, 2H), 7.84 (dd, J = 2.0 Hz, J = 8.0 Hz, 2H), 0.30 (s, 18H); ^{13}C NMR (125 MHz, $CDCl_3$) δ 182.13, 137.16, 133.64, 132.68, 130.97, 129.86, 127.60, 103.40, 100.66, 0.25; APCI-MS (negative mode) *m/z* (%) calcd for $C_{24}H_{24}O_2Si_2$ 401.1, found 400.1 (100) $[M-H]^-$.

S-Decyl phosphonate (85a)

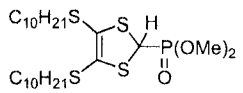

85a

To the solution of **93a** (200 mg, 0.385 mmol) in MeCN (20 mL) was added NaI (110 mg, 0.733 mmol). Then $P(OMe)_3$ (0.1 mL, 0.6 mmol) was added. The mixture was stirred for 2.5 h and then evaporated under vacuum. To the residue H_2O and CH_2Cl_2 were added. The organic layer was washed with H_2O, dried over $MgSO_4$ and evaporated under vacuum to afford **85a** as a pale brown liquid (146 mg, 0.269 mmol, 70%). ^1H NMR (500 MHz, $CDCl_3$) δ 4.74 (d, J = 5.5 Hz, 1H), 3.87 (d, J = 10.5 Hz, 6H), 2.90-2.84 (m, 2H) 2.78-2.72 (m, 2H), 1.70-1.61 (m, 4H), 1.41-1.39 (m, 4H), 1.26 (s, 24H), 0.89-0.87 (m, 6H); ^{13}C NMR (125 MHz, $CDCl_3$) δ 125.5, 54.7, 54.6, 42.0, 40.7, 36.3, 31.9, 29.8, 29.6, 29.3, 29.24, 29.20, 28.6, 22.7, 14.1; APCI-MS (positive mode) *m/z* (%) calcd for $C_{25}H_{49}O_3PS_4$ 556.2, found 893.3 (27), 767 (10), 557.1 (63) $[M+H]^+$, 447.2 (100).

Synthesis of *S*-methyl phosphonate (85b)

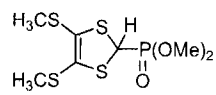

85b

To a solution of **93b** (6.1 g, 22 mmol) in MeCN (50 mL) was added NaI (4.0 g, 27 mmol) under N_2. $P(OMe)_3$ (3.3 mL, 28 mmol) was added. The mixture was stirred for 3 h and then evaporated under vacuum. To the residue H_2O and CH_2Cl_2 were added. The organic layer was washed with H_2O, dried over $MgSO_4$, and evaporated under vacuum to afford a dark red liquid **85b** (4.6 g, 15 mmol, 69 %). (In some cases the product was not

pure enough and it was chromatographied by EtOAc/hexane.) ^{1}H NMR (500 MHz, $CDCl_3$) δ 4.75 (d, J = 5.5 Hz, 1H), 3.90 (d, J = 10 Hz, 6H), 2.44 (s, 6H); ^{13}C NMR (125 MHz, $CDCl_3$) δ 125.6, 54.8, 42.4, 41.1, 19.2; APCI-MS (positive mode) *m/z* (%) calcd for $C_7H_{13}PS_4$ 304.4, found 305.0 (12) $[M+H]^+$, 194.9 (100)

(2,5-Bis(decyloxy)-4-iodophenyl)ethynyltrimethylsilane (86)

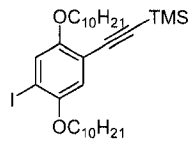

86

To a mixture of diiodo compound **97** (1.8 g, 2.8 mmol), $PdCl_2(PPh_3)_2$ (96 mg, 0.14 mmol), CuI (88 mg, 0.42 mmol) and Et_3N (30 mL) was added TMSA (0.28 mL, 1.9 mmol). The mixture was stirred overnight. After filtration, the filtrate was concentrated under vacuum. The residue was diluted by CH_2Cl_2, washed with aq. HCl (10%), and H_2O, and dried over $MgSO_4$, and evaporated under vacuum. The residue was directly loaded on a silica column and was chromatographied with hexane to recover unreacted **97**. Next, 10% CH_2Cl_2 in hexane was applied as the eluent to elute product **86** (0.96 g, 1.6 mmol, 56%). ^{1}H NMR (500 MHz, $CDCl_3$) δ 7.25 (s, 1H), 6.83 (s, 1H), 3.95-3.92 (m, 4H), 1.81-1.77 (m, 4H), 1.50-1.48 (m, 4H), 1.34-1.27 (m, 24H), 0.90-0.87 (m, 6H), 0.25 (s, 9H).

2,6-Dibromoanthraquinone (88)

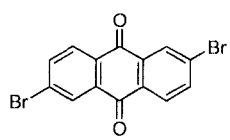

88

To a solution of $CuBr_2$ (3.77 g, 16.9 mmol) in MeCN (50 mL) was added *t*-$BuNO_2$ (2.5 mL, 19 mmol). The mixture was heated to 65 °C and then 2,6-diaminoanthraquinone (4.05 g, 17.0 mmol) was added. After 10 min, *t*-$BuNO_2$ (2.5 mL, 19 mmol) was added. The mixture was stirred for 2 h. Then the mixture was poured into 10% aq. HCl (400 mL). The solid precipitate was collected by filtration, washed with aq. HCl and H_2O, and chromatographied by 1:1 CH_2Cl_2: hexane to yield **88** as a yellow solid (3.02 g, 8.30 mmol, 49%). ^{1}H NMR (300 MHz, $CDCl_3$) δ 8.45 (d, J = 1.5 Hz, 2H), 8.18 (d, J = 8.4 Hz, 2H), 7.96 (dd, J = 1.5 Hz, J = 8.4 Hz, 2H).

Bis(tetraethylammonium) bis(1,3-dithiole-4,5-dithiolate)zincate (89)

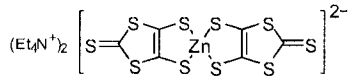

89

A mixture of Na (6.80 g, 0.300 mol) and CS_2 (60 mL, 1.0 mol) was refluxed for 20 min under N_2 protection. Dried DMF (20 mL) was added dropwise over a period of 20 min. The mixture was refluxed for 2 h and then concentrated under vacuum at 30 °C. MeOH (40 mL) was added to the residue with cooling in a H_2O bath. After filtration, a solution of $ZnCl_2$ (7.00 g, 51.3 mmol) in 1:1 MeOH/$NH_3{\cdot}H_2O$ (120 mL) was added carefully to the filtrate. To the resulting mixture, Et_4NBr (20 g, 95 mmol) in H_2O (80 mL) was then added. Then the mixture was left standing overnight. After filtration the residue was sequentially washed with H_2O and Et_2O to yield **89** as a red-colored solid (24 g, 33 mmol, 88 %). M.p. 203-204 °C.

4,5-Bis(decylthio)-1,3-dithiol-2-thione (90a)

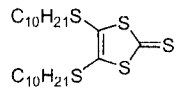

90a

To a solution of compound **89** (2.00 g, 2.78 mmol) in acetone (80 mL) was added $C_{10}H_{21}Br$ (2.80 g, 12.7 mmol). The mixture was refluxed for 2 h and then filtered. The solid residue was washed with acetone (5 mL × 3). To the resulting filtrate, acetonitrile (100 mL) was added. The mixture was then cooled with an ice-water bath. A precipitate was formed and collected by vacuum filtration. The solid was washed with acetonitrile to afford **90a** as a yellow flake-like solid (1.60 g, 3.34 mmol, 60%). M.p. 46-47 °C; IR (neat) 2953, 2915, 2847, 1470, 1057 cm^{-1}; ^1H NMR (500 MHz, $CDCl_3$) δ 2.87 (t, J = 7.5 Hz, 4H), 1.69-1.63 (m, 4H), 1.43-1.38 (m, 4H), 1.27 (s, 24H), 0.90-0.86 (t, J = 7.0 Hz, 6H); ^{13}C NMR (125 MHz, $CDCl_3$) δ 212.0, 136.8, 37.2, 32.3, 30.1, 30.0, 29.9, 29.7, 29.5, 28.9, 23.1, 14.5; APCI-MS (positive mode) *m/z* (%) calcd for $C_{23}H_{42}S_5$ 478.9, found 479.2 (100) $[M]^+$.

4,5-Bis(methylthio)-1,3-dithiol-2-thione (90b)

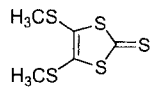

90b

To a solution of **89** (0.52 g, 0.72 mmol) in acetone (40 mL) was added MeI (0.200 mL, 3.21 mmol). The mixture was refluxed for 2 h and filtered. The residue was washed with acetone. The filtrate was evaporated and the residue was quenched with H_2O (80 mL). The mixture was extracted with CH_2Cl_2. The organic layer was washed with H_2O, dried over $MgSO_4$, and evaporated under vacuum. The residue was recrystallized from

MeOH (33 mL) to afford an orange crystal **90b** (0.24 g, 1.1 mmol, 74%). M.p. 107-108 °C; IR (neat) 2984, 2910, 1783, 1470, 1418, 1055,1033 cm^{-1}; ^1H NMR (500 MHz, $CDCl_3$) δ 2.50 (s, 6H); ^{13}C NMR (125 MHz, $CDCl_3$) δ 211.1, 136.2, 19.5.

4,5-Bis(decylthiol)-1,3-dithiol-2-ium tetrafluoroborate (91a)

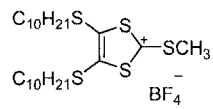

91a

A mixture of DMS (1.5 mL, 15 mmol) and thione **90a** (1.01 g, 2.11 mmol) was heated to 100 °C and stirred for 2 h under N_2. The resulting solution was cooled in an ice bath and $HBF_4{\cdot}Et_2O$ (1.0 mL, 8.0 mmol) was added. Et_2O (3 mL) was added and the mixture was stirred for another 20 min. More Et_2O (20 mL) was added afterwards, which resulted in a precipitate immediately. The solid formed was collected by filtration and washed with ice-cooled Et_2O to afford **90a** as a white solid (1.20 g, 2.07 mmol, 98 %). ^1H NMR (300 MHz, $CDCl_3$) δ 3.25 (s, 3H), 3.18 (t, J = 7.2 Hz, 4H), 1.78-1.70 (m, 4H), 1.49-1.27 (m, 4H), 1.22 (s, 24H), 0.91-0.87 (*t*, J = 6.3 Hz, 6H). APCI-MS (positive mode) *m/z* (%) calcd for cation $[C_{24}H_{45}S_5]^+$ 493.2, found 893.3 (6), 493.1 (100) $[M]^+$, 479.2 (28), 447.2 (15).

4,5-Bis(methylthio)-1,3-dithiol-2-ium tetrafluoroborate (91b)

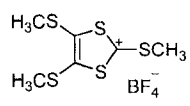

91b

A mixture of thione **90b** (6.75 g, 29.8 mmol) and DMS (15.0 mL, 158 mmol) was heated to 100 °C and stirred for 1.5 h. The mixture was cooled in an ice bath, and

$HBF_4{\cdot}Et_2O$ (0.30 mL, 2.5 mmol) was added. AcOH (15 mL, 342 mmol) was then added. After 10 min, Et_2O (100 mL) was added. The product was collected by filtration and washed with Et_2O to afford a light-brown solid **91b** (9.80 g, 29.2 mmol, 100 %). M.p. 66-68 °C; ^1H NMR (300 MHz, $CDCl_3$) δ 3.24 (s, 3H), 2.78 (s, 6H).

4,5-Bis(decylthio)-2-(methylthio)-1,3-dithiole (92a)

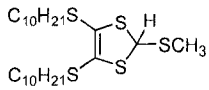

92a

To a solution of compound **91a** (1.20 g, 2.07 mmol) in EtOH (25 mL) cooled with an ice bath was added $NaBH_4$ (200 mg, 5.29 mmol). The mixture was stirred for 2.5 h and then evaporated under vacuum. To the residue H_2O and CH_2Cl_2 were added. The organic layer was washed with H_2O, dried over $MgSO_4$ and then evaporated under vacuum to afford **92a** as a yellow liquid (0.80 g, 1.6 mmol, 78 %). ^1H NMR (300 MHz, $CDCl_3$) δ 5.74 (s, 1H), 2.99-2.90 (m, 2H), 2.75-2.65(m, 2H), 2.26 (s, 3H), 2.19 (s, 3H), 1.73-1.68(m, 4H), 1.50-1.20 (m, 28H), 0.91-0.87 (m, 6H); APCI-MS (positive mode) *m/z* (%) calcd for $C_{24}H_{46}S_5$ 494.2, found 493.2 (26) $[M-H]^+$, 447.2 (100).

4,5-Bis(methylthio)-2-(methylthio)-1,3-dithiole (92b)

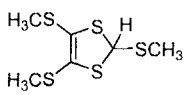

92b

To a solution of compound **91b** (9.8 g, 30 mmol) in EtOH (80 mL) was added $NaBH_4$ (2.8 g, 74 mmol) in an ice bath. After 15 min the mixture was warmed up to r.t. and kept stirring for another 3 h. The mixture was then evaporated under vacuum. H_2O

(20 mL) was added to the residue. The product was collected by filtration to yield **92b** as a pale orange solid (6.4 g, 26.4 mmol, 88%). (In most cases, the product found at this stage was solid. However, it could be a liquid. If that was the case, the product could be extracted with CH_2Cl_2, dried over $MgSO_4$, and evaporated under vacuum to afford a dark-red liquid **92b**, which solidified in a fridge.) ^{1}H NMR (500 MHz, $CDCl_3$) δ 5.79 (s, 1H), 2.41 (d, J = 8.5 Hz, 6H), 2.27 (s, 3H); ^{13}C NMR (125 MHz, $CDCl_3$) δ 124.7, 57.3, 19.4, 13.1; APCI-MS (positive mode) *m/z* (%) calcd for $C_6H_{10}S_5$ 241.9, found 240.9 (9) $[M-H]^+$, 194.9 (100)

_S_-decyl dithiolium salt (93a)

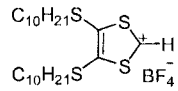

93a

To thiol **92a** (1.00 g, 2.02 mmol) that was cooled in an ice bath was added Ac_2O (8.0 mL, 85 mmol). After 5 min, $HBF_4{\cdot}Et_2O$ (1.0 mL, 8.0 mmol) was added. After another 15 min, Et_2O (20 mL) was added. The formed slurry was filtered, and the solid residue was washed with Et_2O. The filtrate was cooled in a freezer overnight. The resulting yellow crystalline solids were filtered and washed with iced ether to afford pure product **93a** (0.748 g, 1.40 mmol, 70%). ^{1}H NMR (300 MHz, $CDCl_3$) δ 11.37 (s, 1H), 3.22 (t, J = 7.5 Hz, 4H), 1.81-1.76 (m, 4H), 1.49-1.44 (m, 4H), 1.28 (s, 24H), 0.92-0.86 (m, 6H); API-ES-MS (positive mode) *m/z* (%) calcd for cation $[C_{23}H_{43}S_4]^+$ 447.8, found 447.2 (100) $[M]^+$.

_S_-Methyl dithiolium salt (93b)

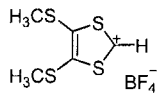

93b

Ac_2O (50 mL, 0.53 mol) was mixed with thiol **92b** (6.4 g, 26 mmol) in an ice bath under N_2. After 10 min, $HBF_4{\cdot}Et_2O$ (5.0 mL, 40 mmol) was added. After another 30 min, Et_2O (100 mL) was added. The product was collected by filtration and washed with Et_2O to afford a yellow solid **93b** (6.1 g, 22 mmol, 83%). M.p. 98-99 °C; ^{1}H NMR (300 MHz, $CDCl_3$) δ 11.29 (s, 1H), 2.82 (s, 6H).

TTFAQ (94) and mono-coupling byproduct (95)

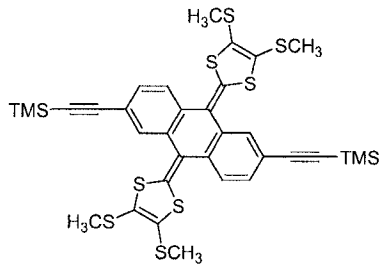

94

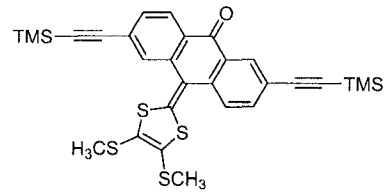

95

To a solution of _S_-methyl phosphonate **85b** (0.71 g, 2.5 mmol) in dried THF (80 ml) at -78 °C was added _n_-BuLi (2.4 mL, 3.8 mmol). After 15 min, a suspension of bisethynylated anthraquinone **84** (0.40 g, 1.0 mmol) in dried THF (20 mL) was added. The mixture was warmed to r.t. and stirred overnight. The mixture was then evaporated under vacuum. H_2O was added to the residue. The mixture was extracted with CH_2Cl_2, dried over $MgSO_4$, and evaporated under vacuum. The residue was purified with chromatography using 9:1 hexane/CH_2Cl_2 as the eluent to yield **94** as a yellow solid (0.67 g, 0.88 mmol, 88% yield). M.p. 290 °C(dec.); IR (neat) 2959, 2359, 2341, 2148, 1670,

1490, 1246, 841 cm^{-1}; ^1H NMR (500 MHz, $CDCl_3$) δ 7.62 (d, J = 1.5 Hz, 2H), 7.48 (d, J = 8.5 Hz, 2H), 7.41 (dd, J = 8.0, 1.5 Hz, 2H), 2.44 (s, 6H), 2.42 (s, 6H), 0.30 (s, 18H); ^{13}C NMR (125 MHz, $CDCl_3$) δ 134.6, 134.4, 133.0, 130.1, 128.4, 126.6, 125.6, 125.3, 122.4, 121.2, 104.9, 95.2, 19.3, 19.1, 0.02; APCI-MS (positive mode) *m/z* (%) calcd for $C_{34}H_{32}S_8Si_2$ 757.8, found 829.1 (17), 757.1 (68) $[M]^+$, 685.0 (57), 613.0 (100), 579.1 (18)

The column chromatography was further eluted by 70% CH_2Cl_2 in hexane to afford red crystal **95**. M.p. 223-224 °C; IR (neat) 2956, 2924, 2855, 2348, 2157, 1649, 1591, 1517, 1433,1420, 1248,1211, 840 cm^{-1}; ^1H NMR (500 MHz, $CDCl_3$) δ 8.34 (s, 1H), 8.19 (d, J = 7.5 Hz, 1H), 7.83 (d, J = 1.5 Hz, 1H), 7.70 (d, J = 1.0 Hz, 2H), 7.50 (dd, J = 1.5 Hz, J = 7.5 Hz, 1 H), 2.44 (s, 6H), 2.43 (s, 6H), 0.30 (s, 9H), 0.27 (s, 9H); ^{13}C NMR (125 MHz, $CDCl_3$) δ 182.4, 142.8, 138.8, 138.5, 135.2, 131.3, 130.8, 130.6, 130.2, 129.7, 128.2, 127.7, 127.5, 127.4, 126.6, 122.1, 118.5, 104.7, 104.4, 99.0, 96.5, 19.9, 19.7; APCI-MS (positive mode) *m/z* (%) calcd for $C_{29}H_{30}OSi_2S_4$ 579.5, found 579.1 (100) $[M]^+$.

1,4-Bis(decyloxy)benzene (96)

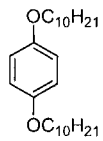

96

Hydroquinone (4.4 g, 40 mmol), KOH (5.6 g, 99 mmol), $C_{10}H_{21}Br$ (17.8 g, 80 mmol) and EtOH (90 mL) were mixed in a 250 mL round-bottom flask. After refluxing the mixture overnight, the reaction was quenched with H_2O (100 mL) and extracted with CH_2Cl_2 (150 mL). The organic layer was separated and washed with water, brine, and then dried over $MgSO_4$. The solvent was removed under vacuum. The residue was

recrystallized from MeOH (150 mL) to afford **96** as a white flake-like solid (10.0 g, 25.6 mmol, 64%). ^{1}H NMR (500 MHz, $CDCl_3$) δ 6.81 (s, 4H), 3.90 (t, J = 6.5 Hz, 4H), 1.78-1.71 (m, 4H), 1.46-1.40 (m, 4H), 1.35-1.27 (m, 24H), 0.90-0.86 (t, J = 7.0 Hz, 6H).

1,4-Bis(decyloxy)-2,5-diiodobenzene (97)

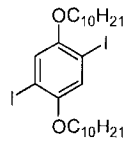

97

To a mixture of compound **96** (5.9 g, 15 mmol), $Hg(OAc)_2$ (11.5 g, 36.0 mmol), I_2 (9.3 g, 37 mmol) was added CH_2Cl_2 (80 mL). The mixture was stirred at r.t. for 20 h and then filtered through a 1 cm thick diatomaceous earth pad. The residue was washed with CH_2Cl_2. The filtrate was washed with $Na_2S_2O_4$ (20%, 150 mL), satd. $NaHCO_3$ (100 mL) and brine (100 mL). After dried over $MgSO_4$, the solvent was evaporated under vacuum. The residue was recrystallized from EtOH (70 mL) to afford a white solid **97** (8.1 g, 13 mmol, 84%). ^{1}H NMR (500 MHz, $CDCl_3$) δ 7.17 (s, 2H), 3.93 (t, J = 7.0 Hz, 4H), 1.82-1.77 (m, 4H), 1.52-1.46 (m, 4H), 1.38-1.28 (m, 24H), 0.91-0.87 (t, J = 7.0 Hz, 6H).

TTFAQ phenylethynylene derivative (100) and dimer (101)

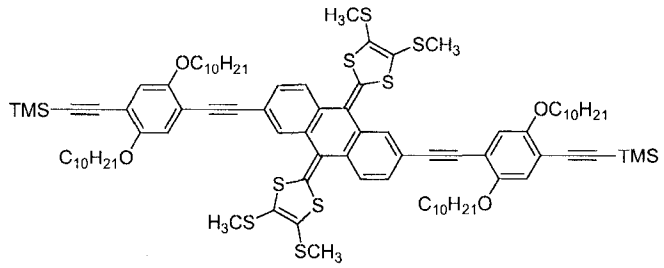

100

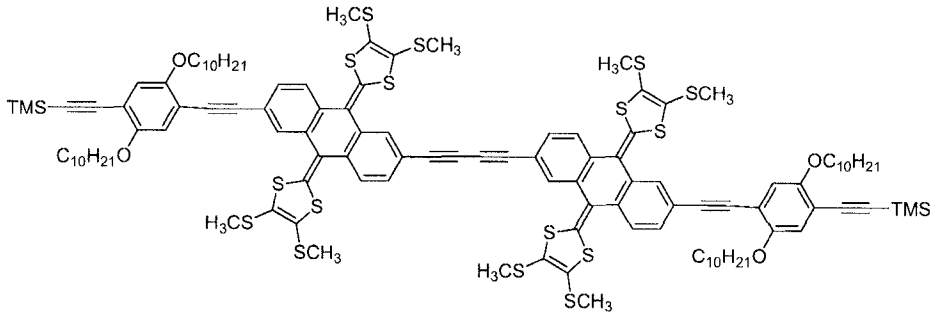

101

A mixture of TTFAQ **94** (38 mg, 0.050 mmol), K_2CO_3, and 1:1 MeOH/THF (20 mL) was stirred at r.t. for 30 min. It was then evaporated under vacuum. The residue was dissolved in CH_2Cl_2 and quenched with H_2O. The organic layer was separated, washed with H_2O, dried over $MgSO_4$, and evaporated under vacuum to obtain desilylated product **98** (28 mg, 0.046 mmol, 92%).

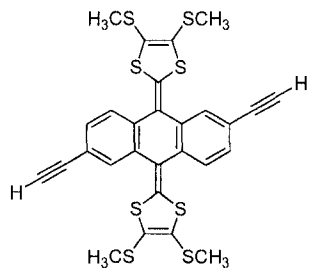

98

To a mixture of the deprotected product **98** (100 mg, 0.165 mmol), iodo compound **86** (465 mg, 0.660 mmol), and $PdCl_2(PPh_3)_3$ (12 mg, 0.017 mmol) was added Et_3N (60 mL). Under N_2 protection, CuI (9.5 mg, 0.050 mmol) was added. The mixture was stirred

at r.t. overnight. Then it was evaporated *in vacuo*, followed by dilution with CH_2Cl_2. The solution was sequentially washed with aq. HCl, aq. NH_4Cl and H_2O, then dried over $MgSO_4$ and evaporated *in vacuo*. The residue was chromatographied by hexane to recovered **86**, then 30% CH_2Cl_2 in hexane to afford **100** (129 mg, 0.82 mmol, 50%) as a solid. M.p. 147.0-148.5 °C; IR (KBr) 2924, 2853, 1622, 1384 cm^{-1}; ^1H NMR (500 MHz, $CDCl_3$) δ 7.67 (d, J = 1.5 Hz, 2H), 7.53 (d, J = 8.5 Hz, 2H), 7.45 (dd, J = 8.0, 1.5 Hz, 2H), 7.00 (s, 2H), 6.95 (s, 2H), 4.02-3.99 (m, 8H), 2.40 (d, J = 4.5 Hz, 12H,), 1.87-1.80 (m, 8H), 1.55-1.51 (m, 8H), 1.40-1.25 (m, 48H), 0.90-0.85 (m, 12H), 0.27 (s, 18H); ^{13}C NMR (125 MHz, $CDCl_3$) δ 154.2, 153.6, 134.6, 134.3, 132.9, 129.6, 128.1, 126.6, 125.9, 125.5, 122.5, 121.5, 117.4, 117.0, 114.2, 113.9, 101.2, 100.2, 94.9, 86.8, 69.7, 69.6, 31.94, 31.91, 29.70, 29.67, 29.64, 29.61, 29.53, 29.48, 29.44, 29.41, 29.38, 29.36, 26.11, 26.07, 22.7, 19.3, 19.2, 14.15, 14.13; MALDI-TOF MS (dithranol) (%) calcd for $C_{90}H_{124}O_4S_8Si_2$ 1580.68, found 1578.97 (100) $[M-H]^+$, 1430.21 (16).

The silica column was further eluted with 45% CH_2Cl_2 in hexane to yield dimer **101** (35 mg, 0.016 mmol, 20%). IR (KBr) 2924, 2853, 1635, 1384 cm^{-1}; ^1H NMR (500 MHz, $CDCl_3$) δ 7.69 (d, J = 1.5 Hz, 2H), 7.66 (d, J = 2.0 Hz, 2H), 7.54-7.45 (m, 8H), 6.99 (s, 2H), 6.95 (s, 2H), 4.02-3.99 (m, 8H), 2.43-2.40 (m, 24H), 1.87-1.80 (m, 8H), 1.55-1.51 (m, 8H), 1.40-1.25 (m, 48H), 0.90-0.85 (m, 12H), 0.27 (s, 18H); ^{13}C NMR (125 MHz, $CDCl_3$) δ 135.4, 134.7, 134.5, 134.2, 133.8, 133.5, 130.5, 129.7, 129.0, 128.1, 126.6, 126.4, 126.02, 126.00, 125.6, 125.5, 122.2, 122.0, 121.6, 119.5, 117.4, 116.9, 114.2, 113.9, 101.2, 100.2, 94.9, 86.9, 82.2, 74.9, 31.94, 31.92, 29.71, 29.67, 29.64, 29.63, 29.48, 29.45, 29.42, 29.39, 29.37, 26.12, 26.08, 22.72, 22.70, 19.32, 19.26, 19.18, 19.14, 14.16, 14.13 (one alkyl carbon signal in the region of 29-30 ppm is missing due to overlap); MALDI-

TOF MS (dithranol) *m/z* calcd for $C_{118}H_{142}O_4S_{16}Si_2$ 2190.6, found 2189.58 $[M-H]^+$, 2040.16 (12), 2011.23 (16), 681.69 (16).

C_{60}-TTFAQ-TTFAQ-C_{60} tetrad (102)

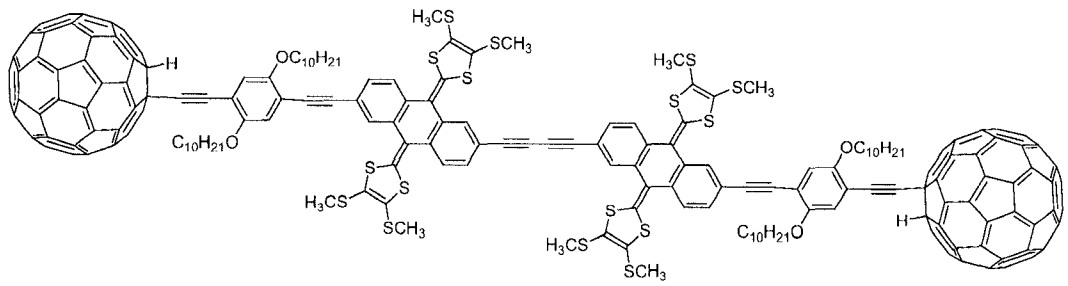

102

To a solution of TTFAQ dimer **101** (36 mg, 0.016 mmol) in THF (15 mL) was added TBAF (0.5 mL, 0.5 mmol). The mixture was stirred for 5 min. Et_2O and H_2O were added. The organic layer was washed by H_2O, dried over $MgSO_4$, and evaporated *in vacuo* to form a red orange solid **101a** (30 mg, 0.015 mmol, 92%).

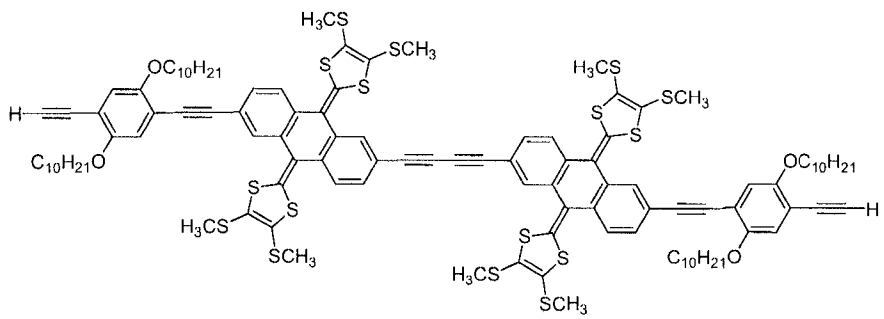

101a

To an oven-dried round-bottom flask **101a** (30 mg, 0.015 mmol) and C_{60} (58 mg, 0.080 mmol) were added. The flask was flame-dried for 15 min under vacuum and then purged with pure N_2 three times. Dried THF (60 mL) was added via a syringe. The mixture was sonicated for 3.5 h to form a good suspension of C_{60}. LHMDS (0.40 mL, 0.40 mmol) was added slowly. 30 min after the base addition was complete, TFA (0.10

mL, 13 mmol) was added to quench the reaction. The resulting mixture was filtered and the filtrate was evaporated under vacuum. CS_2 was then added. The solution was filtered through a short silica plug, eluted by 1:20 $CHCl_3/CS_2$. The resulting brown solution was concentrated *in vacuo*. Another portion of CS_2 was added, and the solution was loaded on a silica column and eluted with 3:3:2 $CHCl_3$/hexane/CS_2 to afford tetrad **102** (6 mg, 0.002 mmol, 13%) as a brown solid. ^{1}H NMR (500 MHz, $CDCl_3$) δ 7.73 (m, 2H), 7.50-7.59 (m, 8H), 7.30 (s, 2H), 7.19 (s, 2H), 7.18 (s, 2H), 4.21-4.14 (m, 8H), 2.45-2.43 (m, 24H), 1.97-1.92 (m, 8H), 1.70-1.58 (m, 8H), 1.47-1.20 (m, 48H), 0.91-0.80 (m, 12H); MALDI-TOF MS (dithranol) *m/z* (%) calcd for $C_{232}H_{126}O_4S_{16}$ 3486.52, found 3486.47 (100) $[M]^+$.

2,2'-(2,6-Bis((4-nitrophenyl)ethynyl)anthracene-9,10-diylidene)-bis(4,5-bis(methylthio)-1,3-dithiole (103a)

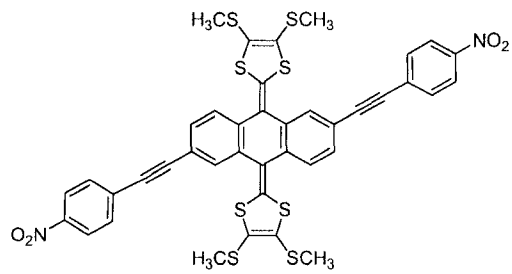

103a

To a mixture of deprotected TTFAQ **98** (35 mg, 0.058 mmol), CuI (8 mg, 0.04 mmol), $PdCl_2(PPh_3)_2$ (6 mg, 0.008 mmol) and 1-bromo-4-nitrobenzene (60 mg, 0.30 mmol) was added Et_3N (30 mL). The mixture was stirred overnight under protection of N_2 atomsphere. After the reaction was complete, the mixture was evaporated *in vacuo*, and the residue was diluted with CH_2Cl_2. This solution was washed with aq. NH_4Cl, H_2O, dried over $MgSO_4$, and then evaporated *in vacuo*. The crude product was chromatographied with 60% CH_2Cl_2 in hexane to afford a red orange solid **103a** (26 mg, 0.031 mmol, 53%). M.p. 50-52 °C; IR (neat) 3073, 2922, 2852, 2206, 1914, 1730, 1589, 1515, 1338, 895, 748 cm^{-1}; ^{1}H NMR (500 MHz, $CDCl_3$) δ 8.25 (d, J = 8.5 Hz, 4H), 7.72-

7.70 (m, 6H), 7.58-7.50 (m, 4H), 2.42 (d, J = 2.0 Hz, 12H); ^{13}C NMR (125 MHz, $CDCl_3$) δ 147.1, 135.2, 134.7, 134.2, 132.4, 130.1, 130.0, 128.3, 127.0, 125.7, 125.6, 123.7, 121.8, 120.1, 94.6, 88.4, 19.4, 19.1; MALDI-TOF MS (dithranol) *m/z* (%) calcd for $C_{40}H_{26}N_2O_4S_8$ 853.97, found 854.28 (100) $[M]^+$..

2,2'-(2,6-Bis((4-cyanophenyl)ethynyl)anthracene-9,10-diylidene)-bis(4,5-bis(methylthio)-1,3-dithiole (103b)

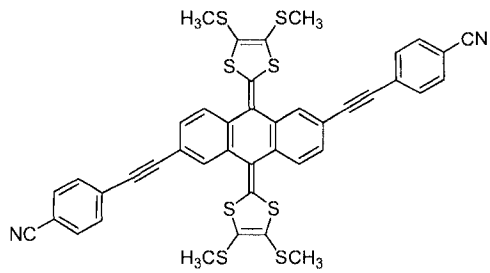

103b

To a mixture of deprotected TTFAQ **98** (30 mg, 0.050 mmol), CuI (5 mg, 0.03 mmol), $PdCl_2(PPh_3)_2$ (6 mg, 0.008 mmol) and 1-bromo-4-cyanobenzene (60 mg, 0.33 mmol) was added Et_3N (35 mL). The mixture was stirred overnight. After evaporated the mixture *in vacuo*, CH_2Cl_2 was added to the residue. The mixture was washed with aq. NH_4Cl, H_2O, dried over $MgSO_4$, and then evaporated *in vacuo*. The crude product was purified through silica chromatography with 80% CH_2Cl_2 in hexane to afford an orange solid **103b** (22 mg, 0.027 mmol, 54%). M.p. 225-226 °C; IR (neat) 3031, 2921, 2853, 2226, 2209, 1914, 1603, 1461, 835 cm^{-1}; ^{1}H NMR (500 MHz, $CDCl_3$) δ 7.69-7.63 (m, 10H), 7.57-7.47 (m, 4H), 2.41 (d, J = 2.0 Hz, 12H); ^{13}C NMR (125 MHz, $CDCl_3$) δ 135.1, 134.7, 134.0, 132.2, 132.1, 129.9, 128.3, 128.1, 127.0, 125.7, 125.6, 123.7, 121.9, 120.2, 118.5, 111.6, 93.7, 88.5, 19.3, 19.1; MALDI-TOF MS (dithranol) *m/z* (%) calcd for $C_{42}H_{26}N_2S_8$ 813.99, found 1426.50 (28), 1277.06 (10), 815.18 (100) $[M+H]^+$.

2,2'-(2,6-Bis((phenyl)ethynyl)anthracene-9,10-diylidene)-bis(4,5-bis(methylthio)-1,3-dithiole (103c)

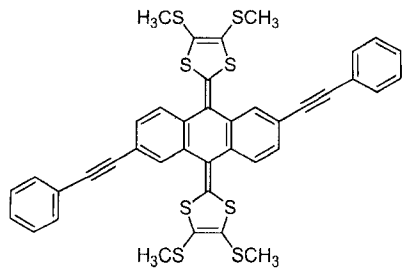

103c

To a mixture of deprotected TTFAQ **98** (35 mg, 0.058 mmol), CuI (3 mg, 0.02 mmol) and $PdCl_2(PPh_3)_2$ (3 mg, 0.004 mmol) was added Et_3N (15 mL), and then 4-iodobenzene (50 mg, 0.24 mmol) was added under N_2 protection. The mixture was stirred overnight at r.t. After the reaction was complete, the mixture was evaporated *in vacuo*, followed by addition of CH_2Cl_2. The mixture was washed with aq. NH_4Cl, H_2O, dried over $MgSO_4$, and then evaporated *in vacuo*. The crude compound was purified through a silica chromatography with 30% CH_2Cl_2 in hexane to afford **103c** as a yellow solid (33 mg, 0.043 mmol, 74%). M.p. 205-207 °C; IR (neat) 3022, 2917, 2206, 1601, 1461, 752, 687 cm^{-1}; ^1H NMR (500 MHz, $CDCl_3$) δ 7.69 (d, J = 1.5 Hz, 2H), 7.58-7.53 (m, 6H), 7.48-7.46 (dd, J = 7.5 Hz, J = 1.5 Hz, 2H), 7.39-7.34 (m, 6H), 2.41 (d, J = 2.0 Hz, 12H); ^{13}C NMR (125 MHz, $CDCl_3$) δ 134.6, 134.3, 133.0, 131.7, 130.2, 129.6, 128.4, 128.1, 126.5, 125.8, 125.5, 123.2, 122.4, 121.3, 116.9, 90.2, 89.4, 19.3, 19.1; APCI-MS (positive mode) *m/z* (%) calcd for $C_{40}H_{28}S_8$ 764.0, found 765.0 (100) $[M]^+$, 571.1 (60).

X-ray crystal data for TTFAQ 94

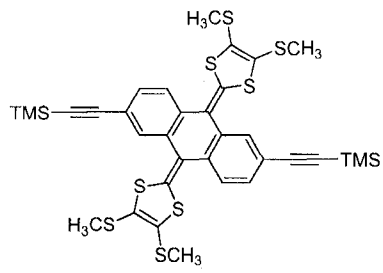

94

Empirical Formula $C_{34}H_{36}S_8Si_2$. Formula Weight 757.31. T -120 °C. Crystal System triclinic. Space Group *P*-1 (#2). a = 9.5782(9) Å; b = 13.3634(12) Å; c = 15.7630(17) Å; α = 78.285(6)°; β = 88.940(7)°; γ = 83.874(7) °. V = 1964.3(3) Å^3. Z value 2. D_{calcd} 1.280 g/cm^3. μ(MoKα) 5.383 cm^{-1}. Trans. factors: 0.8986 – 0.9701. $2\theta_{max}$ 61.3°. Data collected 23293. Data unique 8893. Residuals: R_1 ($I > 2.00\sigma(I)$) 0.0917. Residuals: R (All reflections) 0.1136. Residuals: wR_2 (All reflections) 0.2156. Maximum peak in final diff. map 0.76 e$^-$/Å^3.

General procedures for oxidative titration experiments

1. Prepare a solution of sample (1), and record its concentration.
2. Dilute the solution till its UV-vis maximum absorbance is within 1.0-1.5 au. Calculate the exact diluted concentration C_1.
3. Prepare 100 mL of solution of sample (1) with the concentration C_1.
4. Prepare 10 mL of oxidant solution of $PhI(OAc)_2$ and CF_3SO_3H (1:4) and adjust the concentration of oxidant $C_{PhI(OAc)2}$ to be *ca.* 50 times of C_1 or greater.
5. Add 0.1 mL of oxidant solution to the sample solution to form a mixture, and measure

its UV-vis absorption spectrum.

6. Add another 0.1 mL of oxidant solution to the mixture formed in step 5, and measure its UV-vis absorption spectrum.

7. Repeat step 6 and collect all the absorption data.

Chapter 3

Other Work Related to TTFAQs and Conjugated Oligomers

The successful preparation of the 2,6-dialkynyl-substituted TTFAQ core addressed in the previous chapter also provided a versatile building block for making novel organic-based electroactive materials. As an exploratory study in terms of potential applications, a number of newly designed functional molecular wire systems have been targeted in our work. This chapter will present some related work including the synthetic efforts towards an appealing molecular switch as well as a preliminary investigation of a potentially useful synthetic methodology for making butadiynylene-cored conjugated systems via a one-pot mixed homo-cross-coupling protocol.

3.1 Attempted Synthesis of a TTAFQ Based Redox Molecular Switch

In 2006, Hummelen's group reported a significant conductivity difference in an anthraquinone system between the neutral molecule and its reduced species and predicted that it could be a possible redox molecule switch (Figure 3.1).[69] The concept of this anthraquinone based molecular switch is depicted in Figure 3.1. A key feature embodied in this switch system lies in the swift interconversion between a cross-conjugated ("off") state in structure **104** and a fully conjugated ("on") state in structure **105** controlled by oxidation and reduction. The thiol groups located at each end of the molecule were designed to covalently attach the molecule itself to two microelectrodes, so that each molecule of **104** would function as an individual switching device to bias the electric current passing through it. In an analogous idea, a terminal dithiol functionalized TTFAQ

molecular wire **106** (see Figure 3.2) was designed and envisioned by us to show complementary redox-controlled switching performance when the molecule is sandwiched between electrodes. As discussed previously, the anthracene moiety of the TTFAQ is capable of changing from a cross conjugated backbone to a fully conjugated system upon oxidation. Moreover, this change is accompanied by a conformational change from non-planar to planar. Therefore, the molecular conductivity difference between these two states may be larger than that in the anthraquinone system as shown in Figure 3.1; in other words, the on-and-off ratio of the TTFAQ based molecular switch would be greater. In addition, the dramatic conformational change of the molecule in response to reduction/oxidation may also be useful in such devices as "nano-actuators" or "artificial muscles".

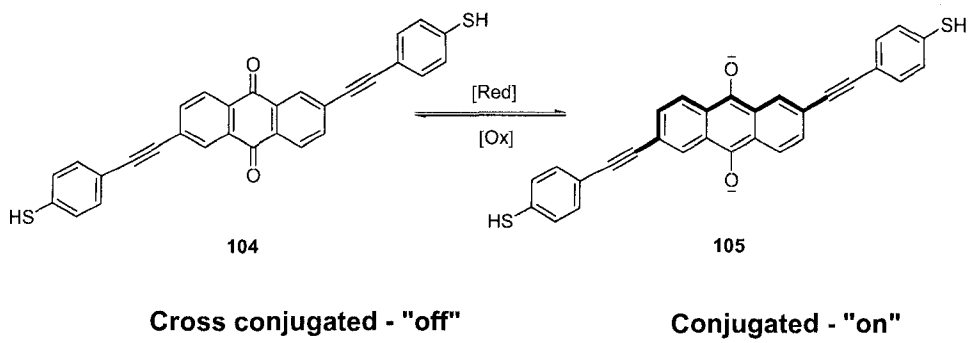

Figure 3.1 A possible oxidation triggered bi-state redox molecular switch.

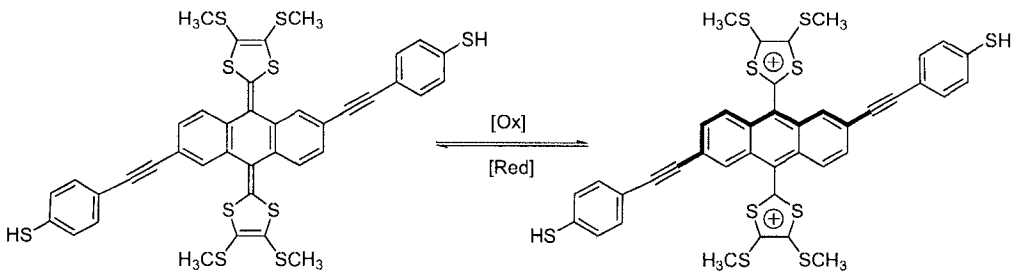

Figure 3.2 Proposed TTFAQ based molecular switch **106**.

The synthesis of compound **106** appeared to be straightforward, since similar TTFAQ derivatives had already been synthesized with ease and high efficiency. Based on our previous results, a synthetic route using Pd-catalyzed coupling reactions was proposed. At first, a protected thiophenyl halide, 4-bromophenyl *tert*-butyl thioether **107** was prepared in order to serve as an essential linker groups for self-assembly on metal electrode surfaces. The synthesis of **107** is outlined in Scheme 3.1.[70] Interestingly, the second step only worked satisfactorily on large scales, whereas attempts in hundred-milligram quantity of starting materials did not give any desired product. It was found that only when the amount of starting material was greater than 0.5 gram would the reaction occur smoothly to afford product **107** with a yield as high as 89%. It is tentatively assumed that good mixing of $AlCl_3$ with other starting materials in bulk quantity is critical to this reaction.

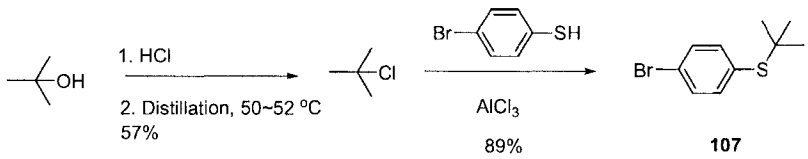

Scheme 3.1 Protection of 4-thiolphenyl bromide with *t*-BuCl.

With aryl bromide **107**, the synthesis of **106** via the Sonogashira coupling reaction should be feasible. However, the attachment of bromide compound **107** to the TTFAQ central core by the Sonagashira reaction (Scheme 3.2) was not successful even though many reaction conditions were investigated. A possible explanation is the extremely low reactivity of **107** towards the Sonagashira reaction. Later it was observed that even the coupling of compound **107** with a much less sterically hindered alkyne, TMSA, using the Pd/Cu catalyst in refluxing THF/Et_3N required more than 48 h to accomplish. Such low reactivity obviously necessitates high temperature for the coupling, which is however not amenable to the heat-sensitive TTFAQ core. Indeed, when the temperature was increased, the TTFAQ starting material quickly disappeared according to TLC analysis, presumably via oxidative decompositions, and the target was not formed.

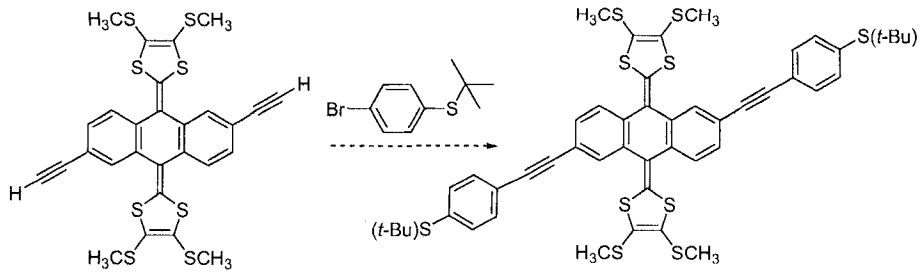

CuI, $PdCl_2(PPh_3)_2$, Et_3N, rt.
CuI, $PdCl_2(PPh_3)_2$, Et_3N, 50 °C
CuI, $PdCl_2(PPh_3)_2$, Et_3N, 40 °C, sonification
CuI, $PdCl_2(PPh_3)_2$, Et_3N,THF, rt.
CuI, $PdCl_2(PPh_3)_2$, toluene, DBU, rt.
CuI, $PdCl_2(PPh_3)_2$, toluene, DBU, reflux
} Disappearance of TTFAQ

CuI, $Pd(PPh_3)_4$, Et_3N, rt. — No reaction

Scheme 3.2 Attempted synthesis of **108** via the Sonogashira coupling.

To avert the reactivity problem in Sonogashira reactions, a Stille coupling was used, which has been useful in the synthesis of sophisticated sulfur containing systems.[70] The Stille coupling required the synthesis of the stannane compound **109** (Scheme 3.3). Unfortunately, the TTFAQ precursor underwent several unwanted side reactions under the basic conditions employed. All of the byproducts were separated and characterized by MS and ^{1}H-NMR, but none of them was identifiable. In fact, when different bases were used, the resulting products were quite different. This indicates that the base was not merely a proton scavenger but an active participant in the reaction. Since the nature of base plays a key role in this reaction, future studies will focus on the use of different base to affect the synthesis. If it is proved to be too difficult to directly connect TTFAQ with the thiolphenyl group at the later stage, especially considering another possibility that sulfur atoms tend to deactivate the Pd catalyst, we may plan strategies other than Pd-catalyzed coupling to prepare the target.

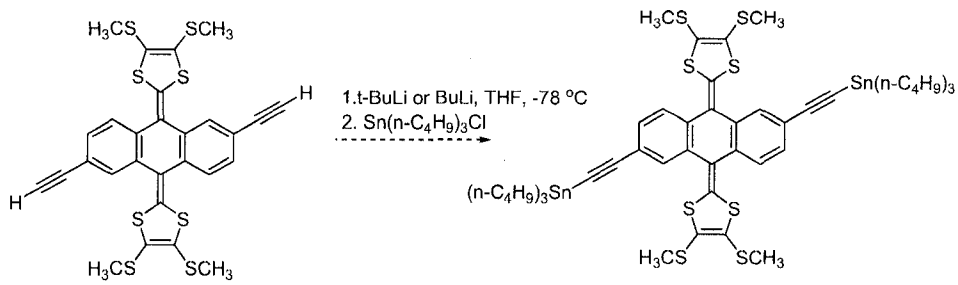

109

Scheme 3.3 Attempted synthesis of a stannyl TTFAQ derivative.

3.2 Strategy and Kinetic Simulations for One-Pot Homo/Cross-Coupling Synthesis of Butadiynylene Cored π-Conjugated Systems

As mentioned in Chapter 2, the extension of a TTFAQ backbone with phenylethynylene units via the Sonagashira reaction also produced an unexpected dimer **101** as a byproduct in significant yields (Scheme 2.11). The formation of such type of dimeric products is not uncommon in many similar Pd-catalyzed coupling cases and can be ascribed to the involvement of a homo-coupling reaction taking place either prior to or after the Pd/Cu catalyzed cross-coupling reaction. Although careful removal of oxygen is supposed to be an efficient way to suppress homo-coupling (if only cross-coupled product(s) is desired), the "side-reaction", on the other hand, may be potentially useful protocol in producing complicated butadiynylene-centered conjugated systems with short synthetic route. It would be much more effective in synthesizing various π-extended molecular wires for such studies as combinatorial oligomer synthesis and structure-property relationships where the electronic and optical properties of various unprecedented ethynylene and butadiynylene based conjugated structures are to be investigated.

As exemplified in Scheme 2.11, the complexity of molecule **101** would have required much more lengthy and tedious efforts to prepare, had a stepwise divergent strategy been implemented. In addition, considering the instability of the TTFAQ core, additional reaction steps would have dramatically lowered the overall yield for certain. In this sense, the surprising one-pot formation of **101** in 20% yield is not inferior to any otherwise designed synthetic route.

The observation of this "side reaction" led to investigations to optimize the yield of dimer **101**. Several reaction conditions were attempted, but variation of the ratio of **86** caused no significant change in the yield of dimer, albeit the yield of the cross-coupled product **100** dropped significantly. TLC analysis showed several other products appeared under these conditions, the identities of which were tentatively assumed to be some higher oligomers.

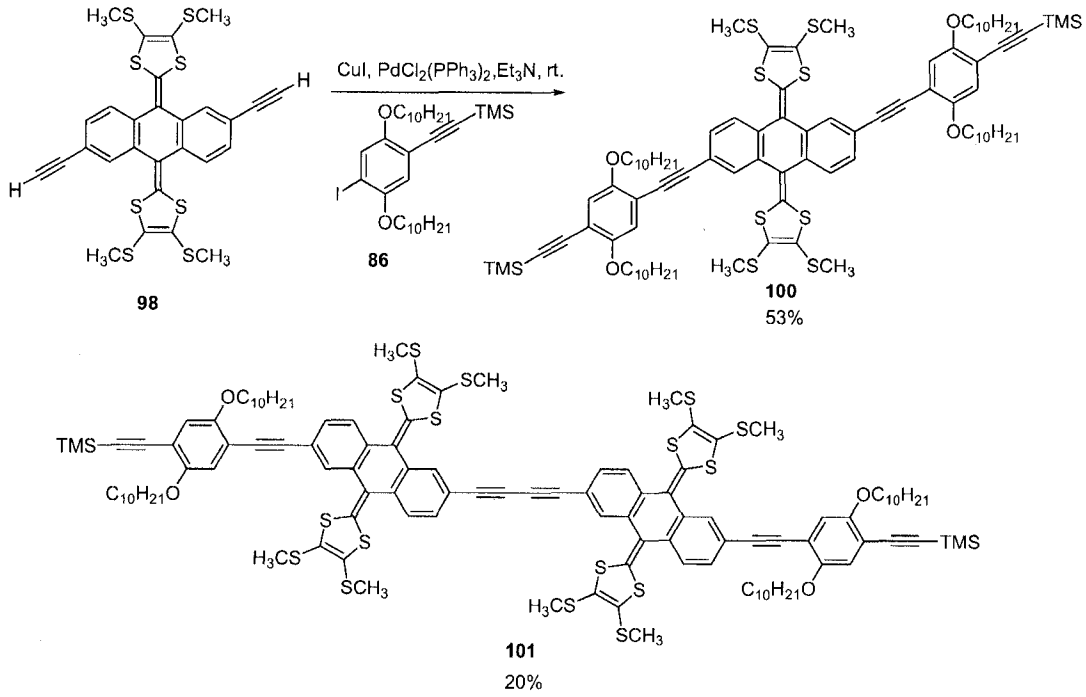

Scheme 2.11. Sonagashira reaction between TTFAQ **98** and iodo compound **86**.

In order to explain these interesting results, the kinetics of such one-pot homo/cross-coupling reactions was studied using computer-assisted kinetic simulations with *Chemical Kinetic Simulator*[71] software package. To perform the simulation appropriately, all significant reaction steps involved in the one-pot reaction need to be adequately defined at first. The possibilities of different reaction pathways could be enormous, however, in our analysis only eight significant pathways were postulated (Figure 3.3) as the input parameters for simulation. Reactions (1) and (2) result in the doubly cross-coupled product (highlighted by the solid-lined box in Figure 3.3) that is normally expected to be the major product in the Sonogashira coupling. Reactions (3)-(7) lead to the formation of homocoupled dimeric product (highlighted by the broken-lined box in Figure 3.3). Moreover, reaction (8) is included in order to take the possibilities of

forming higher oligomers into account. To simplify the analysis, we then made another assumption, that is, all the cross-coupling reactions ((1), (2), (5), (7)) have the same reaction rate constant k_c, and all the homo-coupling reactions ((3), (4), (6), (8)) have the same reaction rate constant k_h.

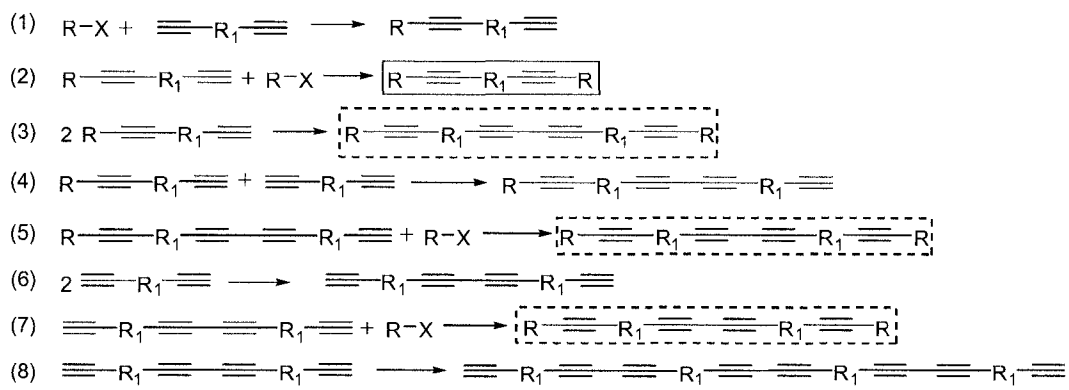

Figure 3.3 Reactions involved in kinetics simulations.

To better understand the analytical results from computer simulations, another important parameter r was defined, which is denoted as the ratio of the reaction rates between the homo- and cross-coupling reactions (*i.e.* $r = k_h/k_c$). With all the parameters specified, the yields of products were calculated via simulation at different concentrations of the halide (R-X). Figure 3.4 gives the relationship between the theoretical yields of the homocoupled dimeric product (Y_h) and the equivalence of halide relative to the dialkyne starting material. Apparently, the correlations in this Figure are drastically different at different r values. In the following examination, however, the trends in these curves will be discussed only in three extreme cases of r values.

(1) The case of $r > 10$. This case encompasses the scenarios that the homo-coupling rate is at least one order of magnitude faster than that of cross-coupling. Under these

conditions, the yield of the homocoupled dimer was found to increase with increasing the equivalence of aryl halide (R-X) until the yield saturates at a maximum value. When Y_h reaches its maximum, the yields of the undesired higher oligomers become nominal, and the yield of doubly cross-coupled product is approximately equal to $(100 - Y_h)\%$. This outcome is suitable for the production of both homocoupled dimer and doubly cross-coupled products. However, it requires a large excess of halide to reach the maximum yield. For example, when $r = 100$ (not shown in Figure 3.4) the maximum yield of homocoupled dimer is calculated at 58% when 100 eq. of aryl halide is applied. With reasonable halide quantities (*ca.* 4 eq.) added, Y_h is however fairly low and the formation of higher oligmers or polymers dominates. This analysis is consistent with the expectation that much faster homo-coupling tends to yield oligomers or polymers as the major products in the reaction. Practically, this condition is not good for making either the doubly cross-coupled or homocoupled dimeric products, because a large amount of aryl halide would be required.

(2) The case of $r < 0.1$. This case is opposite to case 1, *i.e.* the cross-coupling rate is at least one order of magnitude faster than that of homo-coupling. Form Figure 3.4, it can be seen that under such conditions Y_h reaches a maximum when 1 eq. of aryl halide is used. Because the maximal yield of the homocoupled dimer is low, and the reaction mixture contains pronounced higher oligomer species, it is certainly not an ideal condition for preparation of a homocoupled dimeric product. When 2 eq. of aryl halide is applied, this reaction gives the doubly cross-coupled compound as the major product in high yield.

(3) The case of $0.1 < r < 10$. This is the case that really makes the one-pot homo-cross-coupling strategy intriguing. Under these conditions, the homo-coupling and cross-

coupling reactions occur at comparable rates. From Figure 3.4, it can be seen that Y_h reaches its maximum when 1 – 2 eq. of aryl halide is applied. This means that the one-pot reaction will yield both the doubly cross-coupled and homo-coupled dimeric products in moderate to good yields with less amount of starting materials.

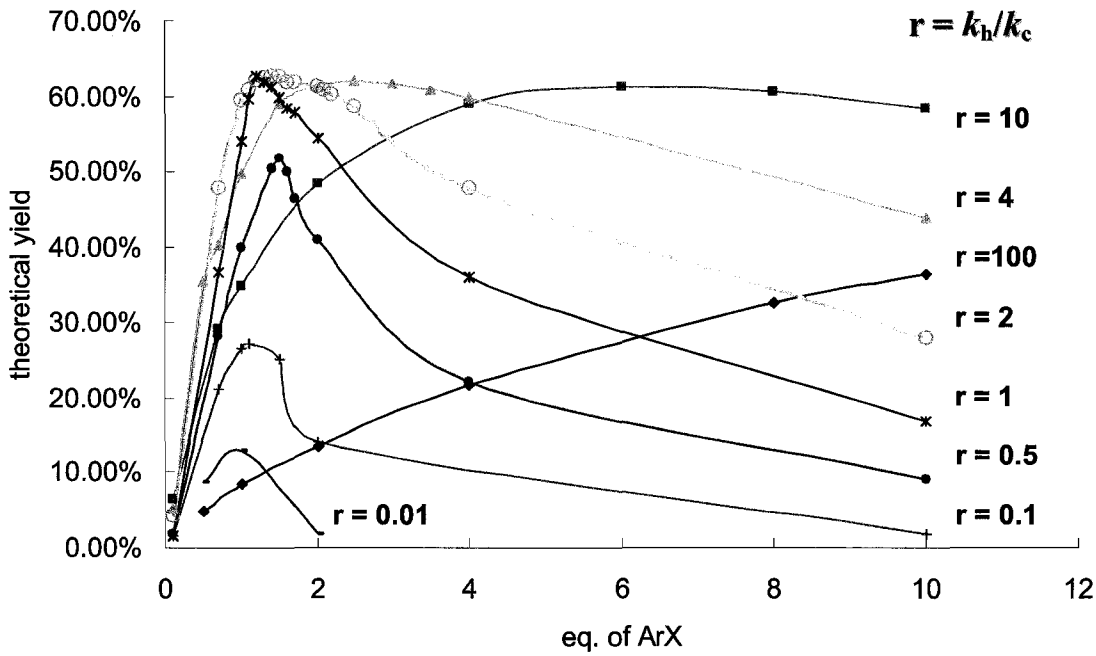

Figure 3.4 Computer-simulated correlation profiles between the yield of homo-coupled dimeric product (Y_h) and the equivalence of halide.

Based on the above analyses, it is reasonable to believe that when k_h and k_c are on a similar scale, it is possible to obtain homo-coupled dimeric product with a reasonable yield in addition to the doubly Sonogashira cross-coupling product. Generally speaking, this one-pot homo-cross-coupling method is not expected to be a very efficient way to synthesize small and simple π-conjugated systems, since alternative stepwise approaches may provide far better yield and efficiency. Nonetheless, when the complexity of the

target compound increases, it might be more powerful than the conventional stepwise divergent oligomer synthesis. As an example, a remarkable OPE/OPV dodecamer (n = 12), **110** (Scheme 3.4), has recently been synthesized in 26% yield along with the doubly cross-coupled product by Ningzhang Zhou in our group.

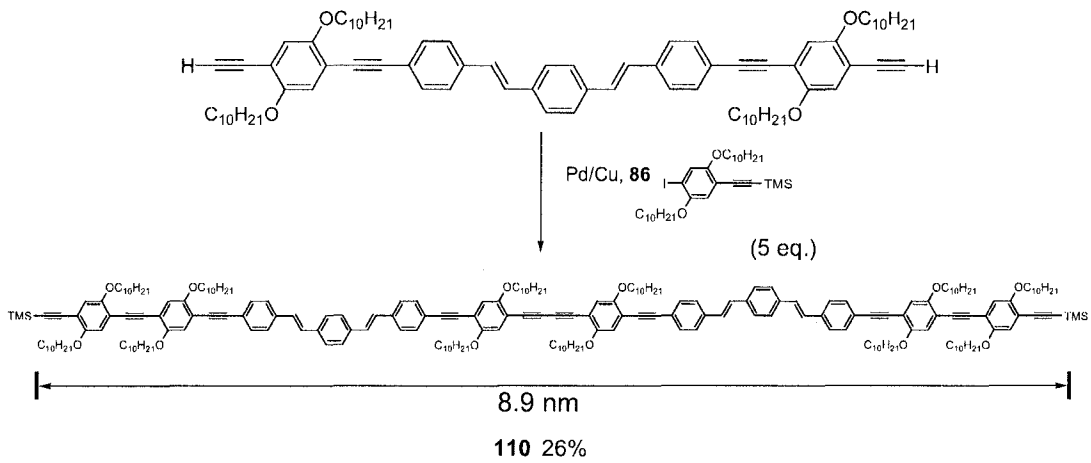

Scheme 3.4 Synthesis of a hybrid OPE/OPV dodecamer **110** via the one-pot homo-cross-coupling protocol.

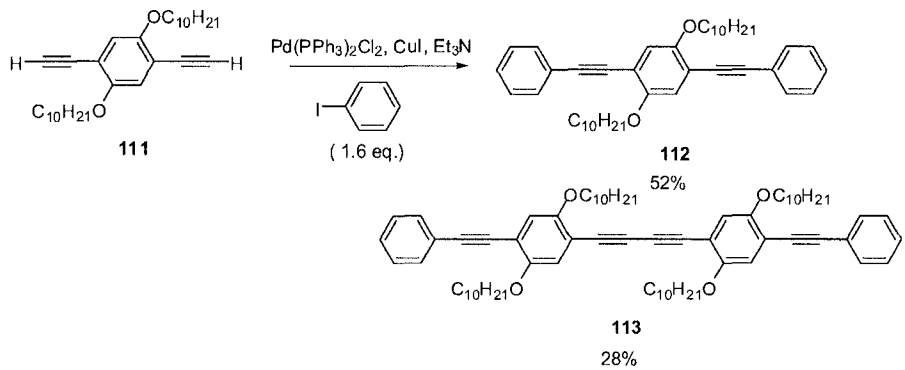

Scheme3.5 Synthesis of butadiynylene **113** via the one-pot homo-cross-coupling protocol

To prove the concept, the synthesis of a butadiynylene cored phenylacetylene

oligomer **113** was performed as shown in Scheme 3.5. In this one-pot reaction, 1.6 eq. of iodobenzene was used under typical Sonogashira coupling conditions without deliberate removal of oxygen. It was postulated that the oxygen participated in this one-pot reaction might increase the reaction rate of homo-coupling. Therefore, the homo- and cross-coupling rates could be of the same order of magnitude. Another method to increase the homo- and cross-coupling reaction rates is to increase the reaction temperature. In our experiment, the product, butadiynylene **113**, was formed in a yield of 28% under typical Sonogashira conditions at room temperature. In the meantime, doubly cross-coupled product **112** was obtained in 52% yield. This outcome is in agreement with the above kinetics analysis, which suggests that the alkyloxy substituted phenylacetylene could be a suitable substrate for implementing the one-pot homo-cross-coupling synthesis. This result also suggests that a further two iterations of the homo-cross-coupling strategy on the phenylacetylene system would afford a series of unprecedented phenyleneacetylene-phenylenebutadiynylene hybrid oligomers such as the decamer and 22-mer as shown in Scheme 3.6. This synthesis, if successful, would considerably speed up the access to some novel one-dimensionally conjugated molecular wires (nanomers).

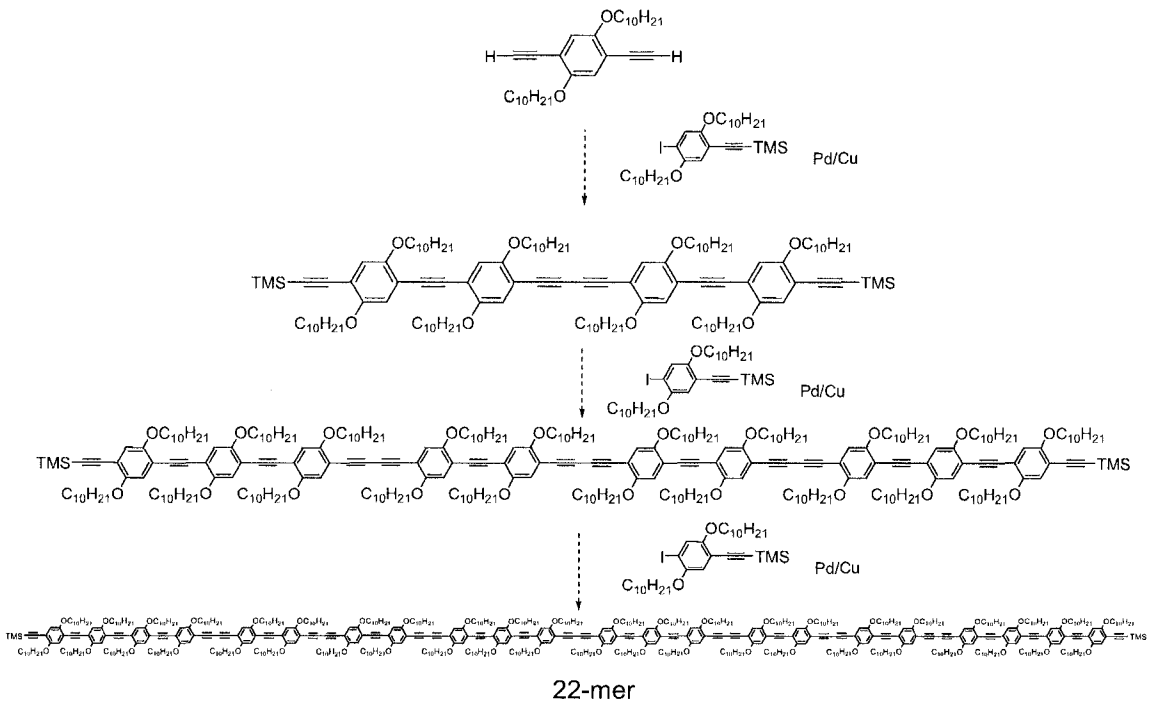

Scheme 3.6 Proposed synthesis of long conjugated oligomer series via iterative one-pot homo-cross-coupling reactions.

3.3 Experimental

General Procedures

All reactions were carried out under a nitrogen atmosphere. All chemicals were of reagent grade. Reaction solvents were dried over appropriate drying agents and used after fresh distillation. Flash column chromatography was performed using 240-400 mesh silica gel. ^{1}H NMR and ^{13}C NMR spectra were measured on the Brunker Advance 500 MHz instrument in $CDCl_3$ using tetramethylsilane as the internal standard. Mass spectra were recorded on a MALDI-TOF spectrometer using a dithranol matrix or obtained from Atmospheric Pressure Chemical Ionization-Mass Spectrometry (GC-MS). Melting points were attained from an uncorrected Fisher-Johns hot stage apparatus.

1-Bromo-4-*t*-butylthiolbenzene (107)

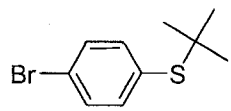

107

To a mixture of 1-bromo-4-thiolbenzene (0.50 g, 2.6 mmol) and *t*-butyl chloride (2 mL, 19 mmol) was added $AlCl_3$ (18 mg, 0.14 mmol). After 30 min, H_2O was added to the reaction. The product was extracted with hexane, washed with H_2O, dried over $MgSO_4$, and evaporated *in vacuo* to afford **107** as a colorless liquid (0.58 g, 2.4 mmol, 91%). ^1H NMR (500 MHz, $CDCl_3$) δ 7.46 (d, J = 8.0 Hz, 2H), 7.39 (d, J = 8.0 Hz, 2H), 1.28 (s, 9H); GC-MS *m/z* calcd for $C_{10}H_{15}BrS$ 246, found 246/244 (20) $[M]^+$, 190/188 (100)

1,4-Bis(decyloxy)-2,5-bis(phenylethynyl)benzene (112) and

1,4-bis(2,5-bis(decyloxy)-4-(phenylethynyl)phenyl)buta-1,3-diyne (113)

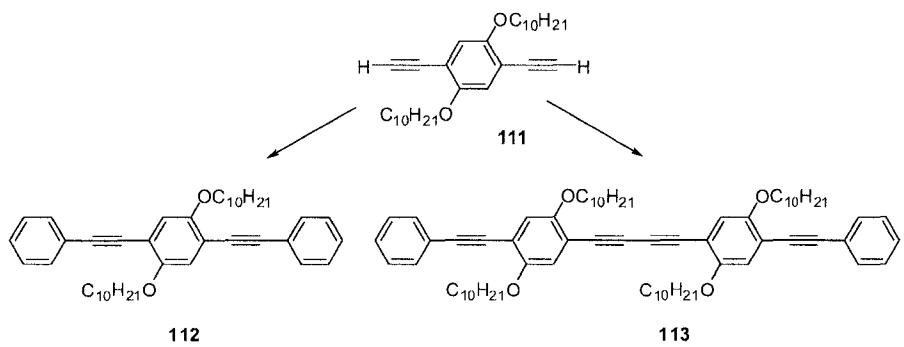

To a mixture of **111** (43 mg, 0.091 mmol), CuI (6 mg, 0.04 mmol) and $PdCl_2(PPh_3)_2$ (7 mg, 0.009 mmol) was added Et_3N (20 mL), and then 4-iodobenzene (30 mg, 0.15 mmol) was added. No deliberate oxygen exclusion was performed. The mixture was stirred overnight at r.t. After the reaction was complete, the mixture was evaporated *in vacuo*, followed by addition of CH_2Cl_2. The mixture was washed by aq. NH_4Cl, H_2O,

dried over $MgSO_4$, and then evaporated *in vacuo*. The crude compound was purified through silica chromatography with 20% CH_2Cl_2 in hexane to afford **112** as a white/pale yellow solid (28 mg, 0.047 mmol, 52%). M.p. 61-62 °C; IR (neat) 3010, 2917, 2851, 2209, 1596, 1486, 1216, 1023 cm^{-1}; ^1H NMR (500 MHz, $CDCl_3$) δ 7.55-7.51 (m, 4H), 7.37-7.31 (m, 6H), 7.02 (s, 2H), 4.03 (t, 4H), 1.87-1.82 (m, 4H), 1.62-1.51 (m, 4H), 1.40-1.25 (m, 24H), 0.87 (t, 6H); ^{13}C NMR (125 MHz, $CDCl_3$) δ 154.1, 132.0, 128.72, 128.66, 123.9, 117.5, 114.5, 95.3, 86.4, 70.1, 32.3, 30.09, 30.01, 29.9, 29.82, 29.78, 26.5, 23.1, 14.5; MALDI-TOF MS (dithranol) *m/z* (%) calcd for $C_{42}H_{52}O_2$ 590.4, found 591.6 (100) $[M+H]^+$.

Compound **113** was then collected as a yellow solid (13 mg, 0.013 mmol, 28%). M.p. 75-76 °C; IR (neat) 3020, 2921, 2849, 2139, 1503, 1389, 1216, 1018 cm^{-1}; ^1H NMR (500 MHz, $CDCl_3$) δ 7.54-7.52 (m, 4H), 7.37-7.34 (m, 6H), 6.99 (d, J = 1.5 Hz, 4H), 4.02-3.98 (m, 8H), 1.86-1.80 (m, 8H), 1.56-1.46 (m, 8H), 1.39-1.20 (m, 48H), 0.89-0.85 (m, 12H); ^{13}C NMR (125 MHz, $CDCl_3$) δ 155.4, 153.9, 132.0, 128.79, 128.74, 123.8, 118.2 117.4, 115.5, 113.0, 95.9, 86.2, 80.0, 79.7, 70.2, 70.1, 32.34, 32.31, 30.13, 30.08, 30.04, 30.02, 30.00, 29.9, 29.79, 29.77, 29.6, 26.5, 26.4, 23.1, 14.5; MALDI-TOF MS (dithranol) *m/z* (%) calcd for $C_{72}H_{98}O_4$ 1026.8, found 1028.5 (33) $[M+H]^+$, 613.2 (100).

Chapter 4

Conclusion

In this thesis work, a novel C_{60}-TTFAQ-C_{60} triad molecule constituted by a highly conjugated 2,6-diethynylated TTFAQ central structure, phenylacetylene bridges, and two ethynylated fullerenyl groups was successfully synthesized. This compound shows no significant electronic interactions among the electroactive groups within the molecule in the ground state; however, it features an intriguingly small HOMO-LUMO bandgap as characterized by electronic absorption spectral and cyclic voltammetric analyses. The photophysical properties of this triad molecule were measured. Substantial fluorescence quenching was observed in steady state emission spectrum in comparison to its TTFAQ precursors. This observation parallels other reported TTFAQ-C_{60} ensemble molecules, suggesting a very fast electron transfer reaction between TTFAQ (donor) to C_{60} (acceptor) could be a dominating pathway in excited state decay. The electronic, optical, and photophysical properties characterized for the C_{60}-TTFAQ-C_{60} compound so far imply its potential applications in photovoltaic devices and photoconducting materials.

A series of TTFAQ based D-A molecules have been synthesized and their spectroscopic and electrochemical properties were investigated. In the ground state, strong electron acceptor (*e.g.* NO_2) can exert very significant influence on the electronic characteristics of the central TTFAQ unit through direct resonance effects. This was mainly reflected by redshifts of the UV-Vis absorption in the high energy region and a

pronounced charge-transfer band in the low energy region. Absorption bands similar to this charge-transfer band were also seen in other TTFAQ reference compounds when they were oxidized into dicationic species. The UV-vis behaviors for these TTFAQ D-A compounds in both the neutral and oxidized forms are essential for future photophysical investigations using nanosecond laser flash photolysis techniques.

A preliminary investigation into a one-pot homo-cross-coupling protocol, aimed at quickly obtaining structurally complex butadiynylene cored π-conjugated oligomeric systems, was undertaken through both theoretical and experimental approaches. Our kinetics simulation study showed that this synthetic strategy would be meaningful only when the homo- and cross-coupling reaction rate constants were of the same order of magnitude. It also suggested that the yield of the butadiynylene product could be optimized by varying the ratio of halide to alkyne. Several synthetic experiments have been performed with product yields consistent with what was predicted by kinetic simulations. Further efforts to explore the synthetic value of this one-pot method are underway.

Finally, a TTFAQ based molecular switch was targeted in this thesis work. Although the synthesis of this molecule has not yet been achieved, the results of this work may pave a way to eventually solve the problem in the future research.

References and Notes

(1) Wudl, F.; Wobschall, D.; Hufnagel, E. J. *J. Am. Chem. Soc.* **1972**, *94* ,670.

(2) Jérome, D. *Chem. Rev.* **2004**, *104*, 5565.

(3) Bryce, M. R. *Adv. Mater.* **1999**, *11*, 11.

(4) Bendikov, M.; Wudl, F.; Perepichka, D. F. *Chem. Rev.* **2004**, *104*, 4891.

(5) Sallé, M.; Jubault, M.; Gorgues, A.; Boubekeur, K.; Fourmigué, M.; Batail, P.; Canadell, E. *Chem. Mater.* **1993**, *5*, 1196.

(6) Roncali, J. *J. Mater. Chem.* **1997**, *7*, 2307.

(7) Kato, R. *Chem. Rev.* **2004**, *104*, 5319.

(8) Pease, A. R.; Jeppesen, J. O.; Stoddart, J. F.; Luo, Y.; Collier, C. P.; Heath. J. R. *Acc. Chem. Res.* **2001**, *34*, 433.

(9) Ho, G.; Heath, J. R.; Kondratenko, M.; Perepichka, D. F.; Arseneault, K.; Pézolet, M.; Bryce, M. R. *Chem. Eur. J.* **2005**, *11*, 2914.

(10) Otero, M.; Herranz, M. Á.; Seoane, C.; Martín, N.; Garín, J.; Orduna, J.; Alcalá, R.; Villacampa, B. *Tetrahedron* **2002**, *58*, 7463.

(11) Moore, A. J.; Bryce, M. R. *Tetraheron Lett.* **1992**, *33*, 1373.

(12) Khanous, A.; Gorgues, A.; Jubault, M. *Tetrahedron Lett.* **1990**, *31*, 7311.

(13) Hansen, T. K.; Lakshmikantham, M. V.; Cava, M. P.; Niziurski-Mann, R. E.; Jensen, F.; Becher, J. *J. Am. Chem. Soc.* **1992**, *114*, 5035.

(14) Bryce, M. R.; Moore, A. J.; Hasan, M.; Ashwell, G. J.; Fraser, A. T.; Clegg, W.; Hursthouse, M. B.; Karaulov, A. I. *Angew. Chem. Int. Ed. Engl.* **1990**, *29*, 1450.

(15) Hurtley, W. R. H.; Smiles, S. *J. Chem. Soc.* **1926**, 2263.

(16) Jigami, T.; Takimiya, K.; Otsubo, T; Aso, Y. *J. Org. Chem.* **1998**, *63*, 8865.

(17) Sugimoto, T.; Awaji, H; Sugimoto, I; Misaki, Y; Kawase, T; Yoneda, S; Yoshida, Z; Kobayashi, T; Anzai, H. *Chem. Mater.* **1989**, *1*, 535.

(18) Yamashita, Y.; Kobayashi, Y. *Angew. Chem. Int. Ed. Engl.* **1989**, *28*, 1052.

(19) Perepichka, D. F.; Bryce, M. R.; Perepichka, I. F.; Lyubchik, S. B.; Christensen, C. A.; Godbert, N.; Batsanov, A. S.; Levillain, E.; McInnes, E. J. L.; Zhao, J. P. *J. Am. Chem. Soc.* **2002**, *124*, 14227.

(20) Watson, W. H.; Eduok, E. E.; Kashyap, R. P.; Krawiec, M. *Tetrahedron* **1993**, *49*, 3035.

(21) Simonsen, K. B.; Zong, K.; Rogers, R. D.; Cava. M. P.; Becher, J. *J. Org. Chem.* **1997**, *62*, 679.

(22) Blower, M. A.; Bryce, M. R.; Devonport, W. *Adv. Mater.* **1996**, *8*, 63.

(23) Li, H.; Jeppensen, J. O.; Levillain, E.; Becher, J. *Chem. Commun.* **2003**, 846.

(24) Schukat, G.; Richter, A. M.; Fanghanel, E. *Sulfur Reports*, **1987**, *7*, 155.

(25) Blanchard, P.; Sallé, M.; Duguay, G.; Jubault, M.; Gorgues, A. *Tetrahedron Lett.* **1992**, *33*, 2685.

(26) Steimecke, G.; Sieler, H. J.; Kirmse, R.; Hoyer, E. Z. *Phosphorus Sulfur* **1979**, *7*, 49.

(27) Svenstrup, N.; Becher, J. *Synthesis* **1995**, 215.

(28) Parg, R. P.; Kilburn, J. D.; Ryan, T. G. *Synthesis* **1994**, 195.

(29) Gorgues, A.; Hudhomme, P.; Sallé, M. *Chem. Rev.* **2004**, *104*, 5151.

(30) Green, D. C. *J. Org. Chem.* **1979**, *44*, 1476.

(31) Simonsen, K. B.; Svenstrup, N.; Lau, J.; Simonsen, O.; Mork, P.; Kristensen, G. J.; Becher, J. *Synthesis* **1996**, 407.

(32) Wang, C.; Guo, Z. X.; Fu, S.; Wu, W.; Zhu, D. *Prog. Polym. Sci.* **2004**, *29*, 1079.

(33) Hirsch, A. *Synthesis* **1995**, 895.

(34) Atienza, C. M.; Fernández, G.; Sánchez, L.; Martín, N.; Dantas, I. S.; Wienk, M. M.; Janssen, R. A. J.; Rahman, G. M. A.; Guldi, D. M. *Chem. Commun.* **2006**, 514.

(35) Herance, J. R.; Peris, E.; Vidal, J.; Bourdelande, J. L.; Marquet, J.; García, H.; *Chem. Mater.* **2005**, *17*, 4097.

(36) Nakamura, E.; Isobe, H. *Acc. Chem. Res.* **2003**, *36*, 807.

(37) Guldi, D. M.; Prato, M. *Acc. Chem. Res.* **2000**, *33*, 695.

(38) Echegoyen, L.; Echegoyen, L. E. *Acc. Chem. Res.* **1998**, *31*, 593.

(39) Shirai, Y.; Zhao, Y.; Cheng, L.; Tour, J. M. *Org. Lett.* **2004**, *6*, 2129.

(40) Diederich, F.; Isaacs, L.; Philp, D. *Chem. Soc. Rev.* **1994**, *23*, 243.

(41) González, S.; Martín, N.; Guldi, D. M. *J. Org. Chem.* **2003**, *68*, 779.

(42) Díaz, M. C.; Herranz, M. A.; Illescas, B. M.; Martín, N.; Godbert, N.; Bryce, M. R.; Luo, C.; Swartz, A.; Anderson, G.; Guldi, D. M. *J. Org. Chem.* **2003**, *68*, 7711.

(43) Nishikawa, H.; Kojima, S.; Kodama, T.; Ikemoto, I.; Suzuki, S.; Kikuchi, K.; Fujitsuka, M.; Luo, H.; Araki, Y.; Ito, O. *J. Phys. Chem. A* **2004**, *108*, 1881.

(44) Maggini, M.; Scorrano, G.; Prato, M. *J. Am. Chem. Soc.* **1993**, *115*, 9798.

(45) Prato, M.; Maggini, M. *Acc. Chem. Res.* **1998**, *31*, 519.

(46) Martín, N.; Pérez, I.; Sánchez, L.; Seoane, C. *J. Org. Chem.* **1997**, *62*, 5690.

(47) Martín, N.; Sánchez, L.; Guldi, D. M. *Chem. Commun.* **2000**, 113.

(48) Herranz, M. A.; Martín, N. *Org. Lett.* **1999**, *1*, 2005.

(49) Herranz, M. A.; Martín, N.; Ramey, J.; Guldi, D. M. *Chem. Commun.* **2002**, 2968.

(50) Giacalone, F.; Segura, J. L.; Martín, N.; Guldi, D. M. *J. Am. Chem. Soc.* **2004**, *126*, 5340.

(51) Atienza, C.; Martín, N.; Wielopolski, M.; Haworth, N.; Clark, T.; Guldi, D. M. *Chem. Commun.* **2006**, 3202.

(52) Sánchez, L.; Sierra, M.; Martín, N.; Guldi, D. M.; Wienk, M. W.; Janssen, R. A. J. *Org. Lett.*, **2005**, *7*, 1691.

(53) Herranz, M. A.; Illescas, B.; Martín, N.; Luo, C.; Guldi, D. M. *J. Org. Chem.* **2000**, *65*, 5728.

(54) Sánchez, L.; Pérez, I.; Martín, N.; Guldi, D. M. *Chem. Eur. J.* **2003**, *9*, 2457.

(55) Kodis, G.; Liddell, P. A.; de la Garza, L.; Moore, A. L.; Moore, T. A.; Gust, D. *J. Mater. Chem.* **2002** *12*, 2100.

(56) Hodge, P.; Power, G. A.; Rabjohns, M. A. *Chem. Commun.* **1997**, 73.

(57) Yang, J.; Dass, A.; Rawashdeh, A. M. M.; Sotiriou-Leventis, C.; Panzner, M. J.; Tyson, D. S.; Kinder, J. D.; Leventis, N. *Chem. Mater.* **2004**, *16*, 3457.

(58) The unknown compound was not mono substituted product. A mixture of this compound and dibromide 6 was subjected to another Sandermayer reaction but no reaction was observed.

(59) Moore, A. J.; Bryce, M. R. *Synthesis* **1991**, 26.

(60) Heinrich, A. PhD thesis **2003**.

(61) MeCN was added by happen.

(62) Christensen, C. A.; Bryce, M. R.; Batsanov, A. S.; Becher, J. *Org. Biomol. Chem.* **2003**, *1*, 511.

(63) Kwang-Fu Shen, C.; Duong, H. M.; Sonmez, G.; Wudl, F. *J. Am. Chem. Soc.* **2003**, *125*, 16206.

(64) Bauld, N. L.; Bellville, D. J.; Pabon, R.; Chelsky, R.; Green, G. *J. Am. Chem. Soc.* **1983**, *105*, 2378.

(65) Zhao, Y.; Shirai, Y.; Slepkov, A. D.; Cheng, L.; Alemany, L. B.; Sasaki, T.; Hegmann, F. A.; Tour, J. M. *Chem. Eur. J.* **2005**, *11*, 3643.

(66) Chen, G.; Zhao, Y. *Tetrahedron Lett.* **2006**, *47*, 5069.

(67) Gautier, N.; Samuel, R.; Sahin, Y.; Levillain, E.; Leroy-Lhez, S.; Hudhomme, P. Org. Lett. **2004**, *6*, 1569.

(68) Giffard, M.; Mabon, G.; Leclair, E.; Mercier, N.; Allain, M.; Gorgues, A.; Molinié, P.; Neilands, O.; Krief, P.; Khodorkovsky V. *J. Am. Chem. Soc.* **2001**, *123*, 3852.

(69) van Dijk, E. H.; Myles, D. J. T.; van der Veen, M. H.; Hummelen, J. C. *Org. Lett.* **2006**, *8*, 2333.

(70) Pinault, T.; Cherioux, F.; Therrien, B.; Suss-Fink, G. *Heteroatom Chem.* **2004**, *15*, 121.

(71) The copyright of the software belongs to IBM.

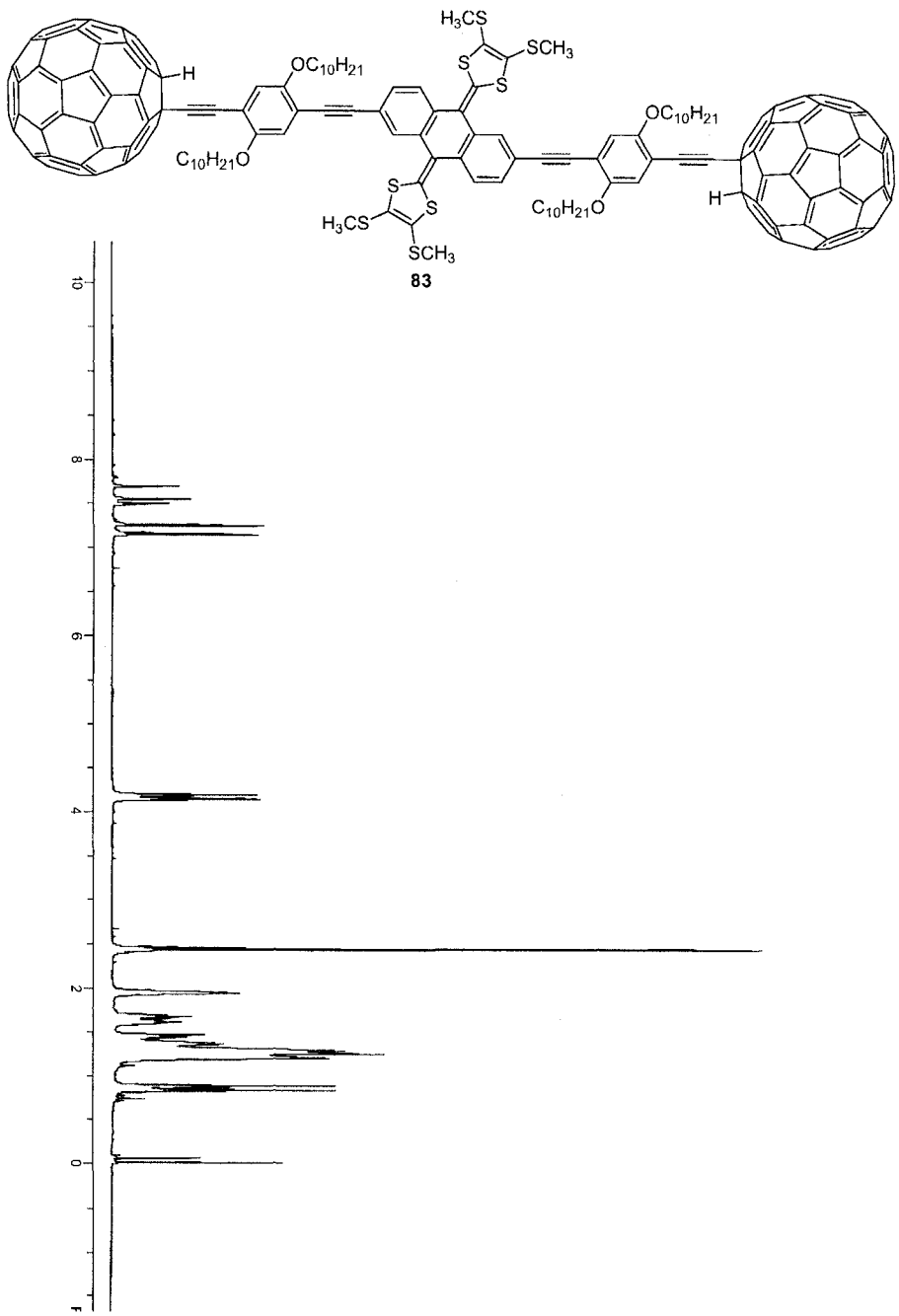

Figure A.1 ^{1}H NMR spectrum for **83**.

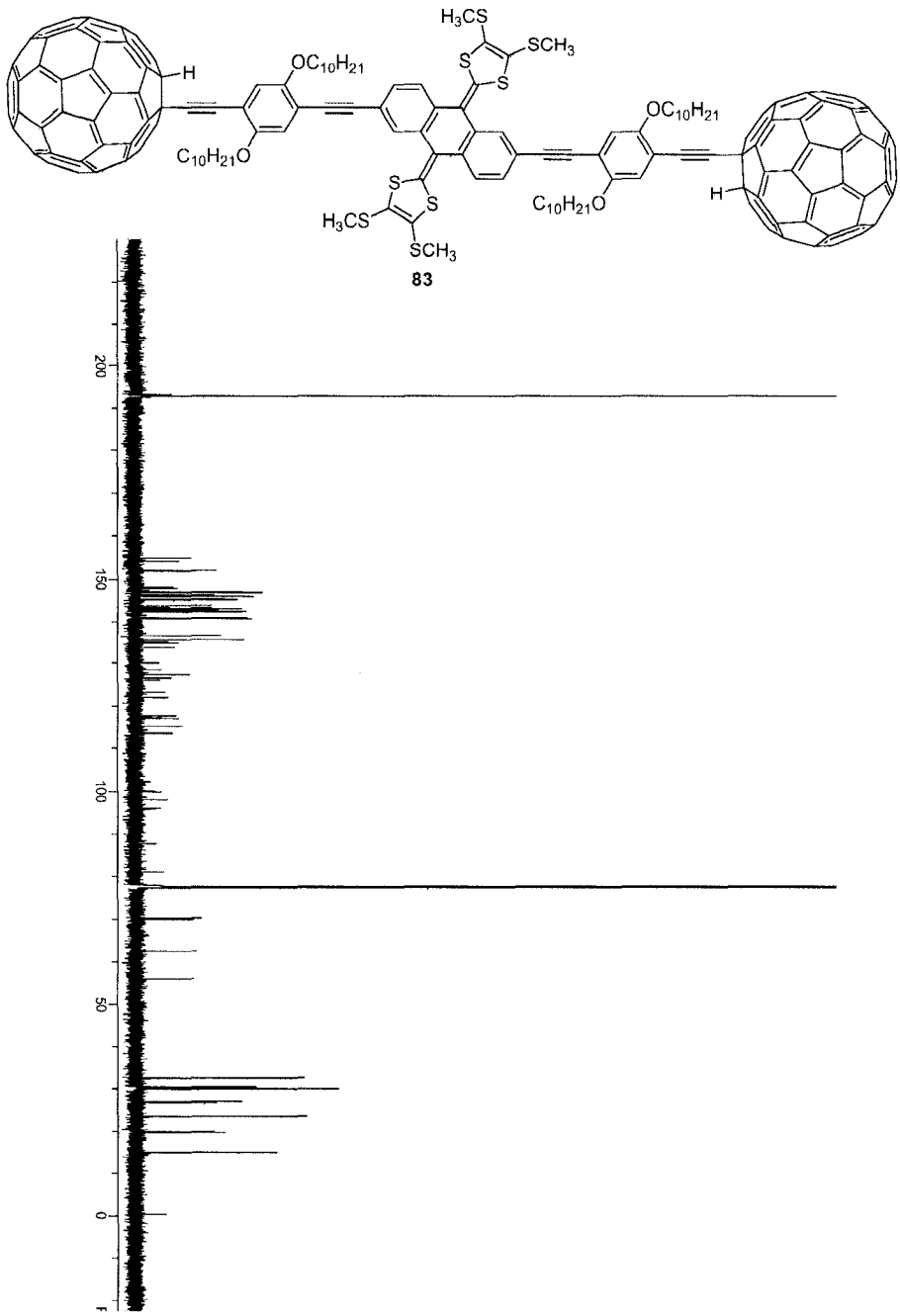

Figure A.2 ^{13}C NMR spectrum for **83**.

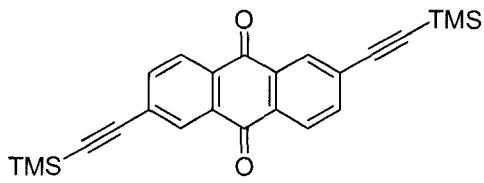

84

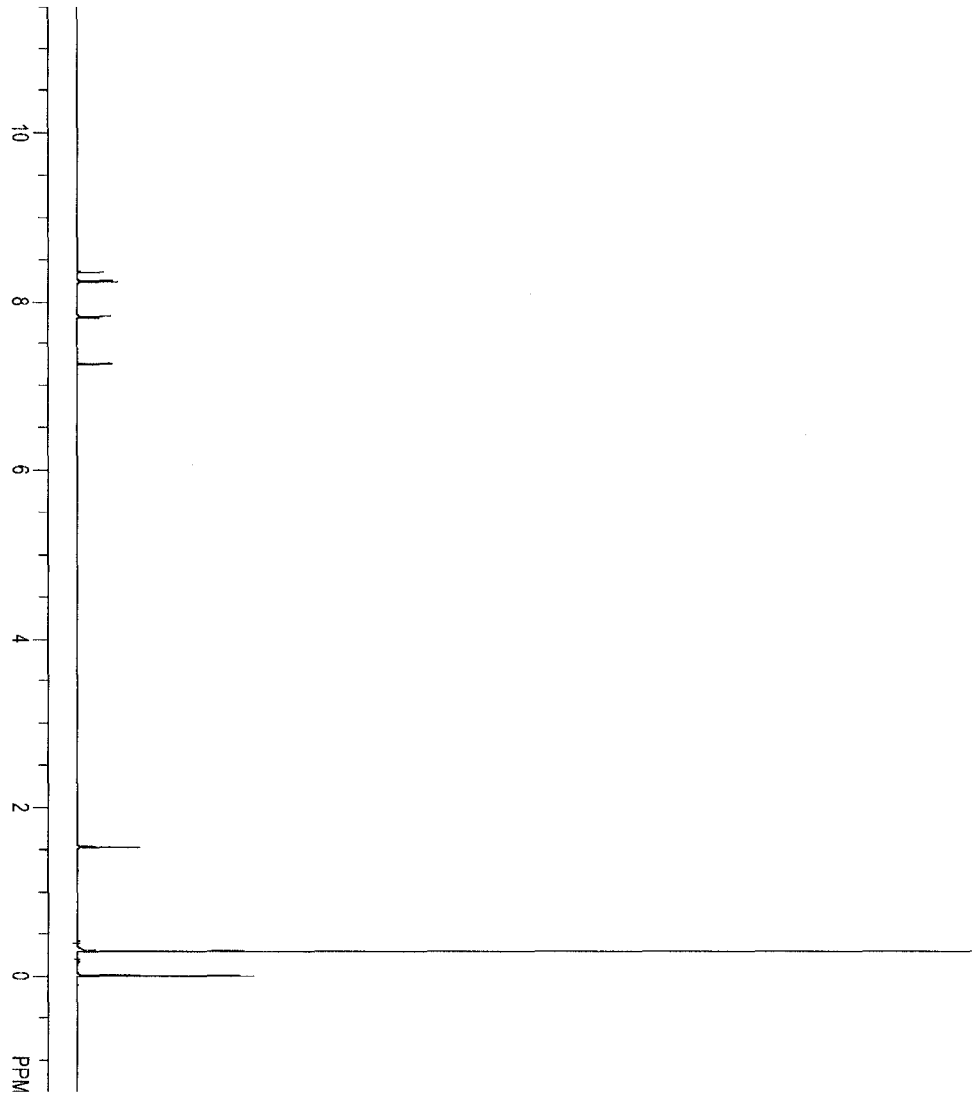

Figure A.3 ^{1}H NMR spectrum for **84**.

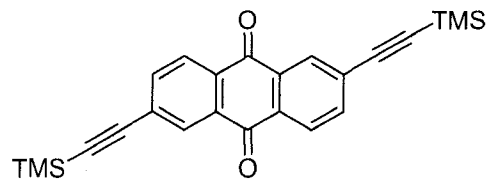

84

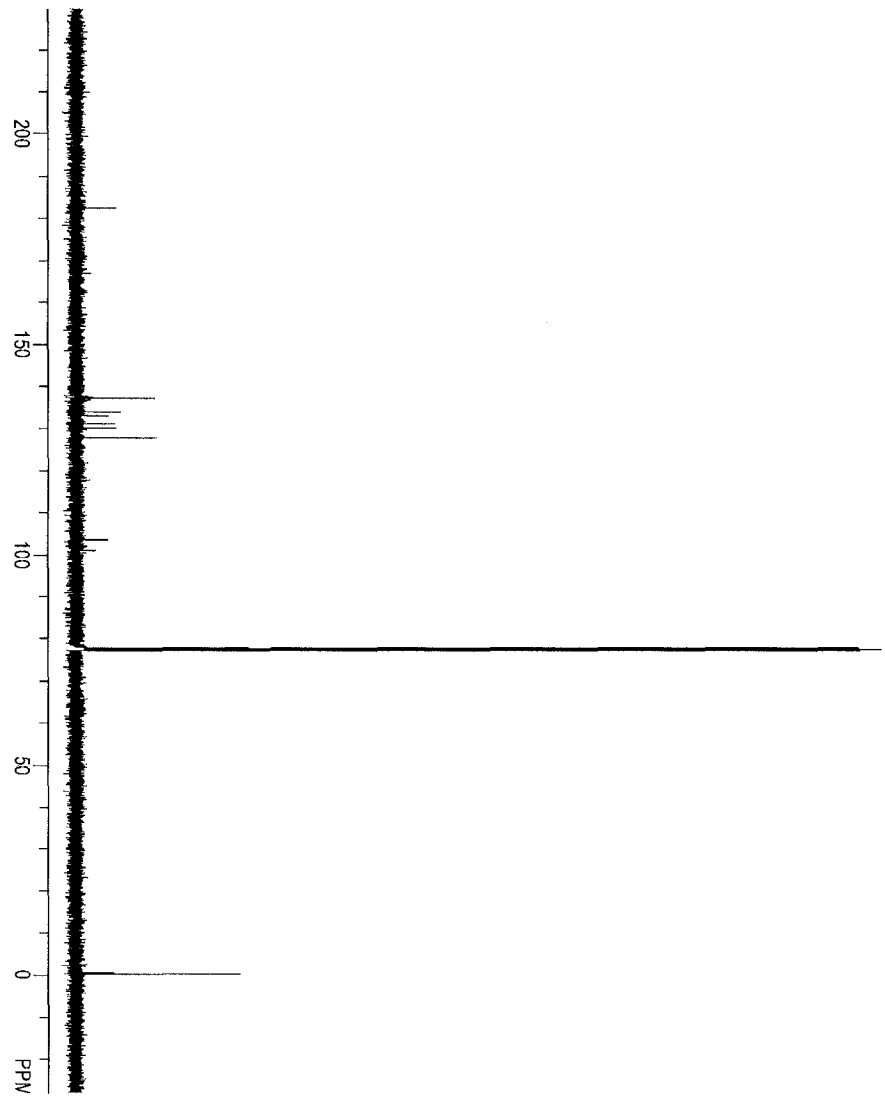

Figure A.4 ^{13}C NMR spectrum for **84**.

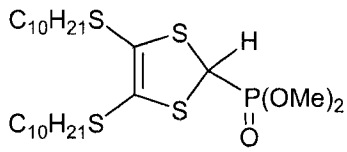

85a

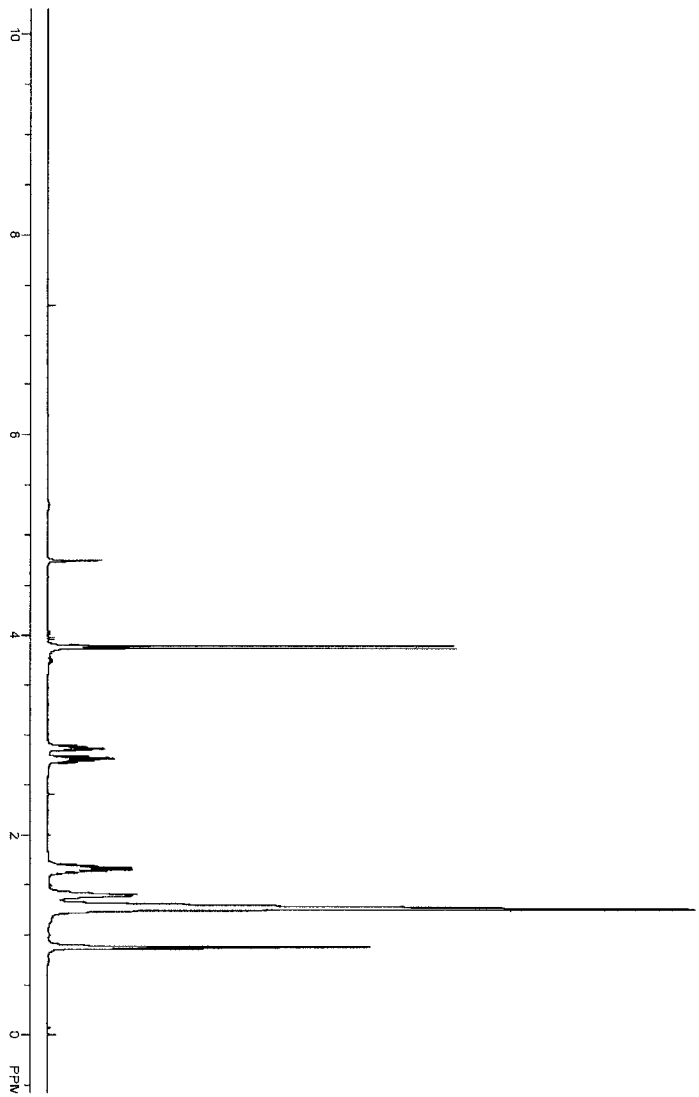

Figure A.5 ^{1}H NMR spectrum for **85a**.

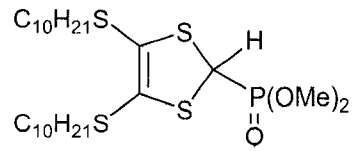

85a

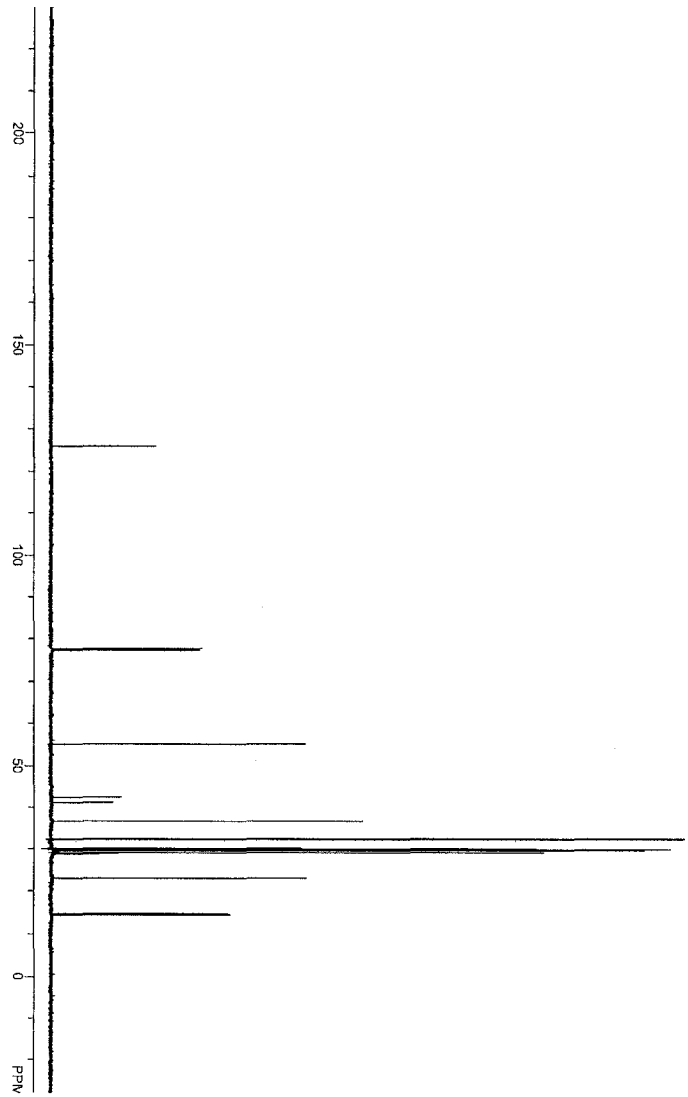

Figure A.6 ^{13}C NMR spectrum for **85a**.

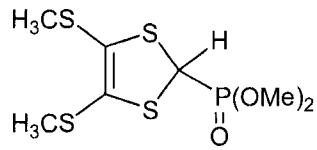

85b

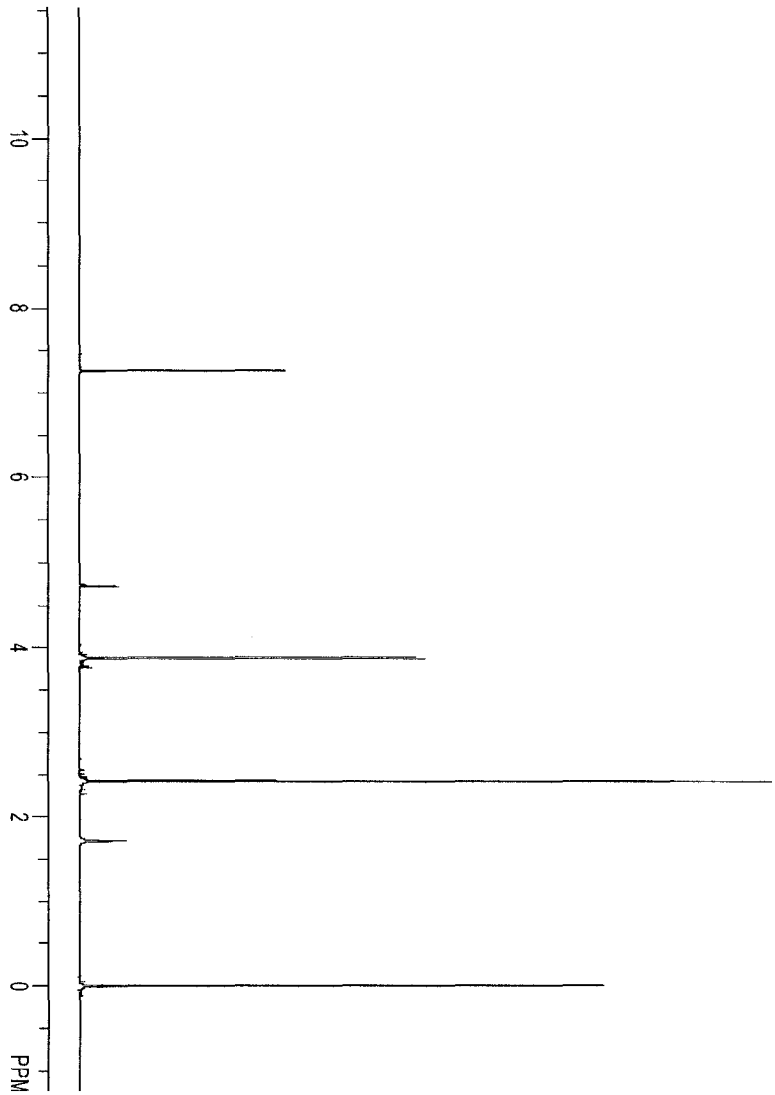

Figure A.7 ^{1}H NMR spectrum for **85b**.

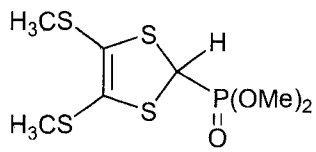

85b

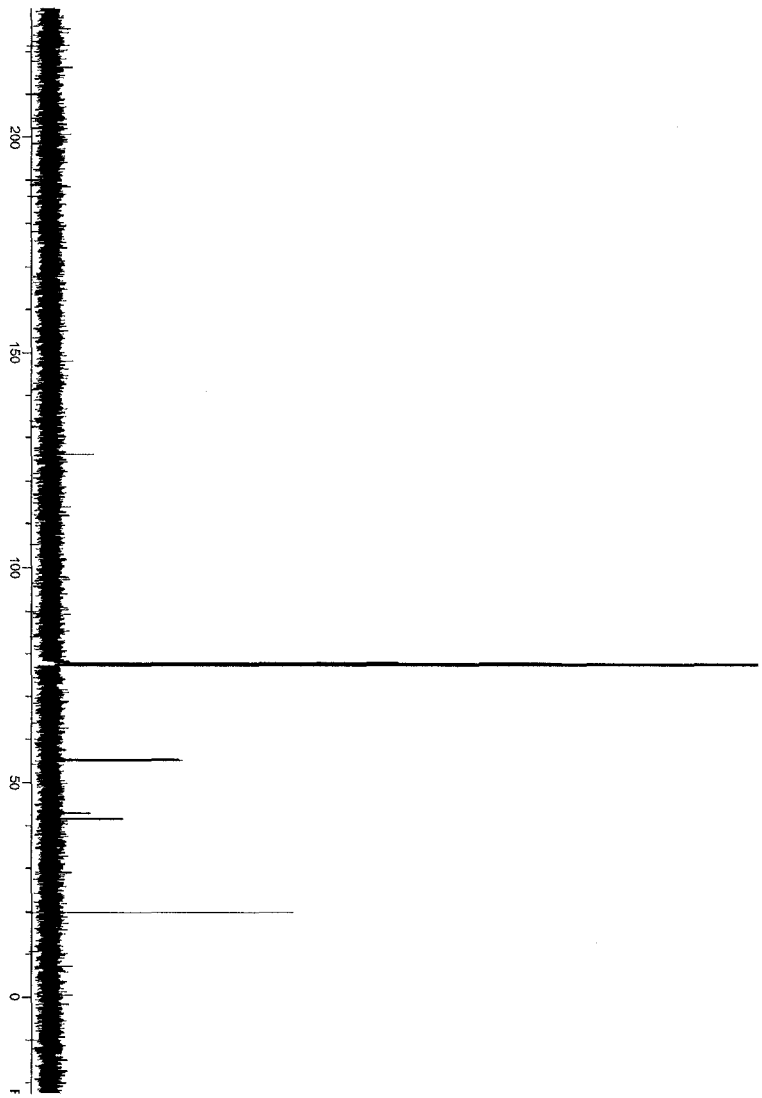

Figure A.8 ^{13}C NMR spectrum for **85b**.

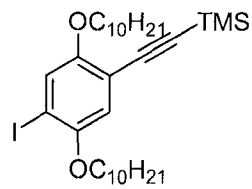

86

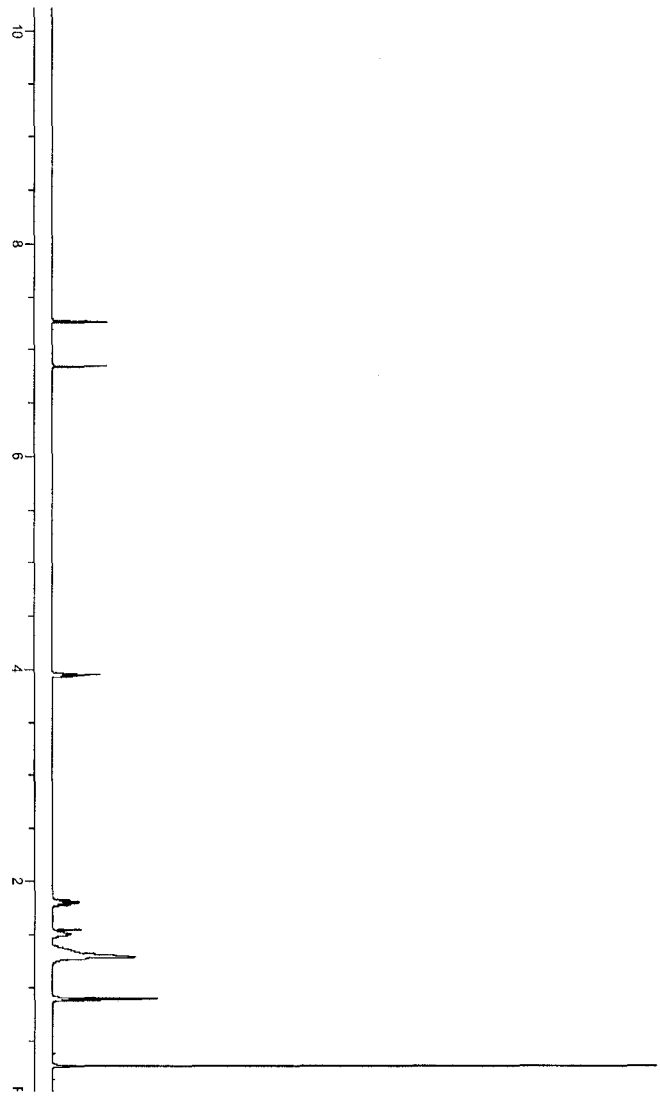

Figure A.9 ^{1}H NMR spectrum for **86**.

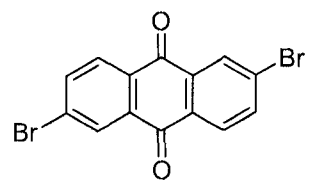

88

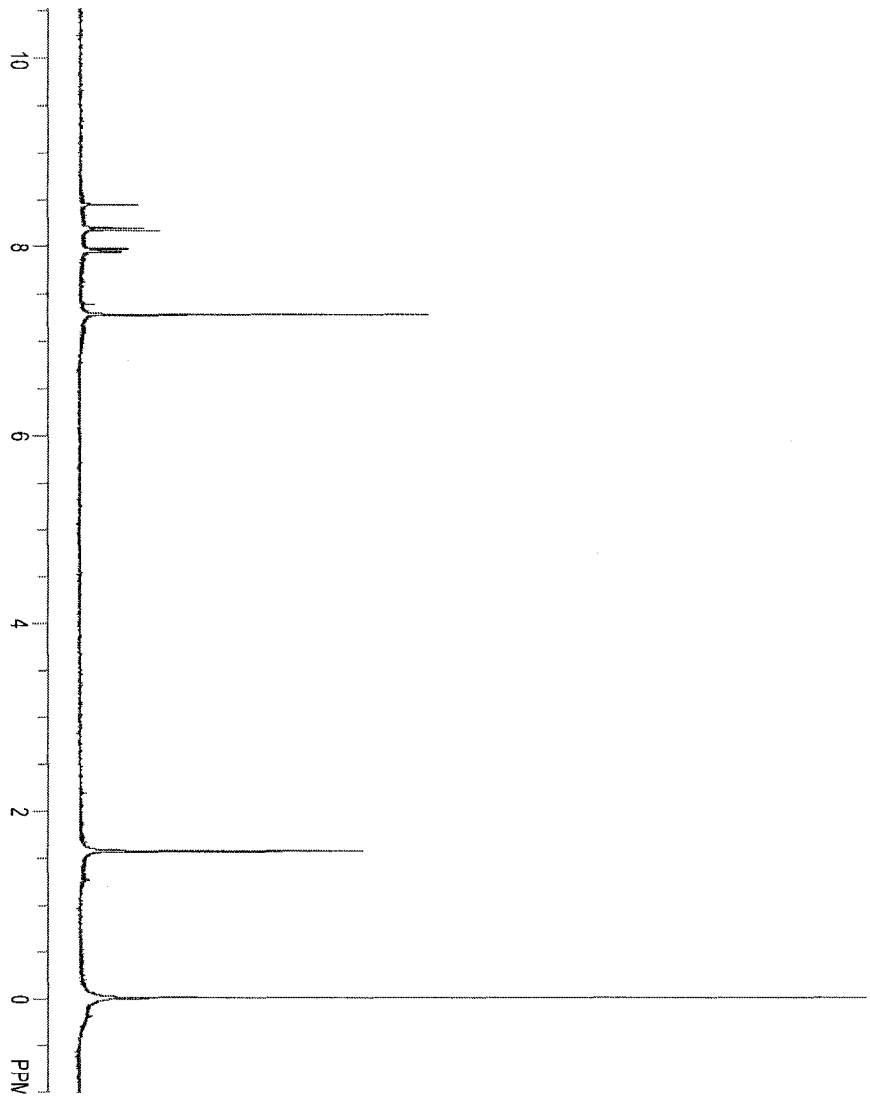

Figure A.10 ^{1}H NMR spectrum for **88**.

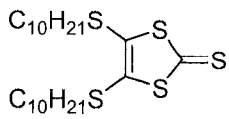

90a

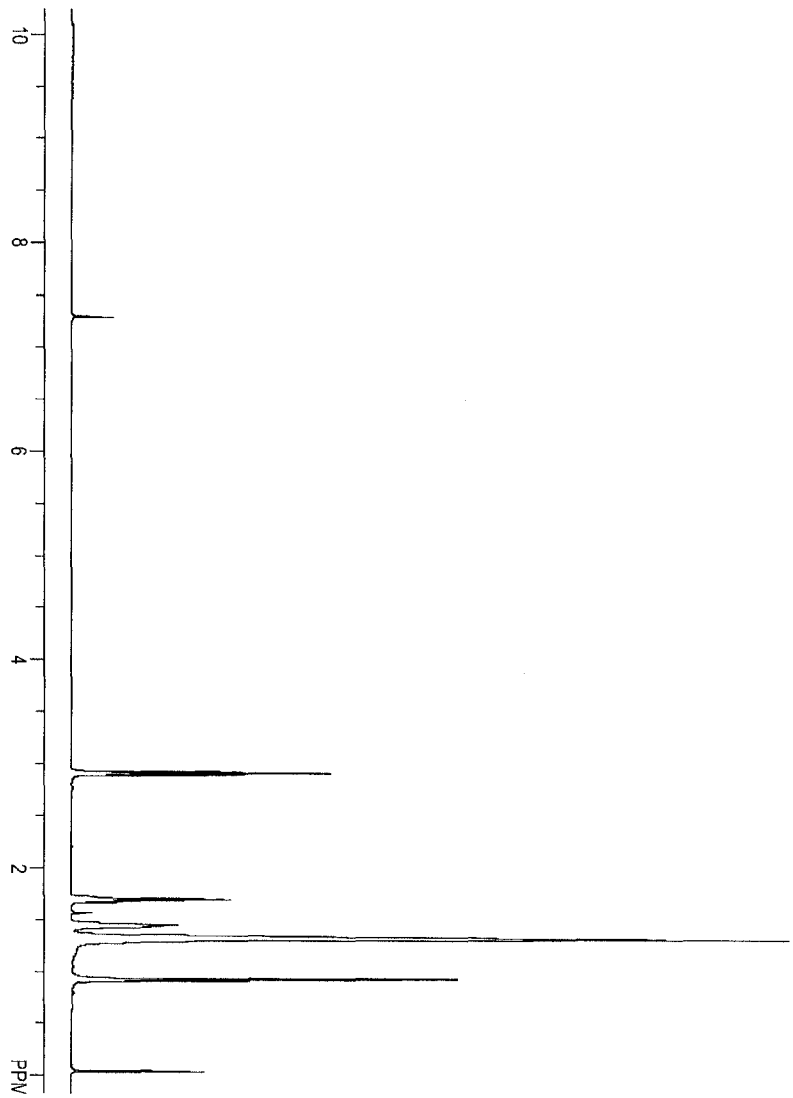

Figure A.11 ^{1}H NMR spectrum for **90a**.

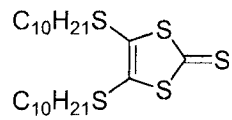

90a

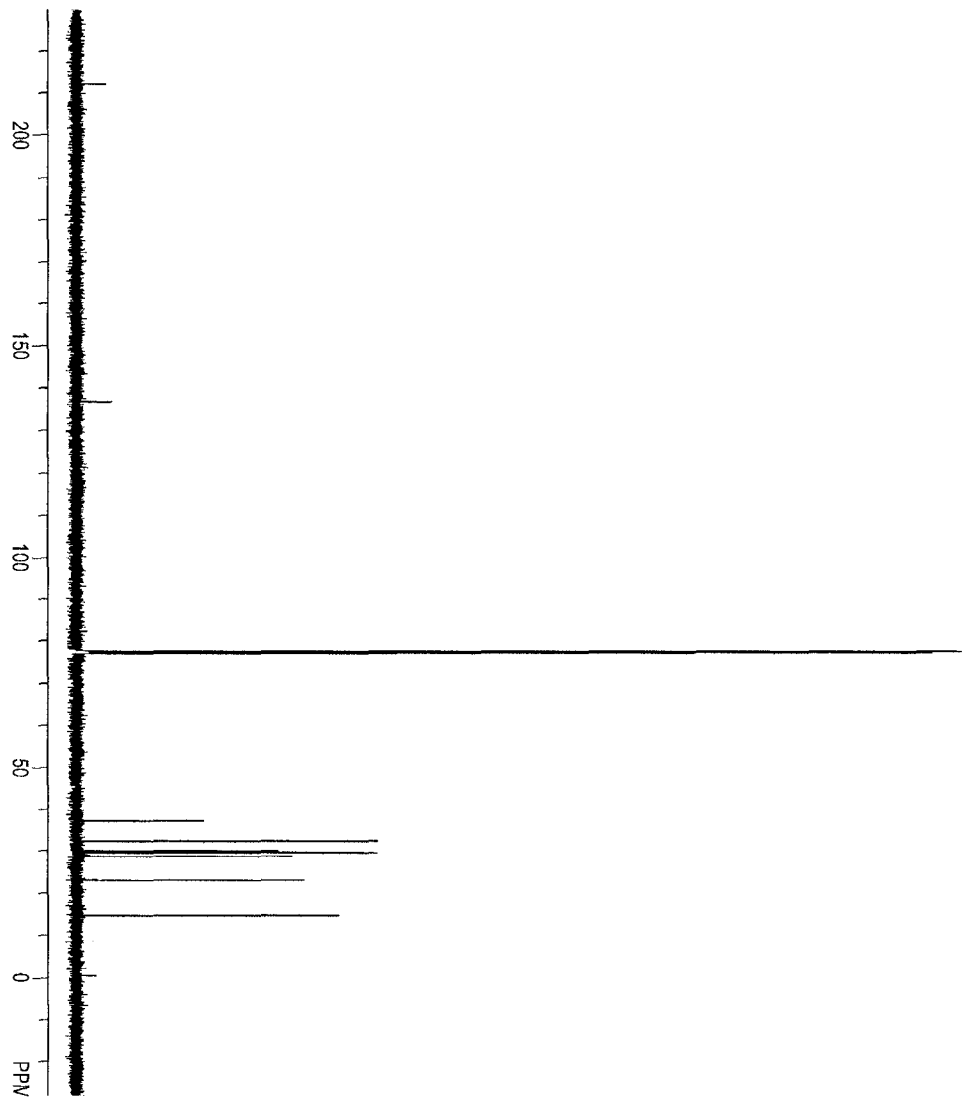

Figure A.12 ^{13}C NMR spectrum for **90a**.

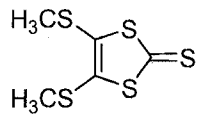

90b

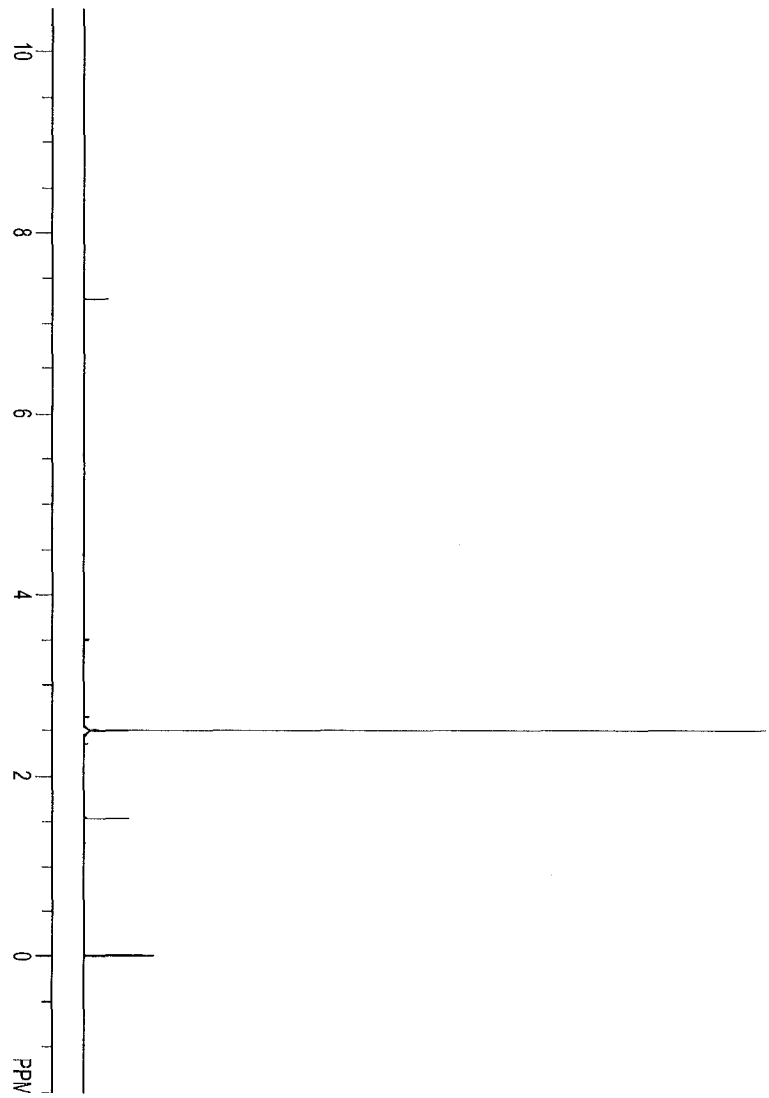

Figure A.13 ^{1}H NMR spectrum for **90b**.

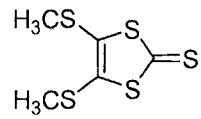

90b

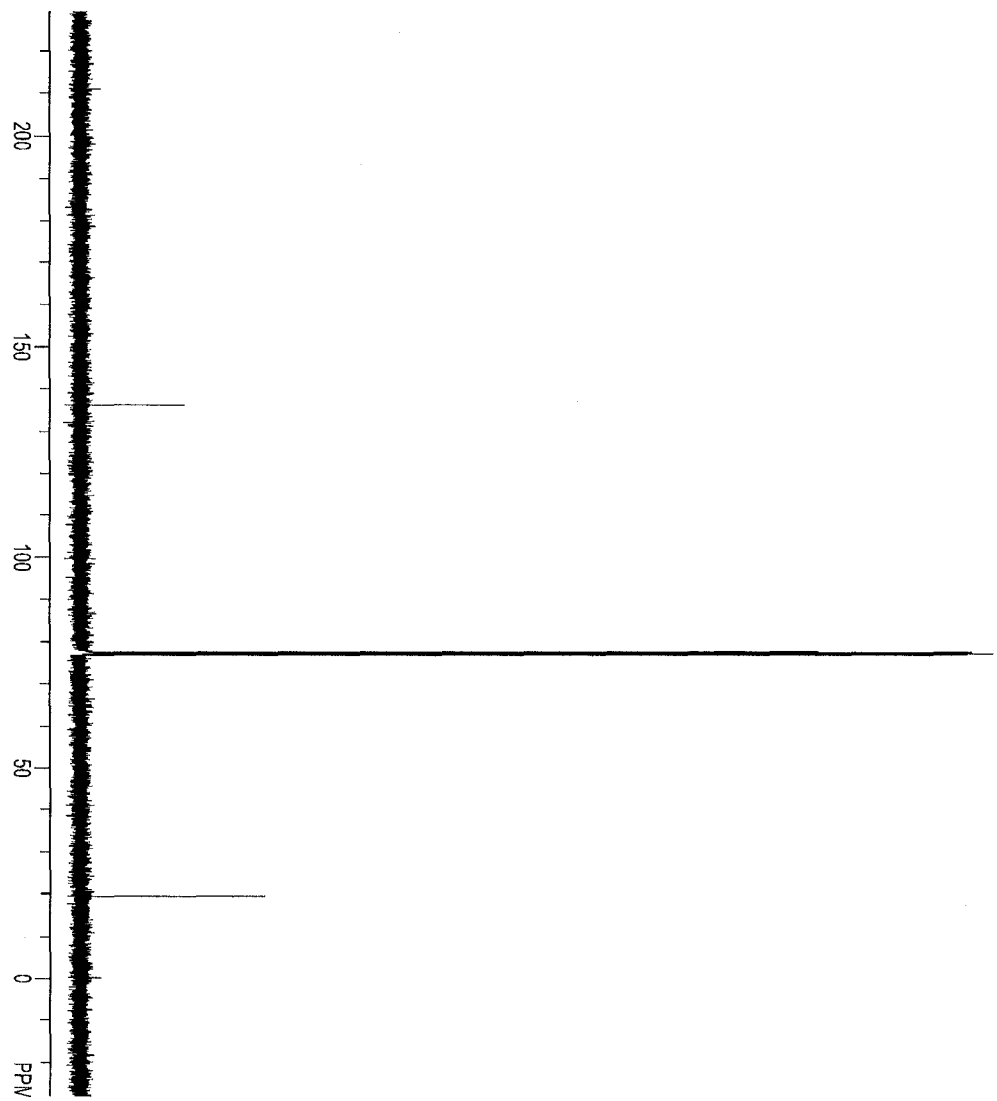

Figure A.14 ^{13}C NMR spectrum for **90b**.

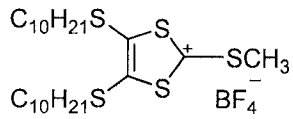

91a

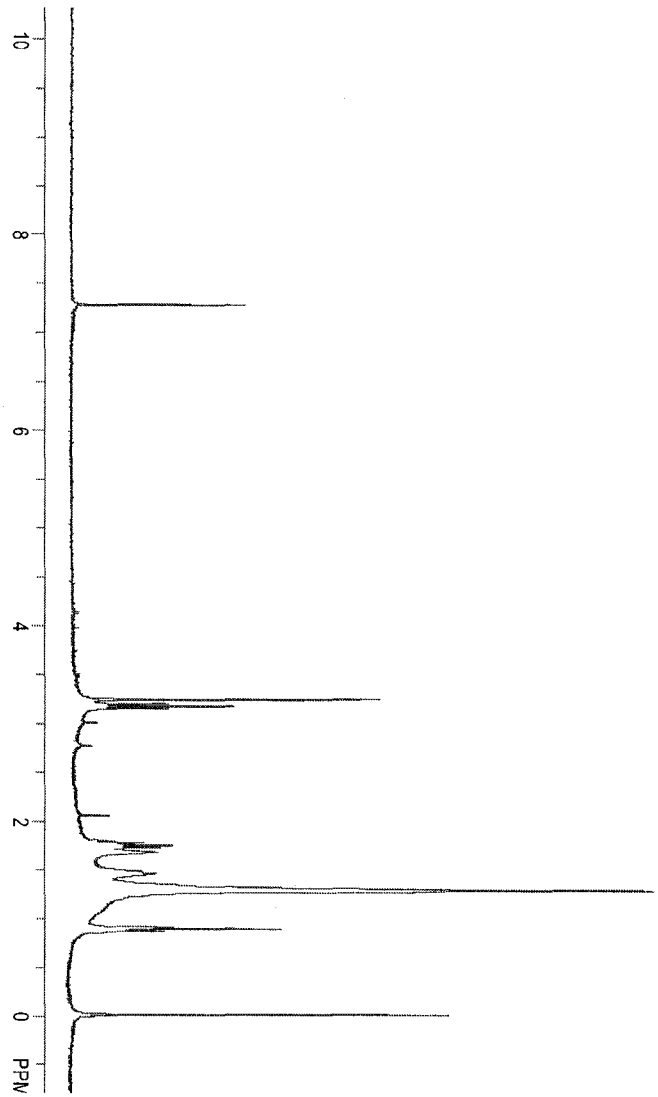

Figure A.15 ^{1}H NMR spectrum for **91a**.

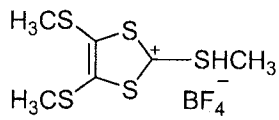

91b

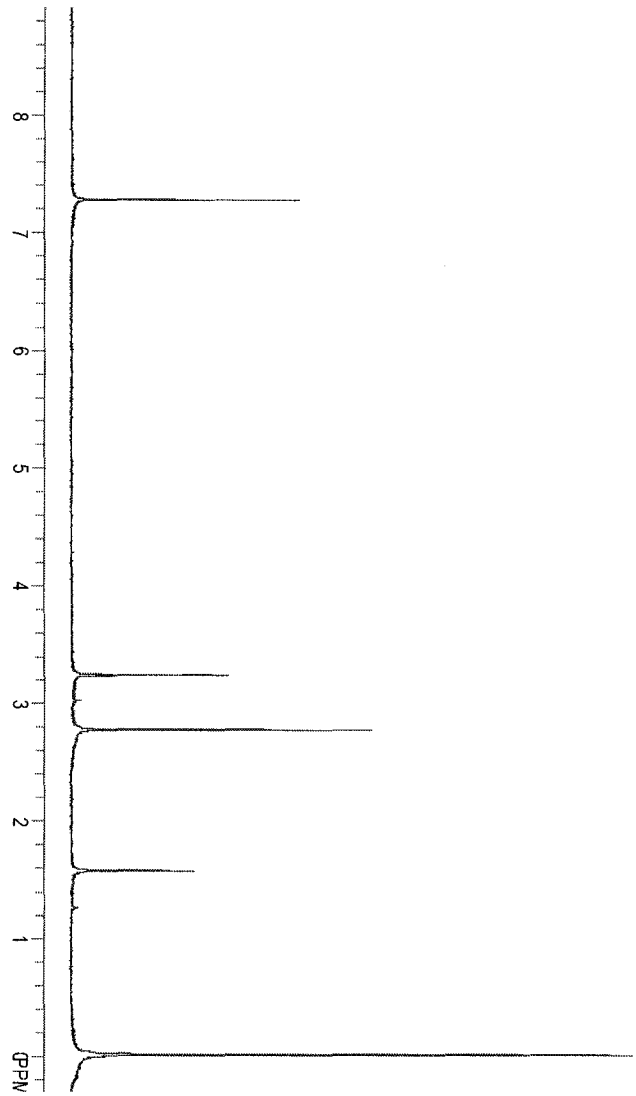

Figure A.16 ^{1}H NMR spectrum for **91b**.

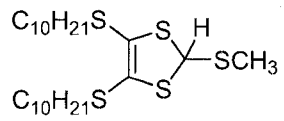

92a

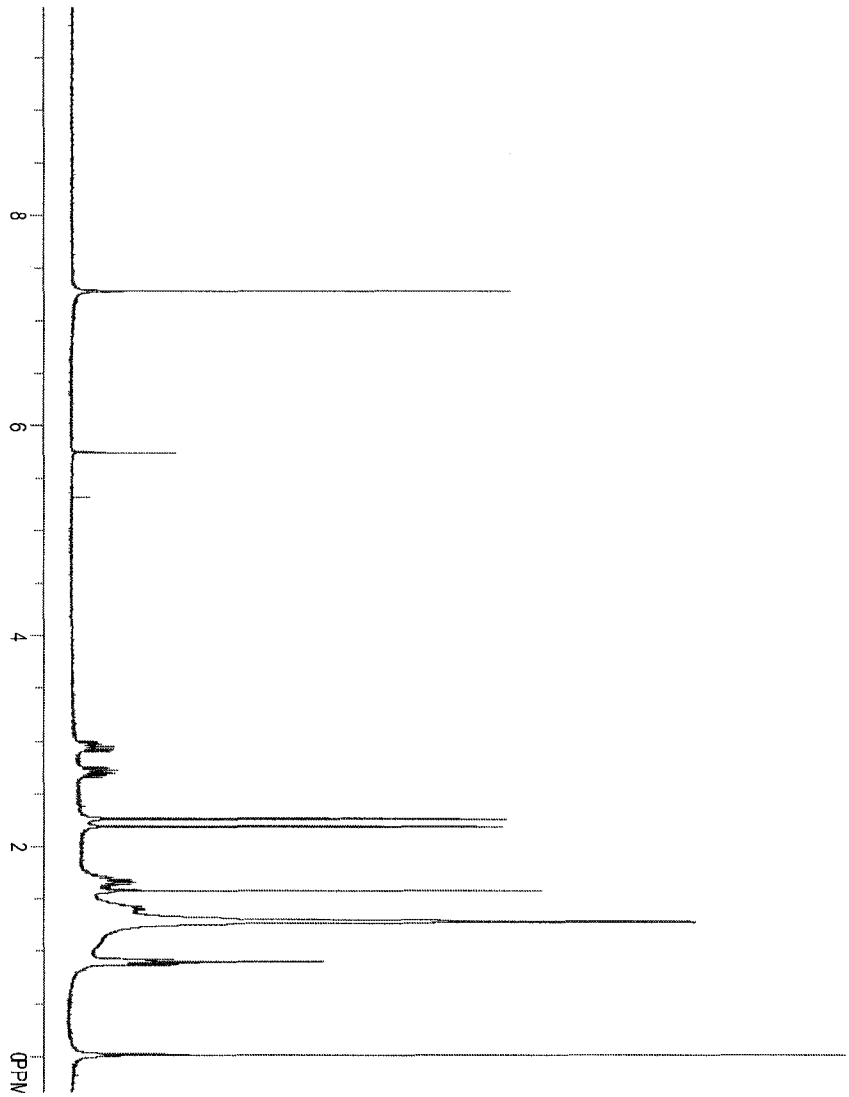

Figure A.17 ^{1}H NMR spectrum for **92a**.

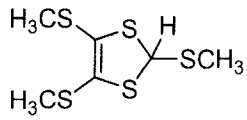

92b

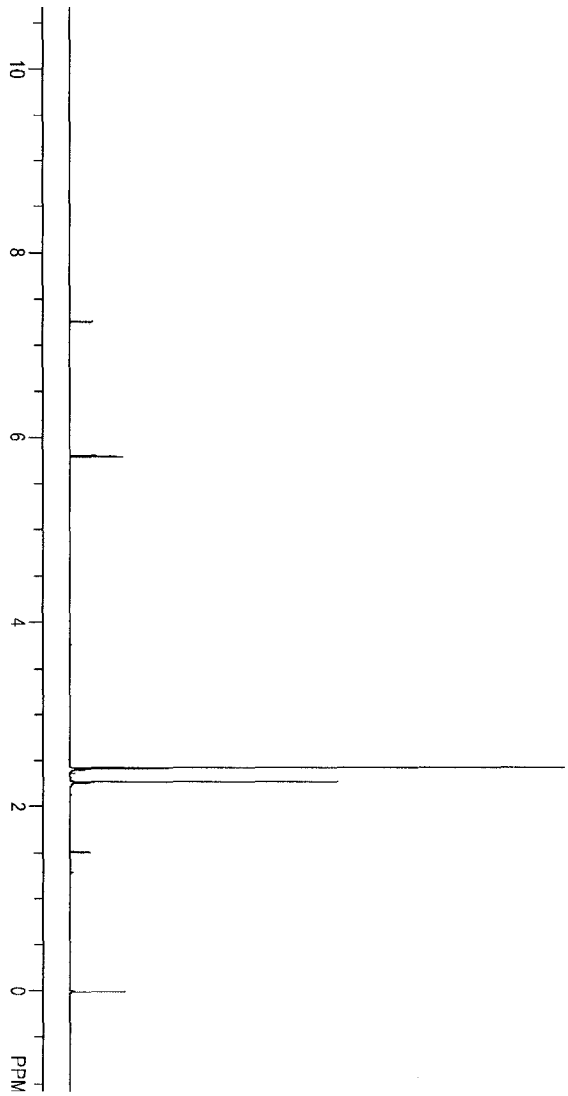

Figure A.18 ^{1}H NMR spectrum for **92b**.

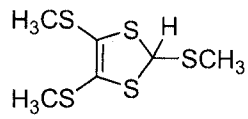

92b

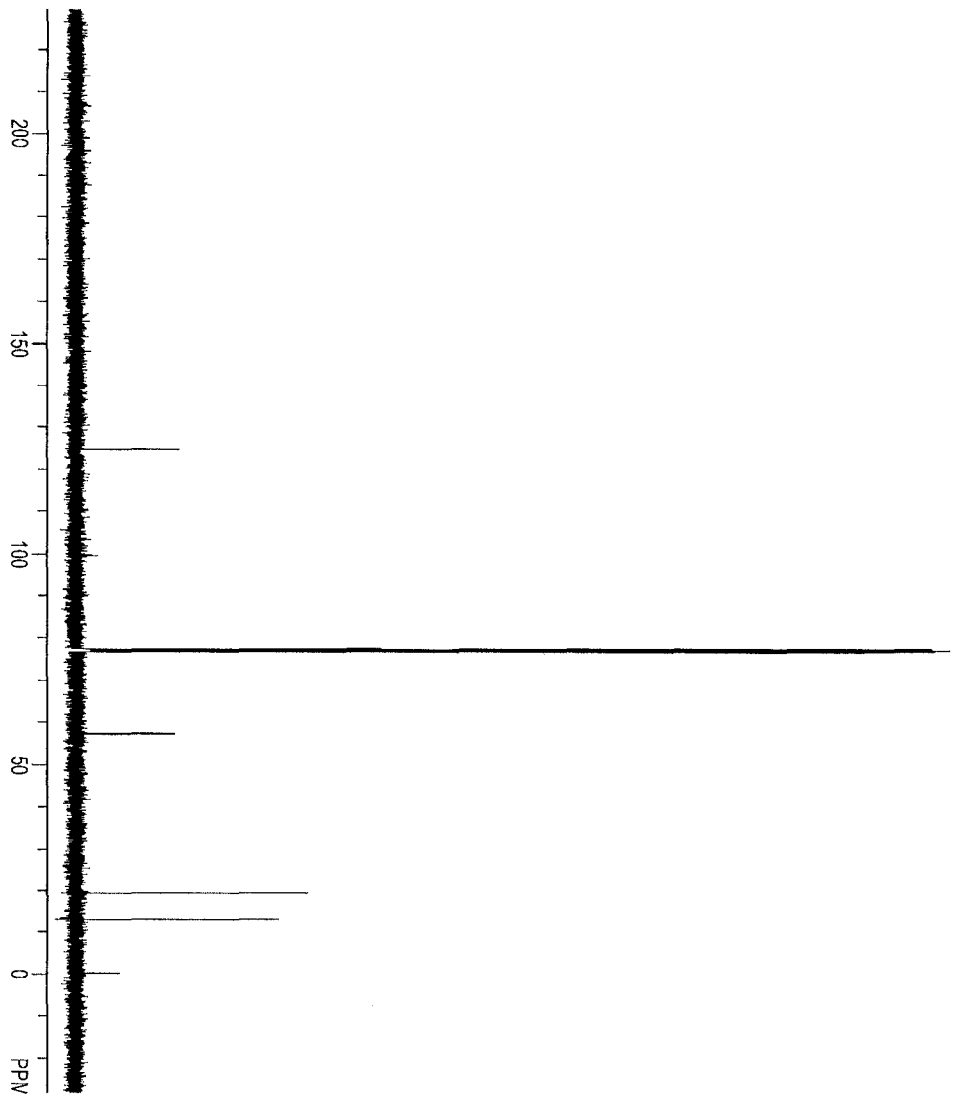

Figure A.19 ^{13}C NMR spectrum for **92b**.

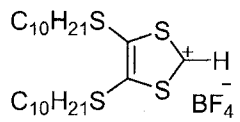

93a

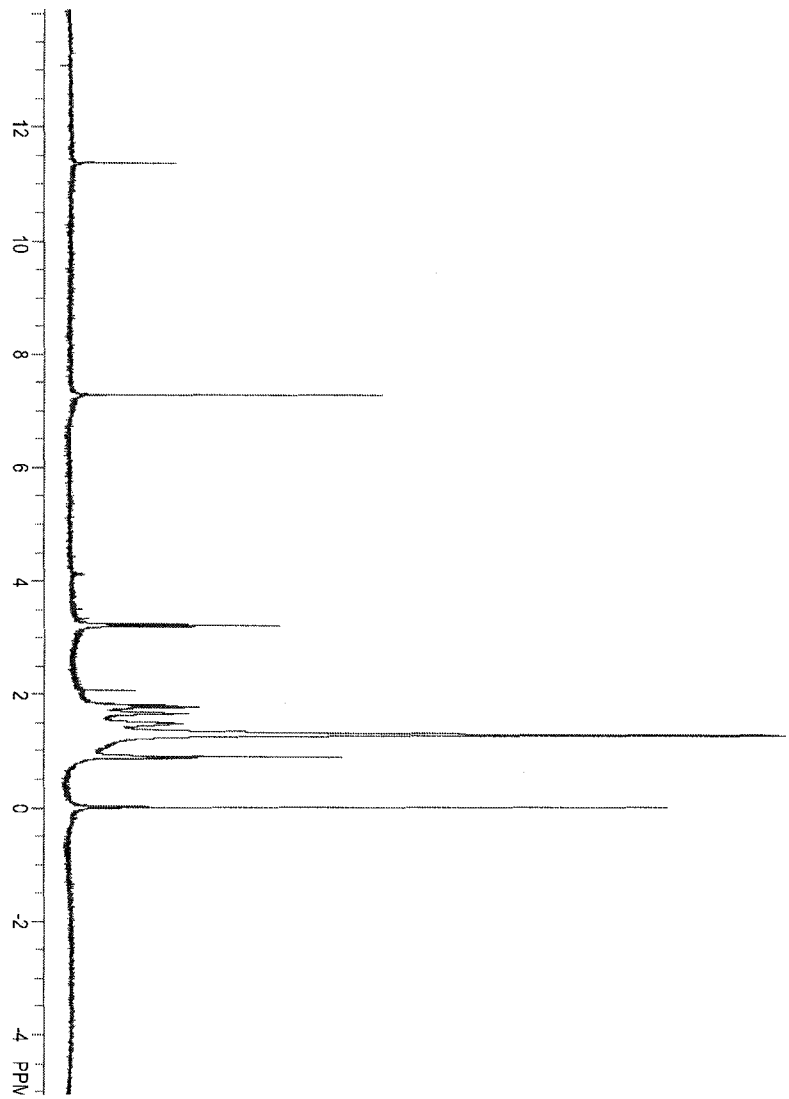

Figure A.20 ^{1}H NMR spectrum for **93a**.

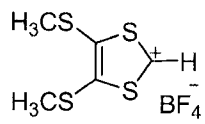

93b

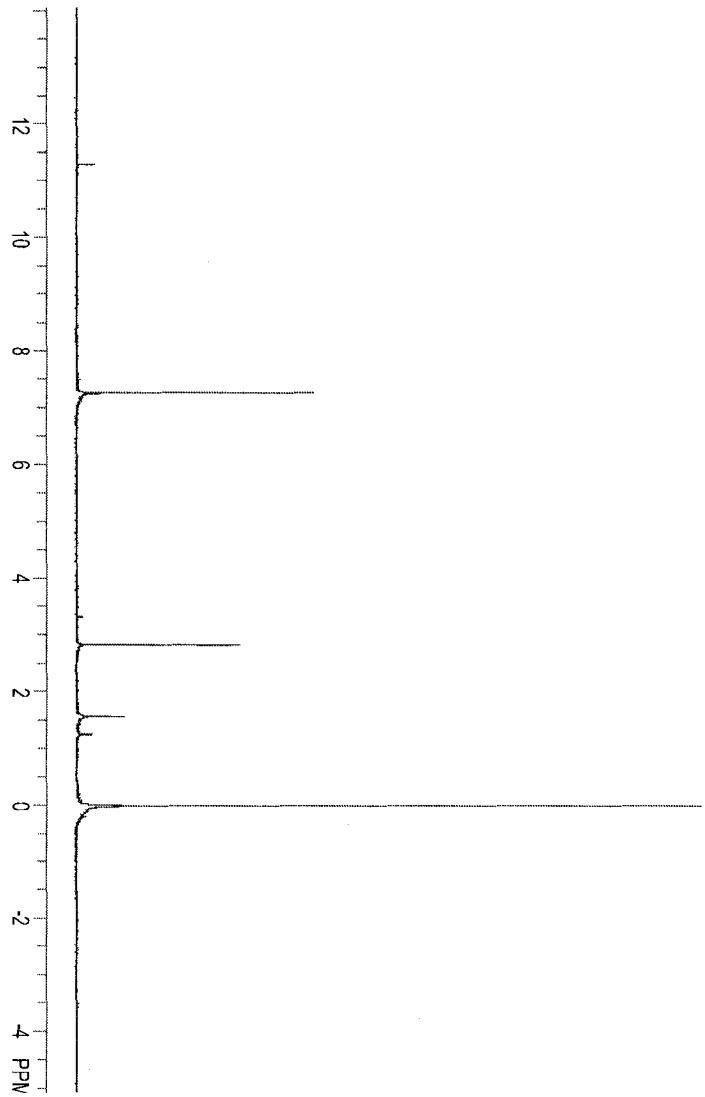

Figure A.21 ^{1}H NMR spectrum for **93b**.

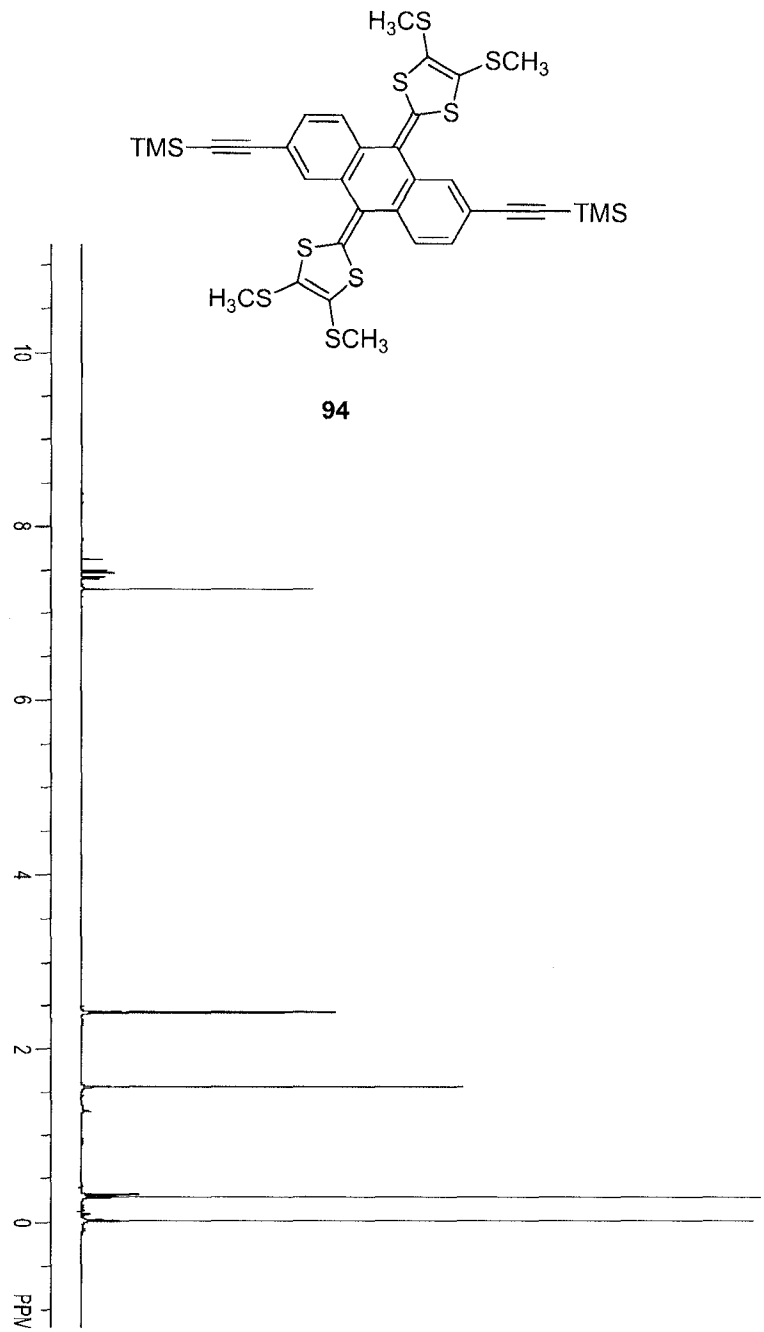

Figure A.22 ^{1}H NMR spectrum for **94**.

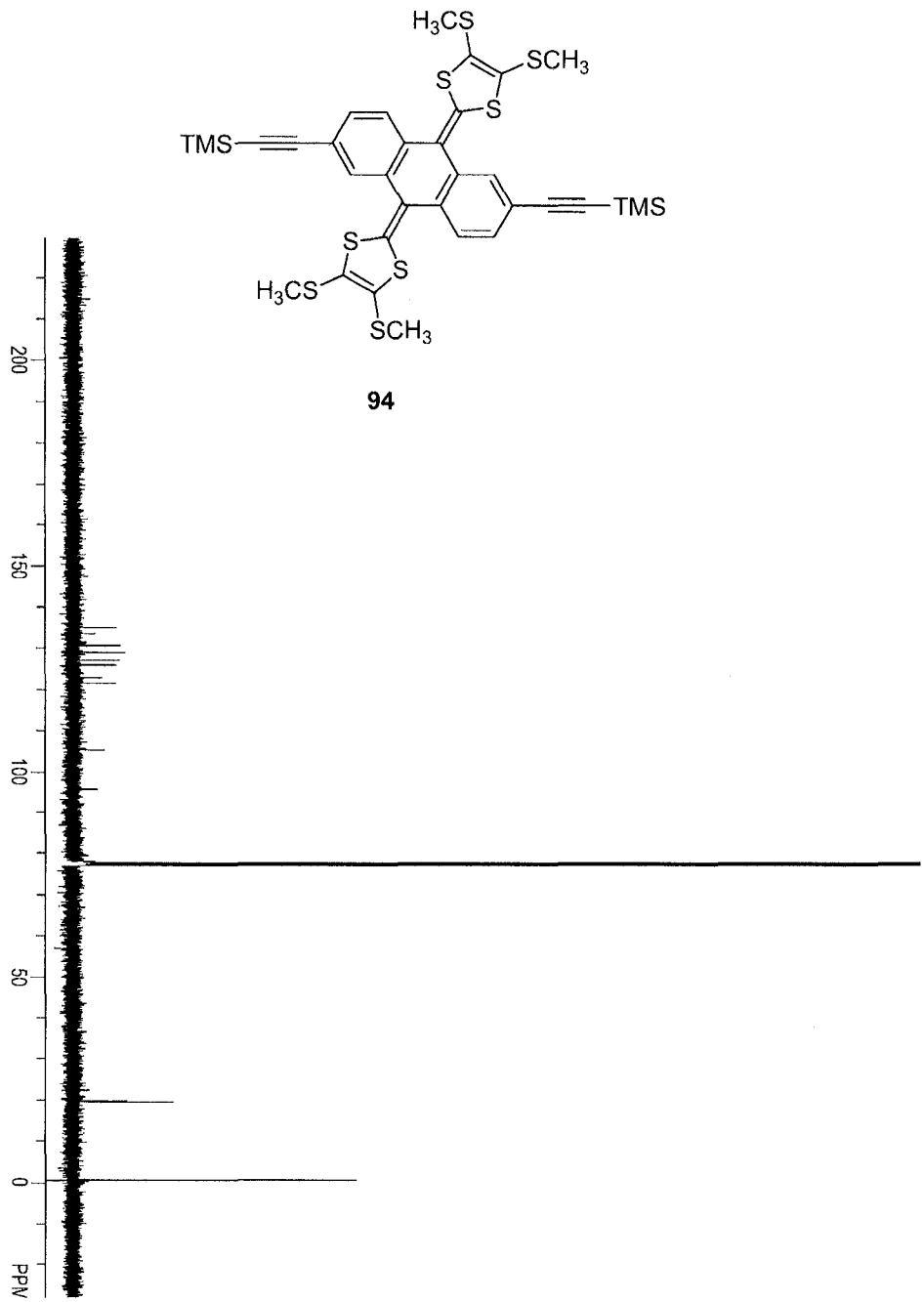

Figure A.23 ^{13}C NMR spectrum for **94**.

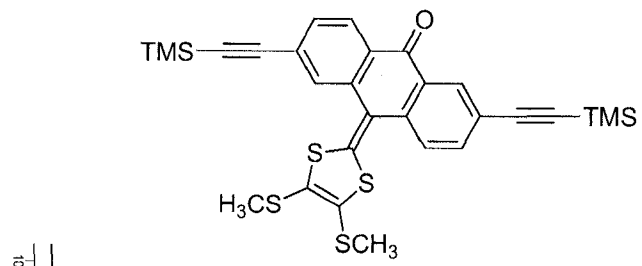

95

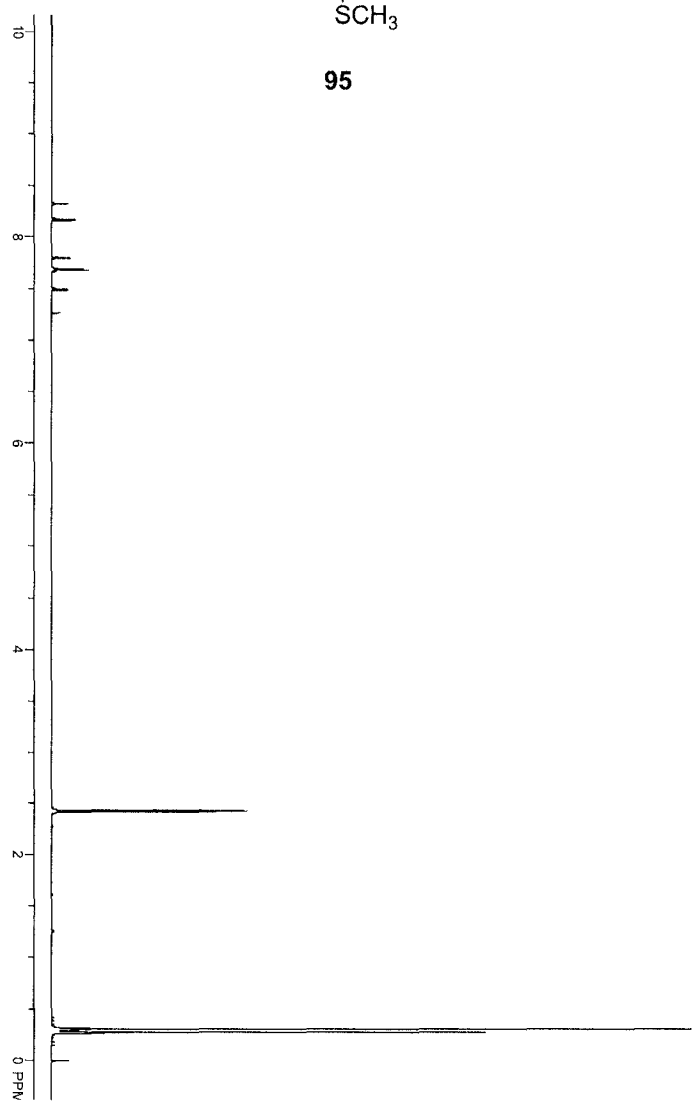

Figure A.24 ^{1}H NMR spectrum for **95**.

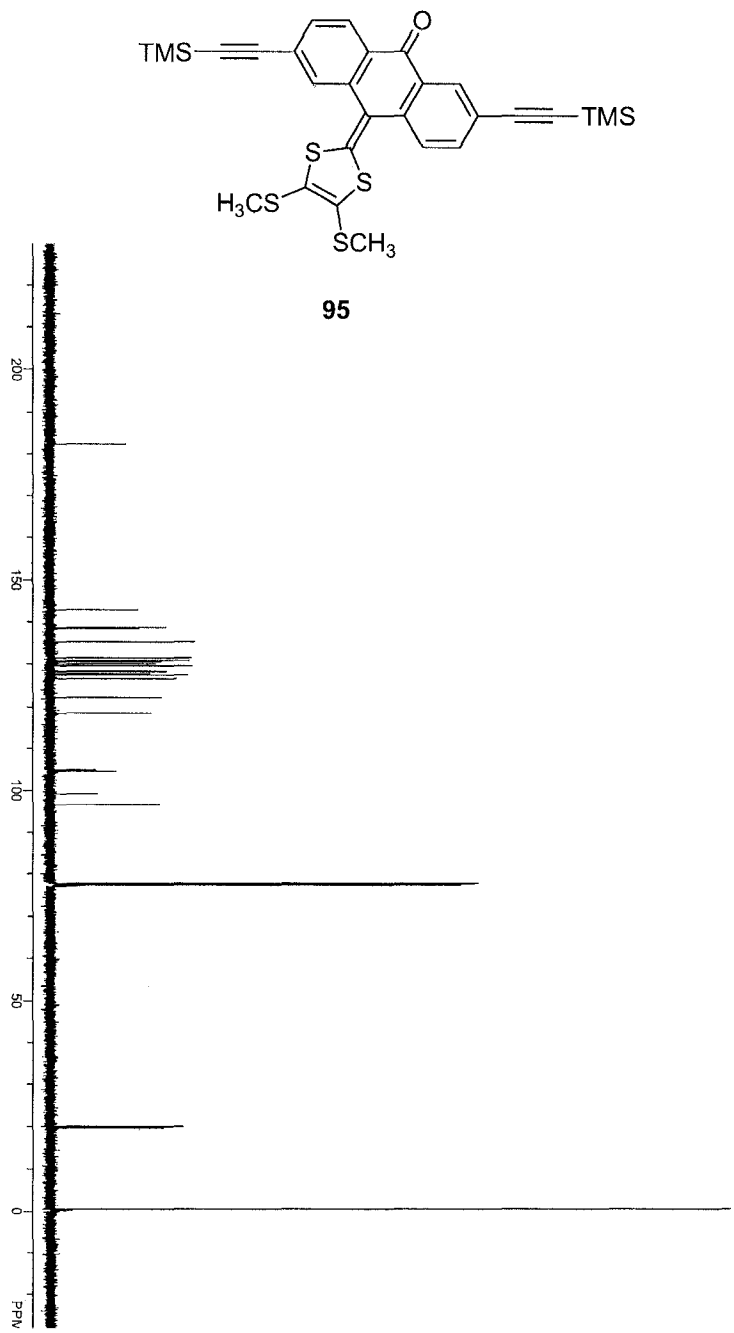

Figure A.25 ^{13}C NMR spectrum for **95**.

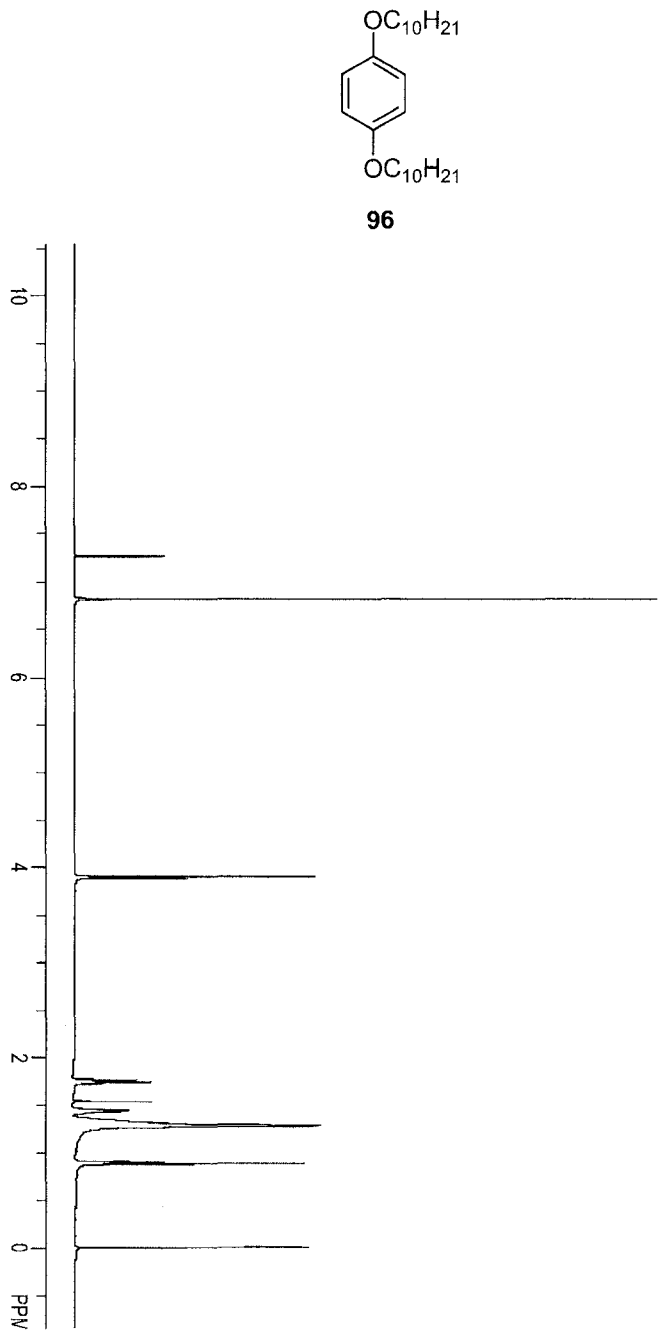

Figure A.26 ^{1}H NMR spectrum for **96**.

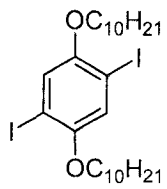

97

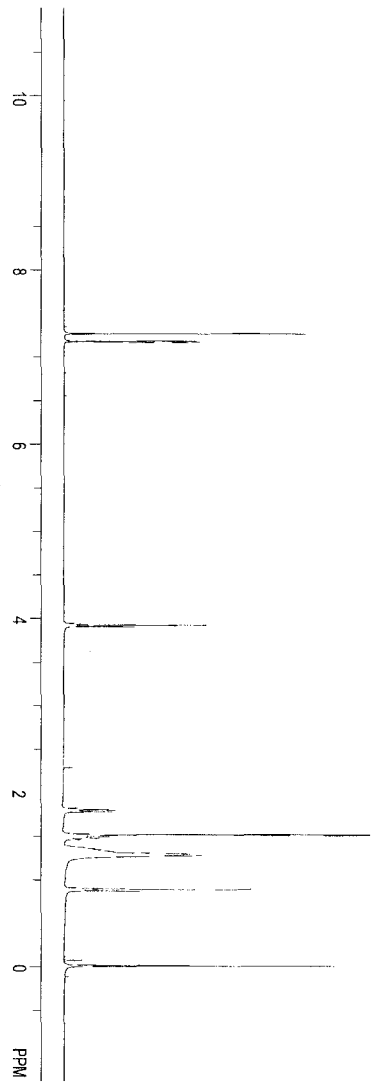

Figure A.27 ^{1}H NMR spectrum for **97**.

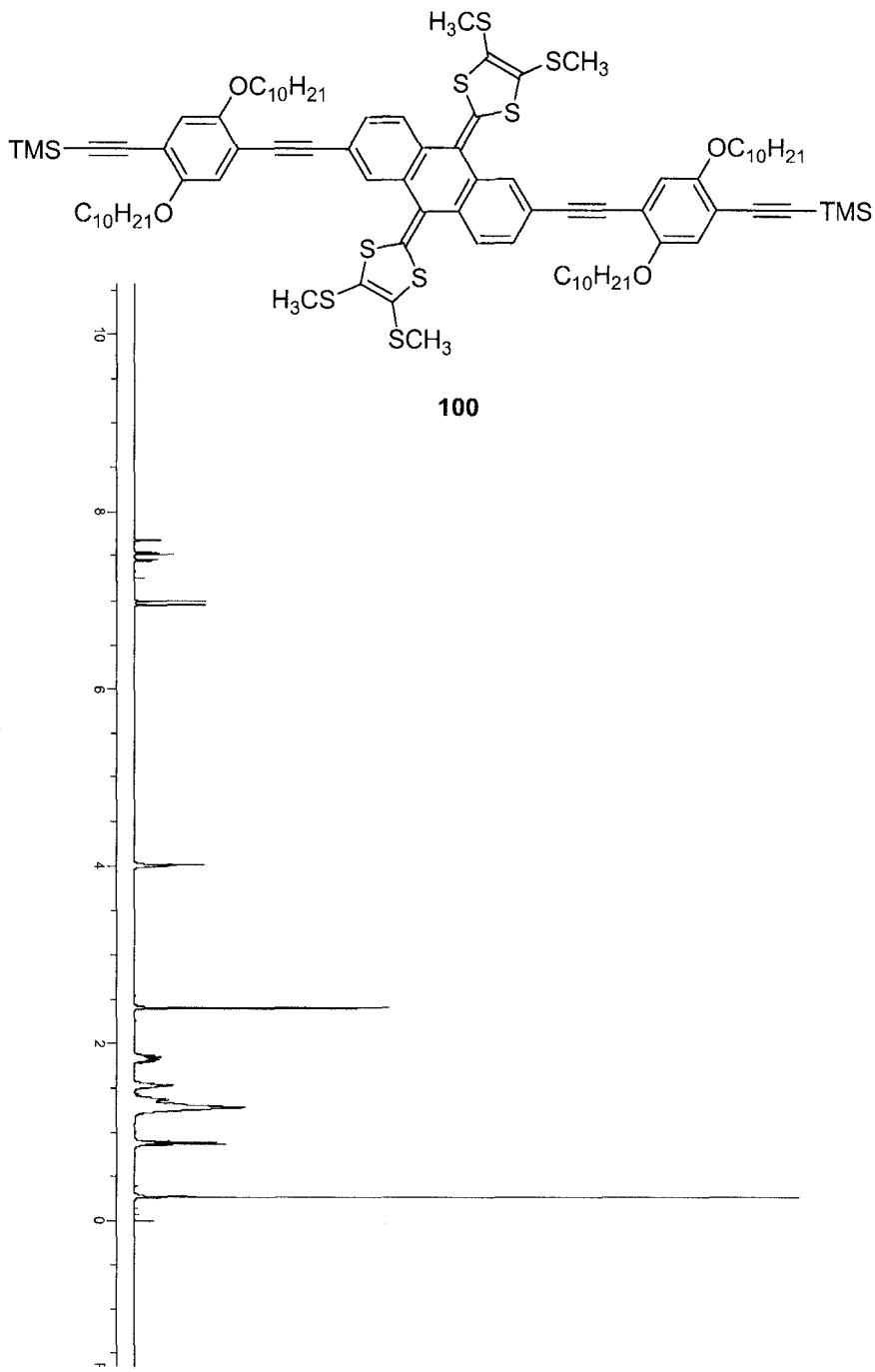

100

Figure A.28 ^{1}H NMR spectrum for **100**.

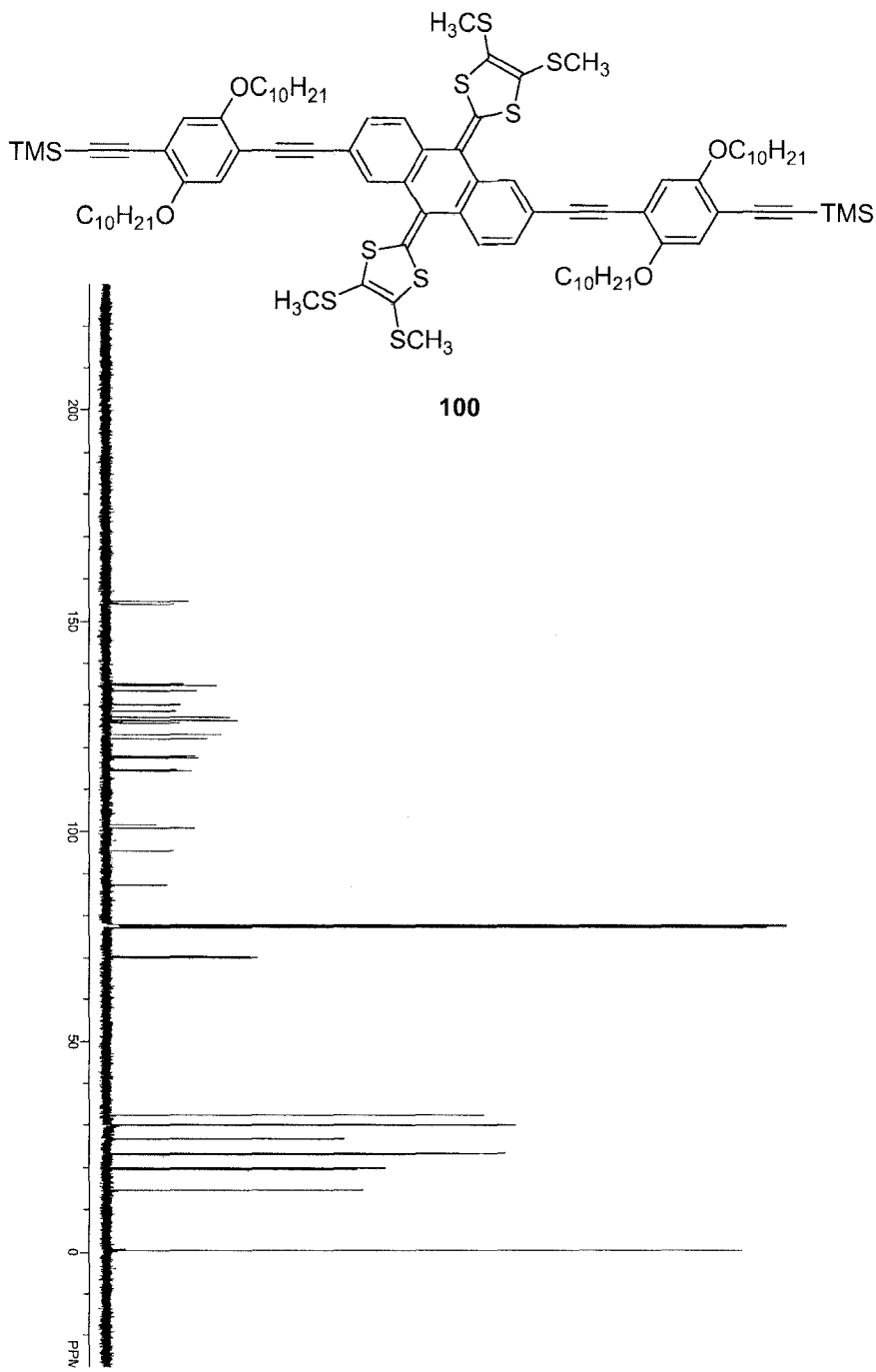

Figure A.29 ^{13}C NMR spectrum for **100**.

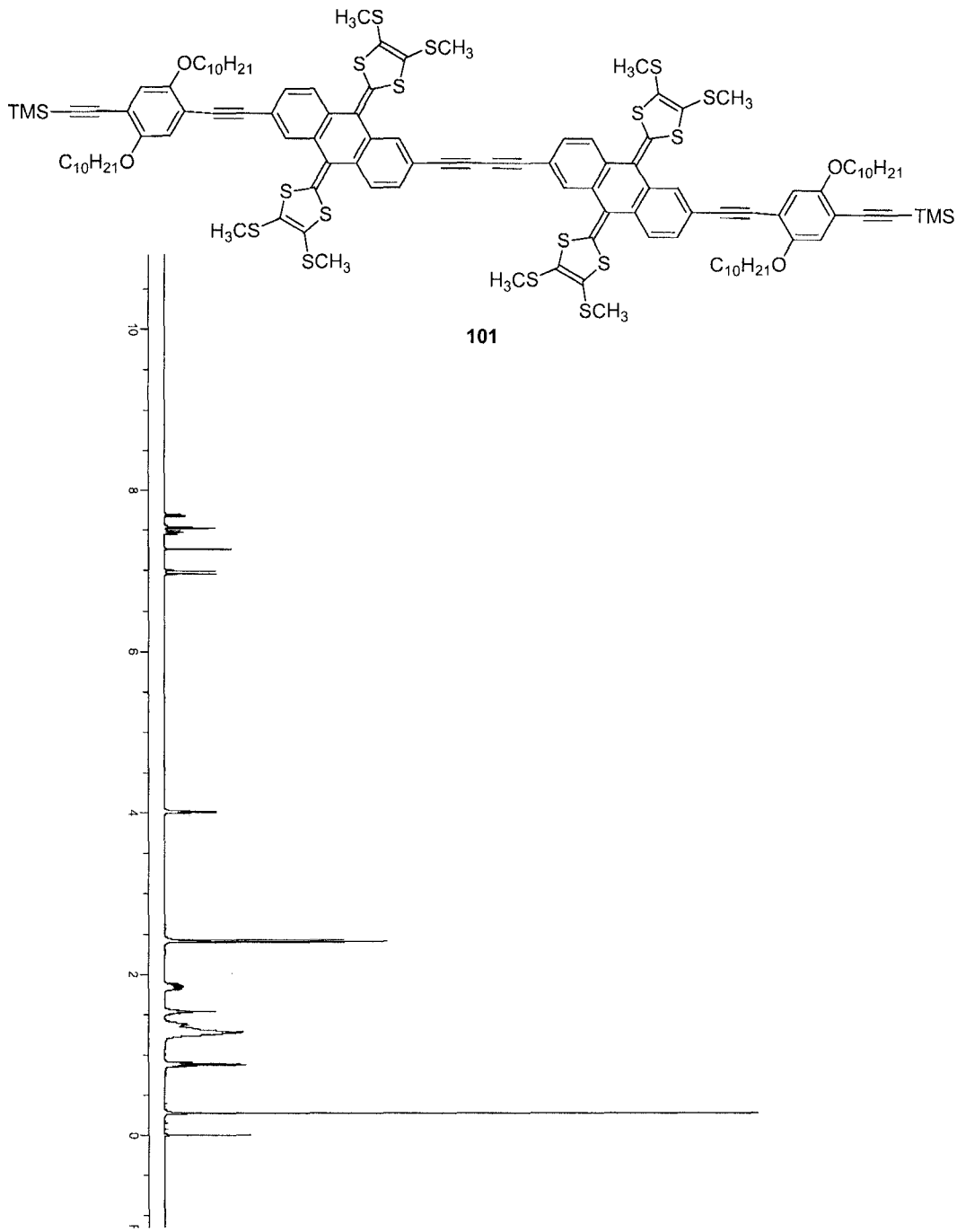

Figure A.30 ^{1}H NMR spectrum for **101**.

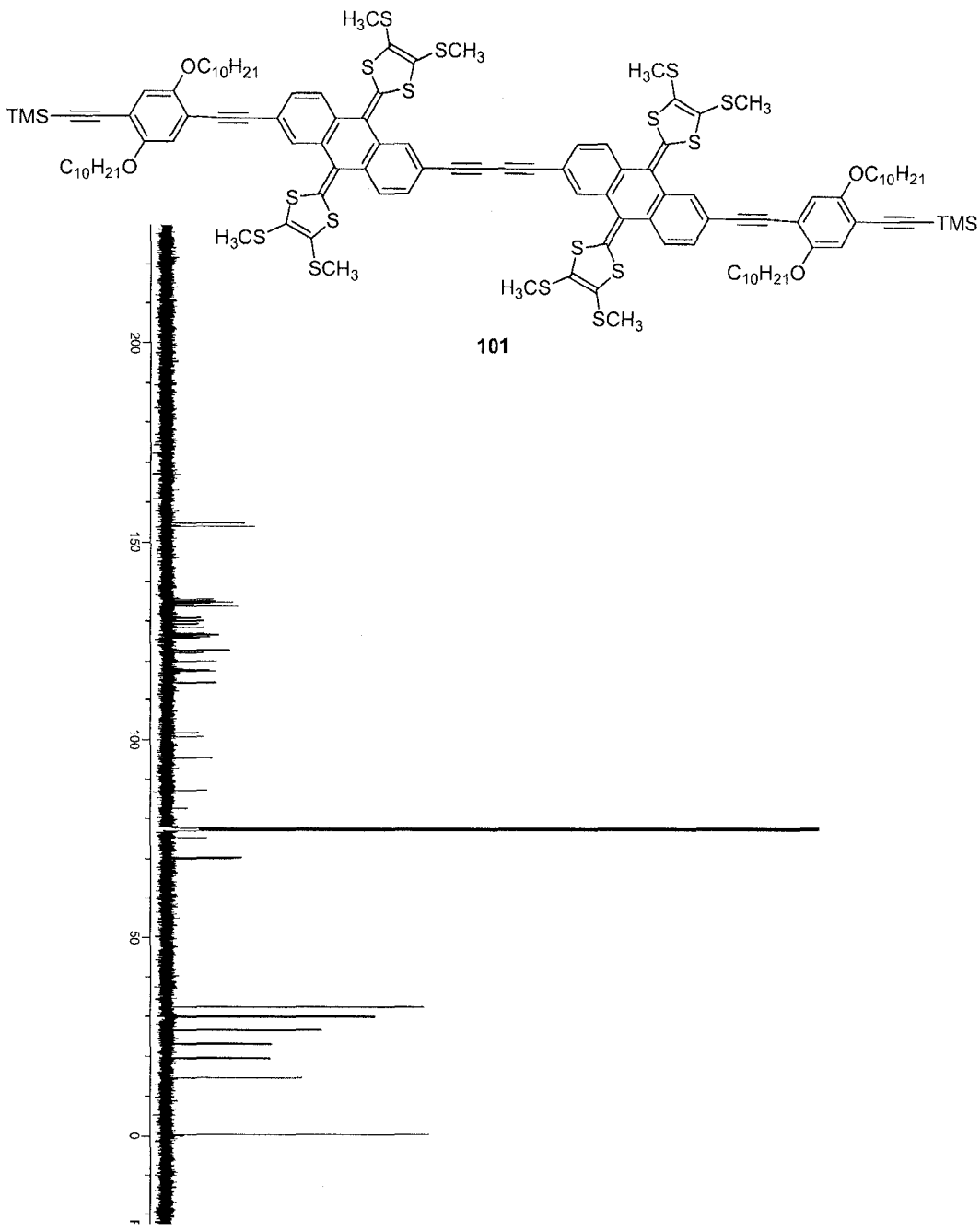

Figure A.31 ^{13}C NMR spectrum for **101**.

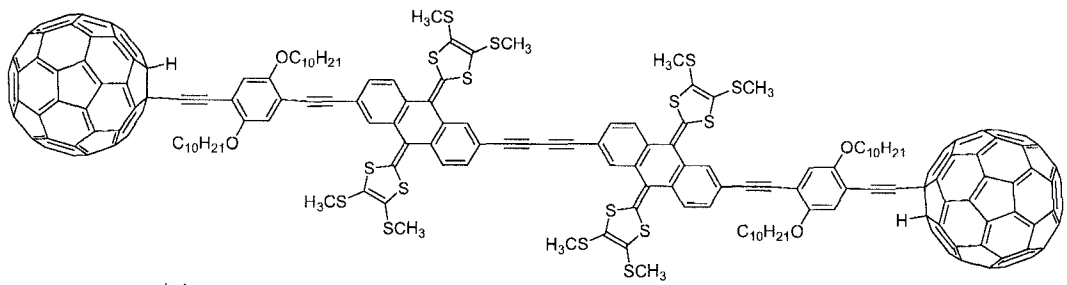

102

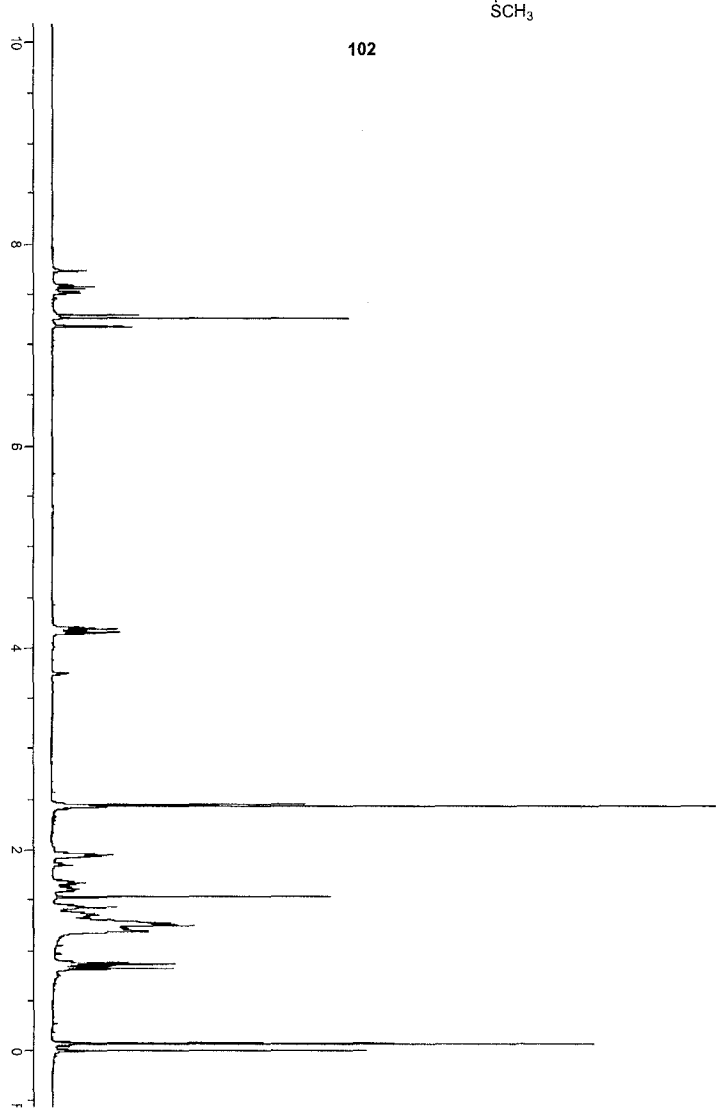

Figure A.32 ^{1}H NMR spectrum for **102**.

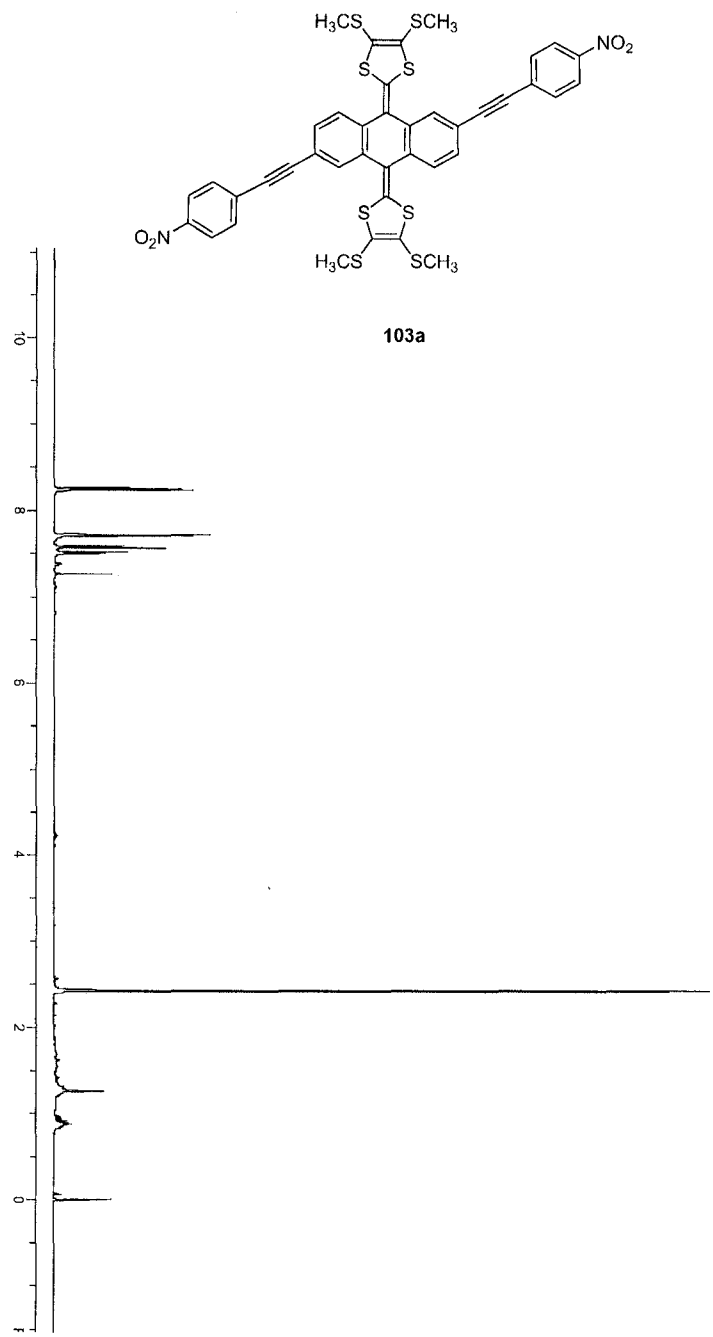

Figure A.33 ^{1}H NMR spectrum for **103a**.

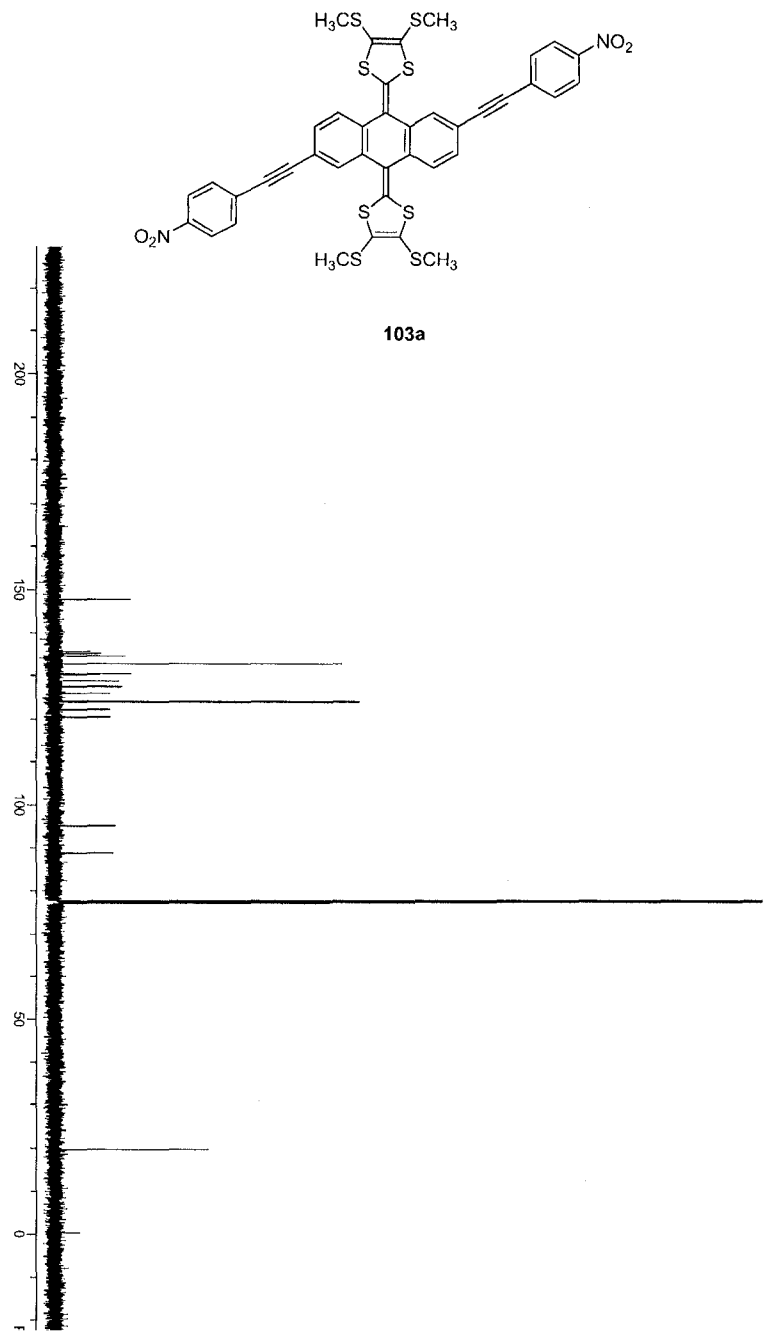

Figure A.34 ^{13}C NMR spectrum for **103a**.

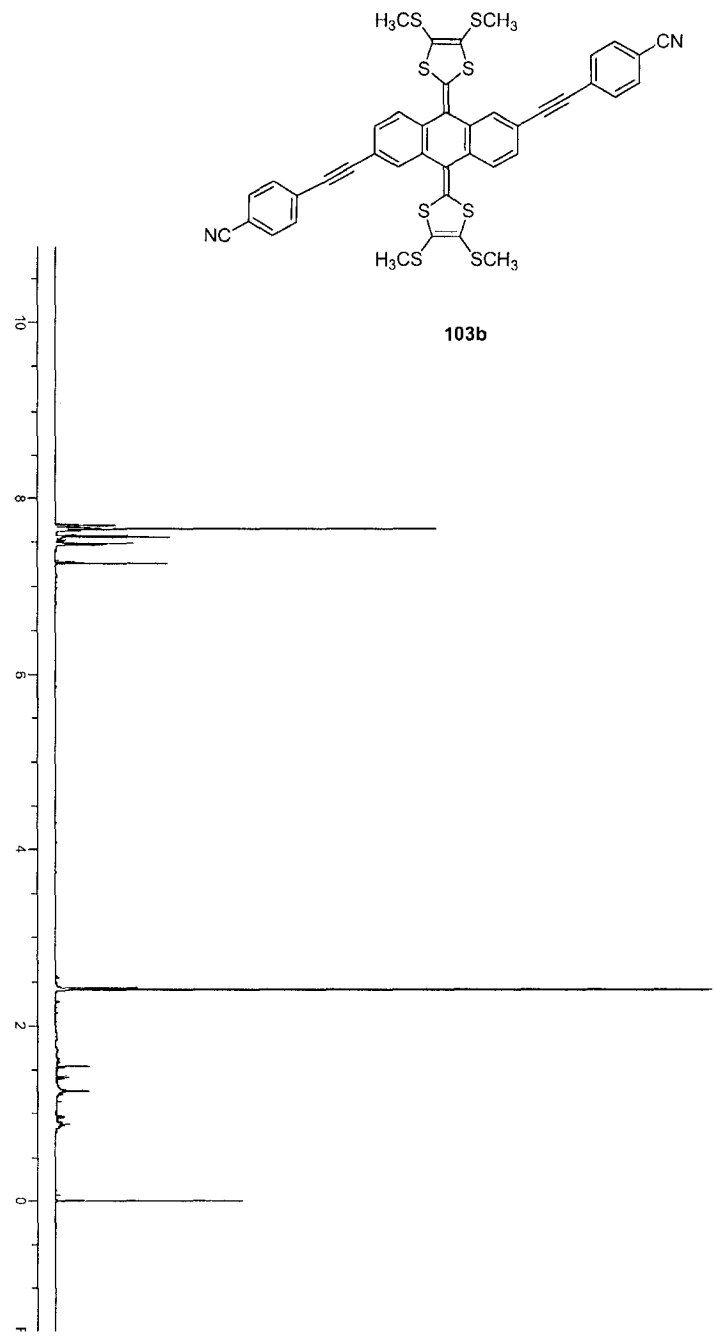

Figure A.35 ^{1}H NMR spectrum for **103b**.

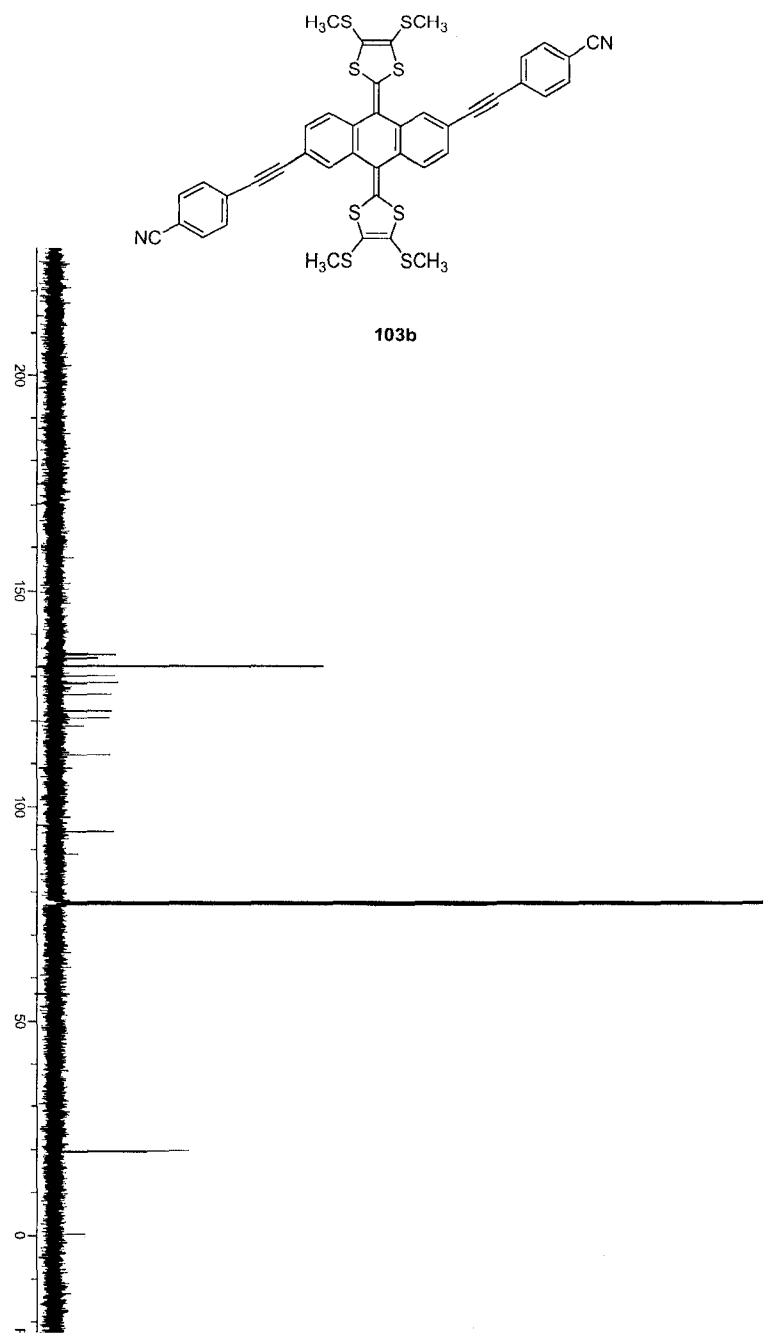

Figure A.36 ^{13}C NMR spectrum for **103b**.

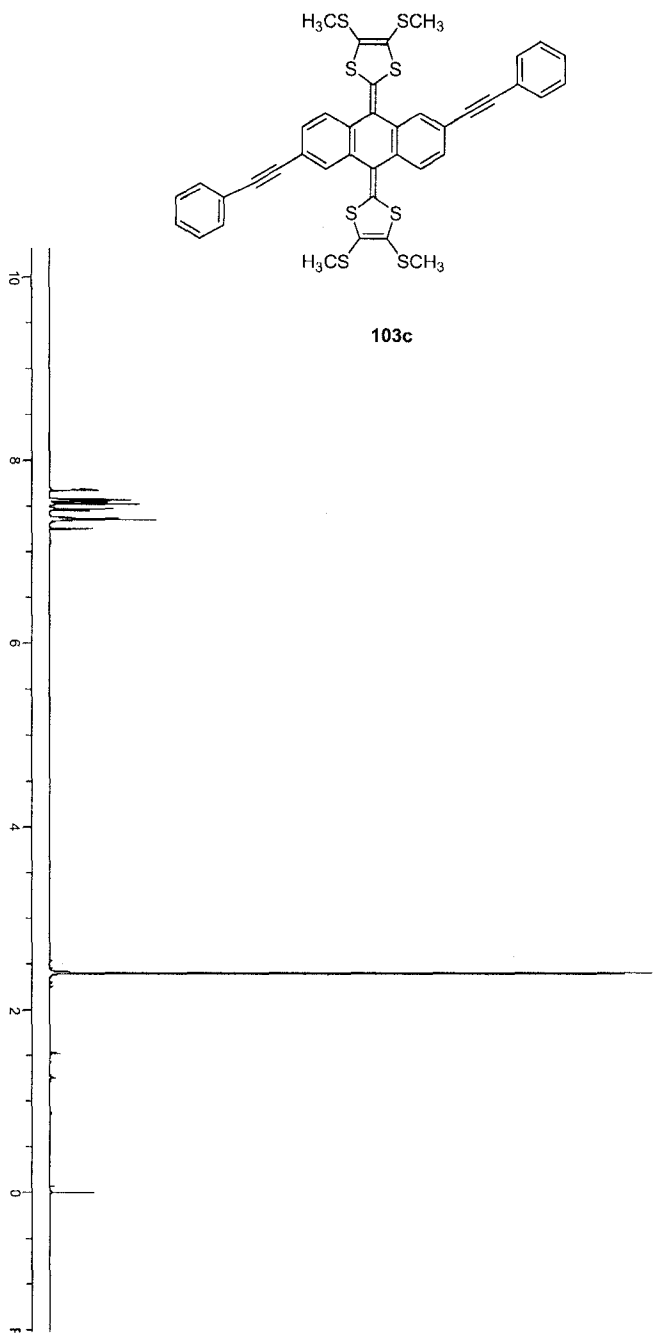

Figure A.37 ^{1}H NMR spectrum for **103c**.

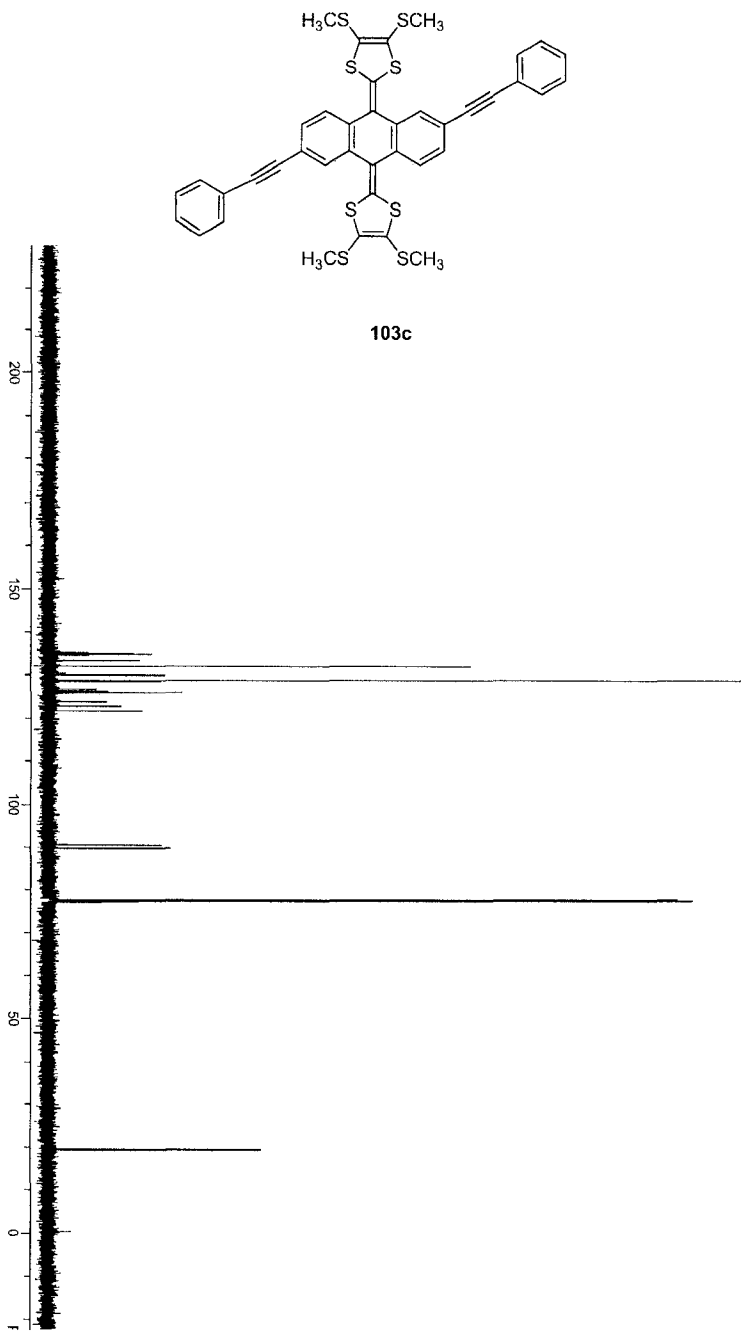

Figure A.38 ^{13}C NMR spectrum for **103c**.

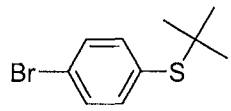

107

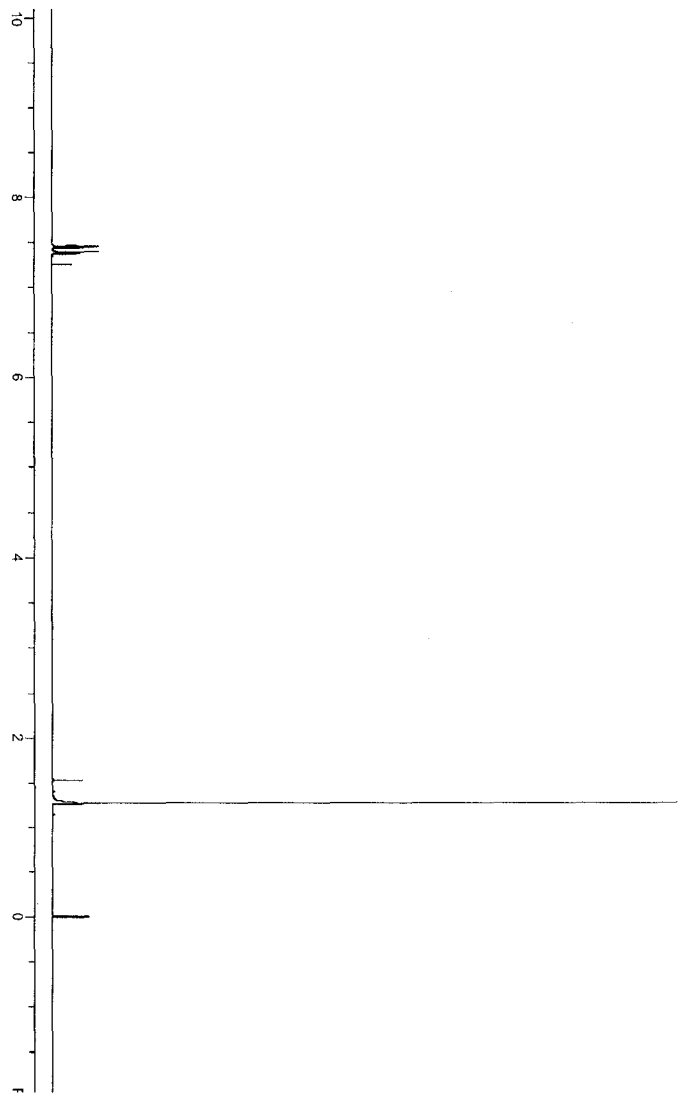

Figure A.39 ^{1}H NMR spectrum for **107**.

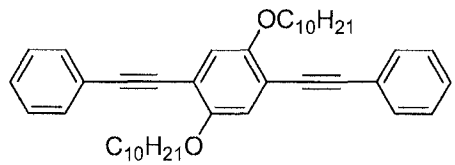

112

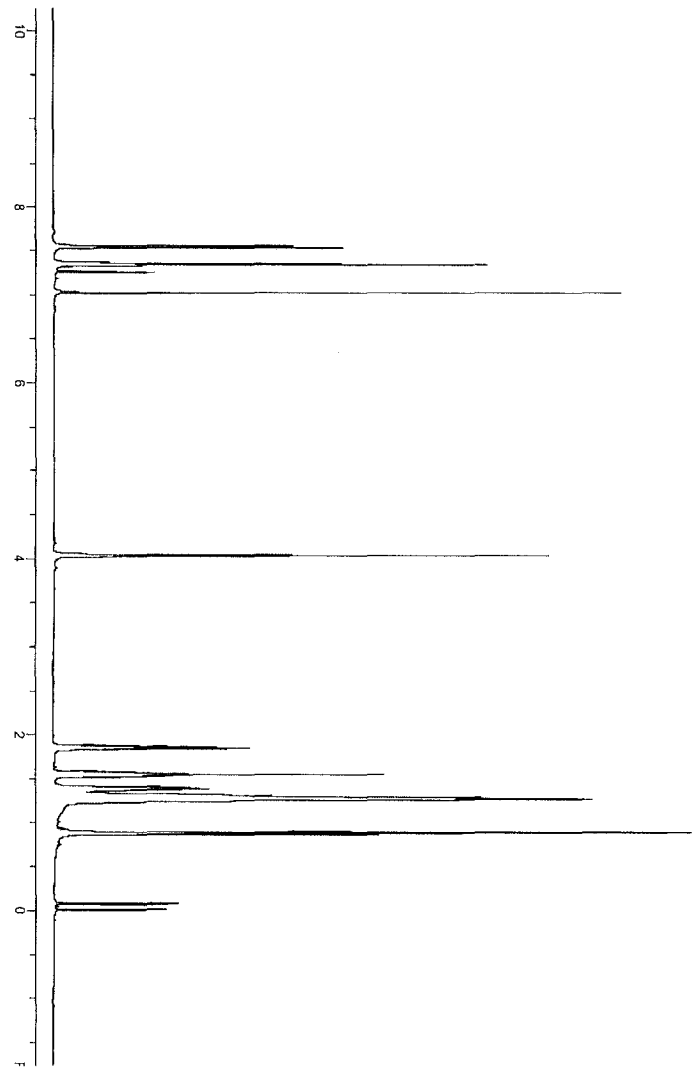

Figure A.40 ^{1}H NMR spectrum for **112**.

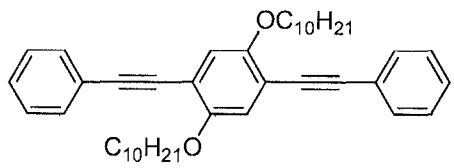

112

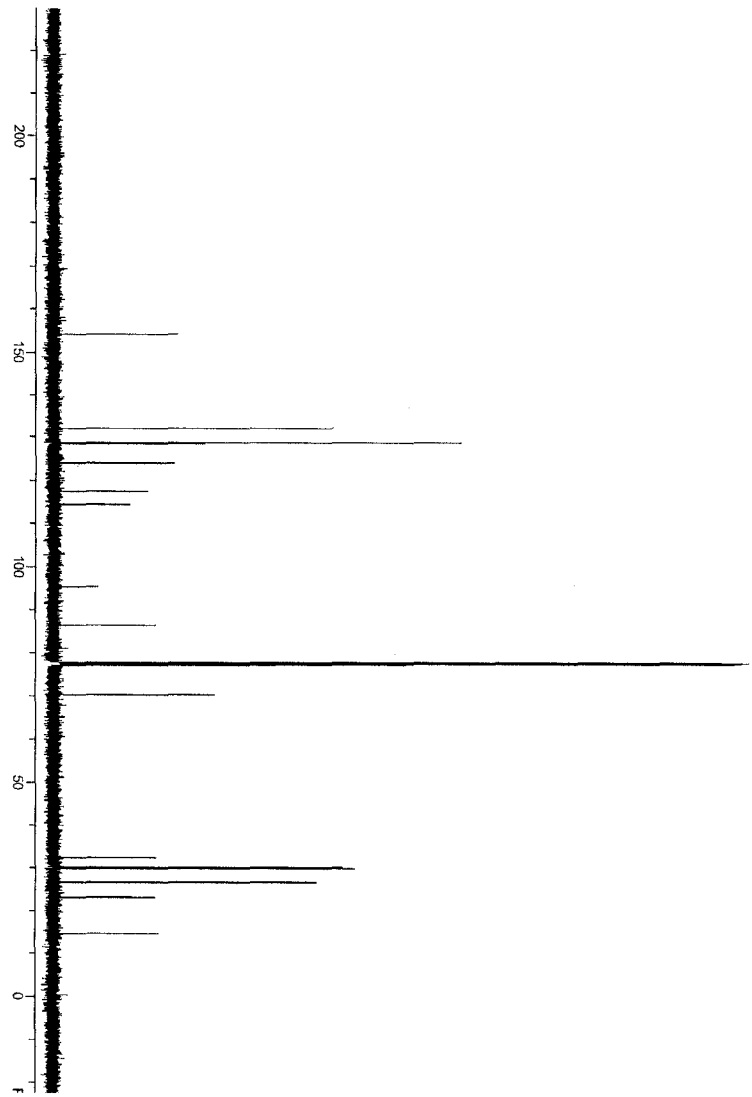

Figure A.41 ^{13}C NMR spectrum for **112**.

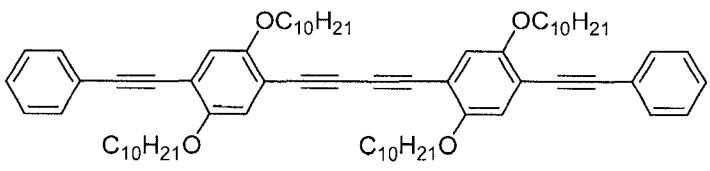

113

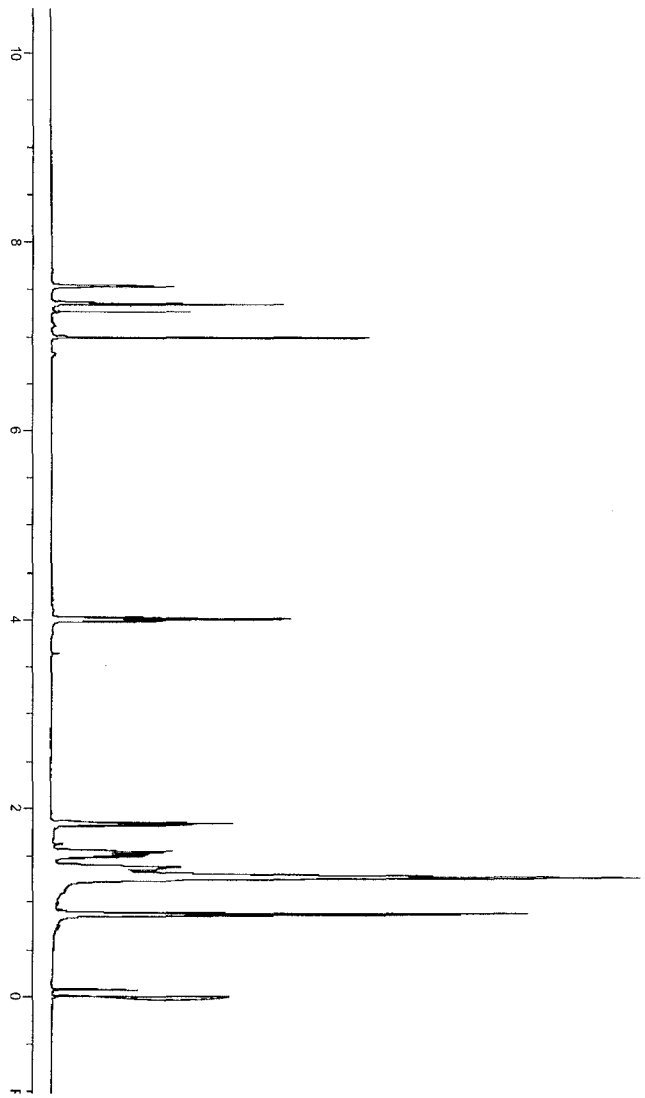

Figure A.42 ^{1}H NMR spectrum for **113**.

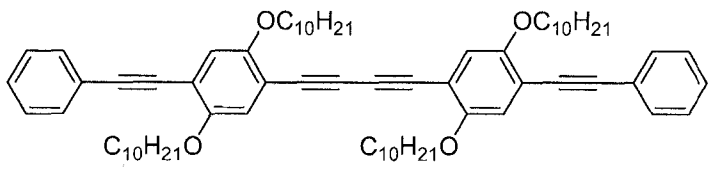

113

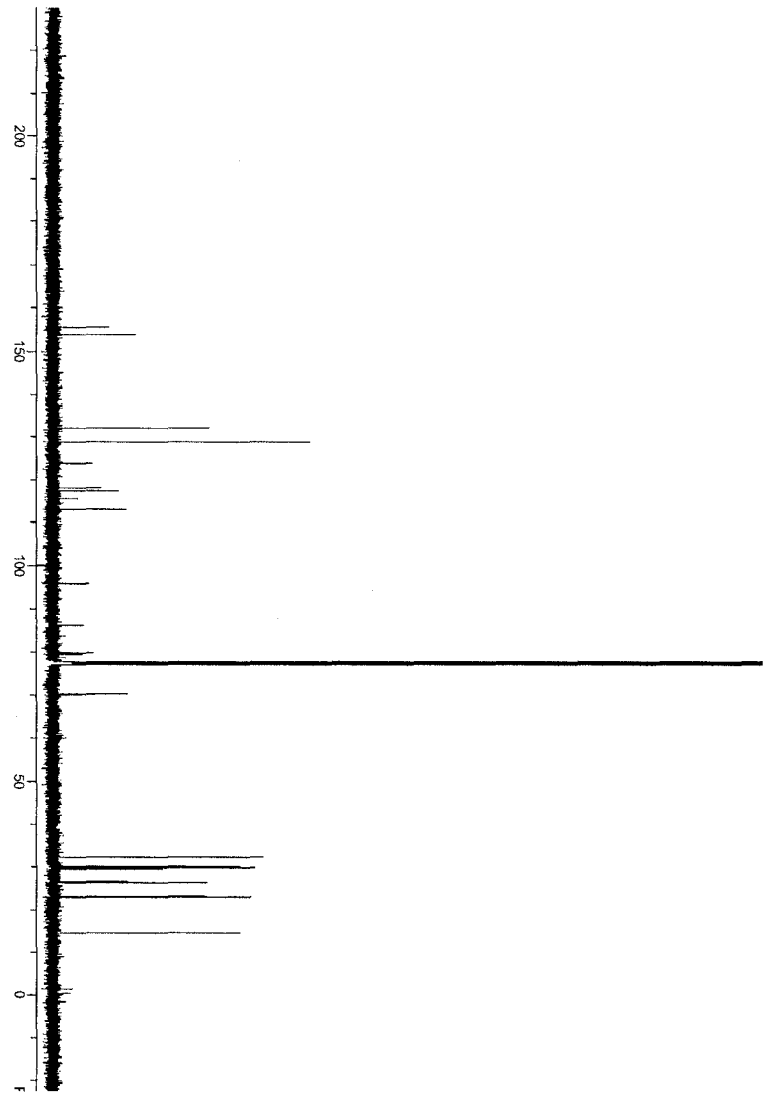

Figure A.43 ^{13}C NMR spectrum for **113**.

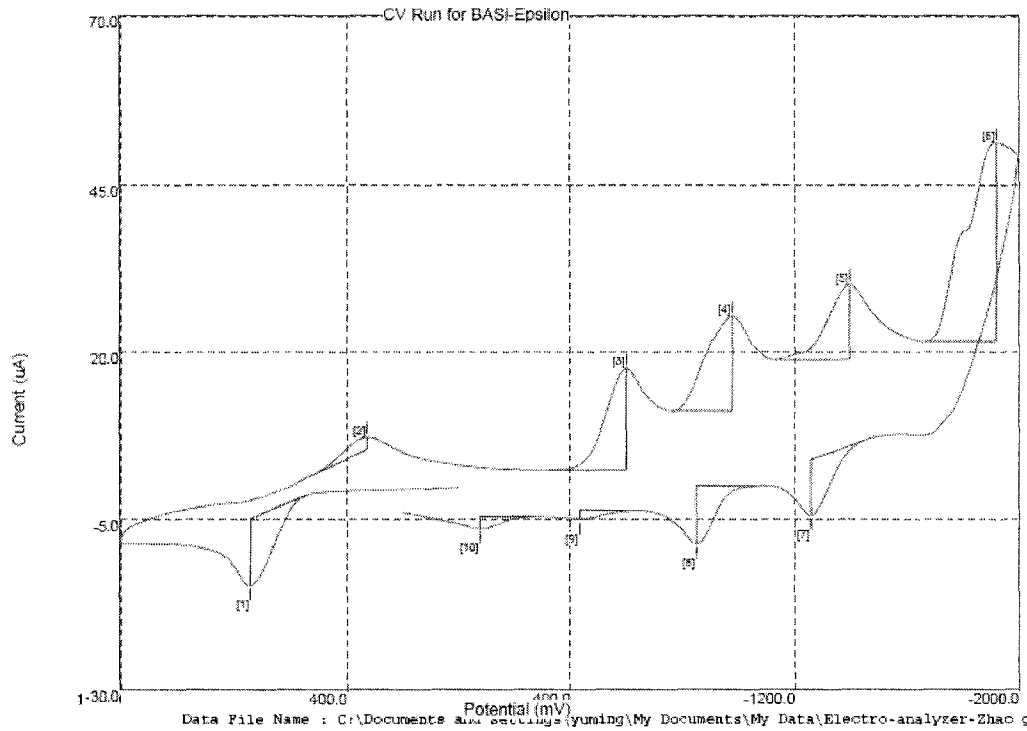

Data File Name : C:\Documents and Settings\yuming\My Documents\My Data\Electro-analyzer-Zhao group\Guang-
Title : CV Run for BASi-Epsilon
Experiment Type : Cyclic Voltammetry (CV)
Printed : 31/12/2006 4:20:47 PM
Date & Time of the run : 2/20/2006 4:02:01 PM
Number of data points : 6600
Display Convention : POLAROGRAPHIC
Initial Potential : 0 (mV)
Switching Potential 1 : 1200 (mV)
Switching Potential 2 : -2000 (mV)
Final Potential : 200 (mV)
Number of segments : 3
Scan rate : 100 (mV/s)
Current Full Scale : 100 uA
Filter : 10 Hz
Quiet Time : 2 (Sec)
Sample Interval : 1 mV

Peak Data:
peak [1] @ 741 [mV], 9.8024 (uA), 9.0453 (uC)
peak [2] @ 328 [mV], 1.7945 (uA), 2.0665 (uC)
peak [3] @ -601 [mV], 15.1186 (uA), 12.6763 (uC)
peak [4] @ -980 [mV], 14.0688 (uA), 14.6552 (uC)
peak [5] @ -1395 [mV], 11.1696 (uA), 9.9388 (uC)
peak [6] @ -1921 [mV], 29.7612 (uA), 36.8594 (uC)
peak [7] @ -1258 [mV], 8.3833 (uA), 6.6075 (uC)
peak [8] @ -852 [mV], 8.6000 (uA), 6.1727 (uC)
peak [9] @ -434 [mV], 1.3153 (uA), 1.1458 (uC)
peak [10] @ -78 [mV], 1.7273 (uA), 1.3462 (uC)

Figure A.44 Cyclic voltammogram of **83**.

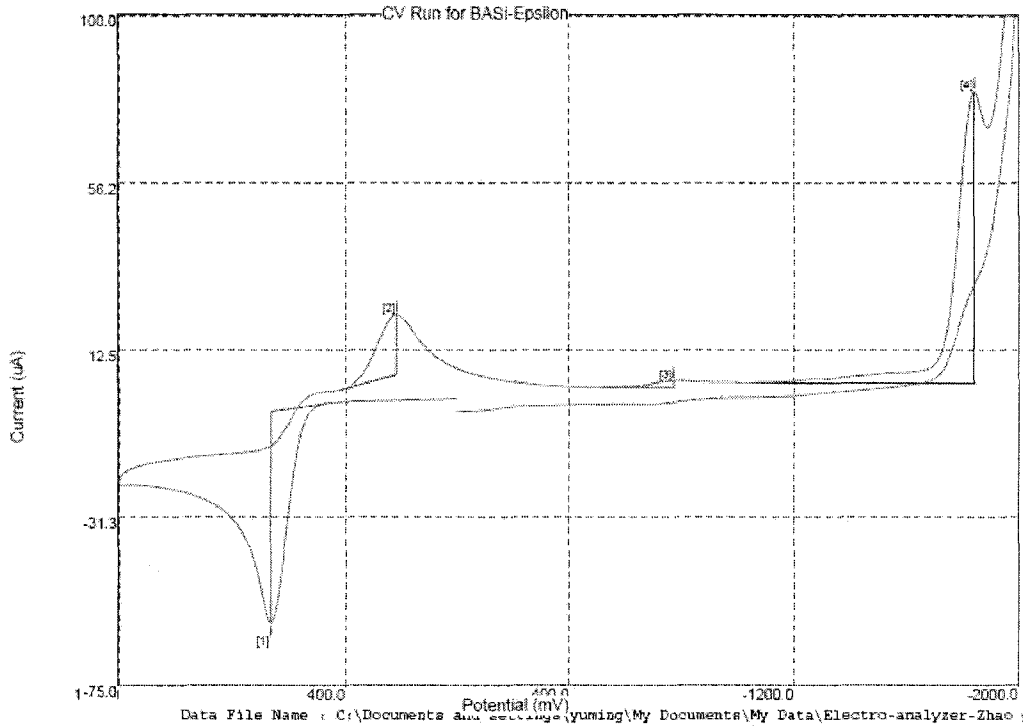

Data File Name : C:\Documents and Settings\yuming\My Documents\My Data\Electro-analyzer-Zhao group\Guang-
Title : CV Run for BASi-Epsilon
Experiment Type : Cyclic Voltammetry (CV)
Printed : 04/01/2007 11:03:22 AM
Date & Time of the run : 2/28/2006 4:51:04 PM
Number of data points : 6400
Display Convention : POLAROGRAPHIC
Initial Potential : 0 (mV)
Switching Potential 1 : 1200 (mV)
Switching Potential 2 : -2000 (mV)
Final Potential : 0 (mV)
Number of segments : 3
Scan rate : 100 (mV/s)
Current Full Scale : 100 uA
Filter : 10 Hz
Quiet Time : 2 (Sec)
Sample Interval : 1 mV

Peak Data:
peak [1] @ 664 [mV], 55.2255 (uA), 36.1805 (uC)
peak [2] @ 217 [mV], 16.0586 (uA), 12.9984 (uC)
peak [3] @ -774 [mV], 1.6144 (uA), 1.4709 (uC)
peak [4] @ -1843 [mV], 76.2585 (uA), 59.7860 (uC)

Figure A.45 Cyclic voltammogram of **94**.

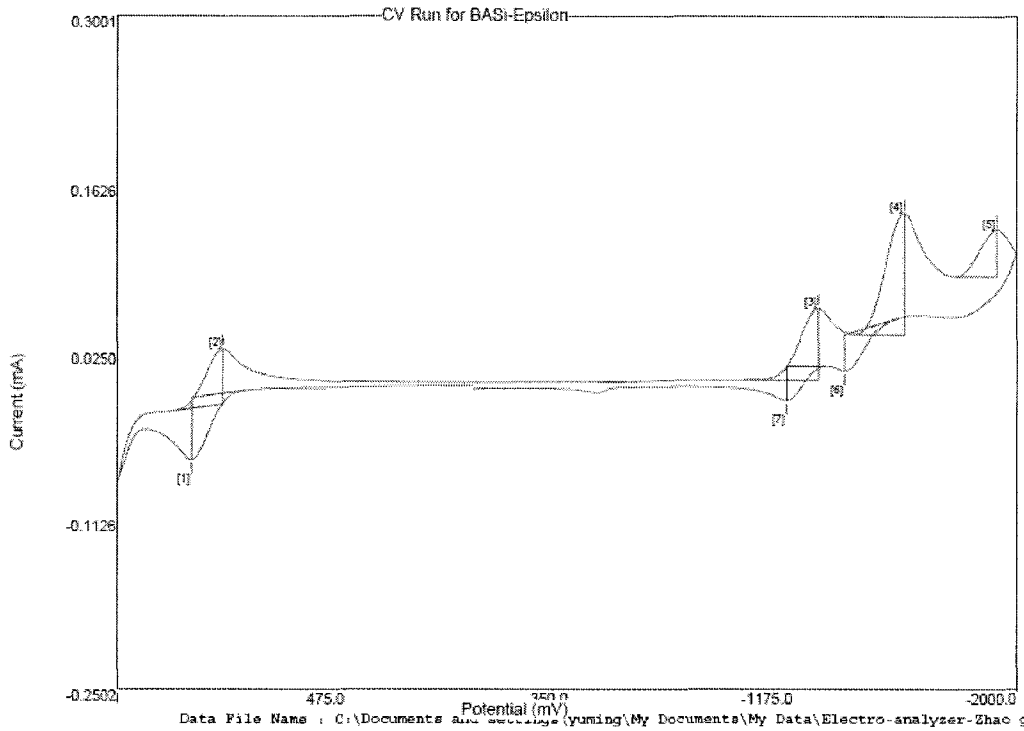

Data File Name : C:\Documents and Settings\yuming\My Documents\My Data\Electro-analyzer-Zhao group\Guang-
Title : CV Run for BASi-Epsilon
Experiment Type : Cyclic Voltammetry (CV)
Printed : 31/12/2006 4:12:03 PM
Date & Time of the run : 2/28/2006 5:19:39 PM
Number of data points : 6600
Display Convention : POLAROGRAPHIC
Initial Potential : 0 (mV)
Switching Potential 1 : 1300 (mV)
Switching Potential 2 : -2000 (mV)
Final Potential : 0 (mV)
Number of segments : 3
Scan rate : 100 (mV/s)
Current Full Scale : 1 mA
Filter : 10 Hz
Quiet Time : 2 (Sec)
Sample Interval : 1 mV

Peak Data:
peak [1] @ 1032 [mV], 0.0513 (mA), 0.0386 (mC)
peak [2] @ 918 [mV], 0.0450 (mA), 0.0331 (mC)
peak [3] @ -1372 [mV], 0.0584 (mA), 0.0466 (mC)
peak [4] @ -1585 [mV], 0.0998 (mA), 0.0770 (mC)
peak [5] @ -1928 [mV], 0.0388 (mA), 0.0270 (mC)
peak [6] @ -1366 [mV], 0.0292 (mA), 0.0241 (mC)
peak [7] @ -1153 [mV], 0.0284 (mA), 0.0185 (mC)

Figure A.45 Cyclic voltammogram of **95**.

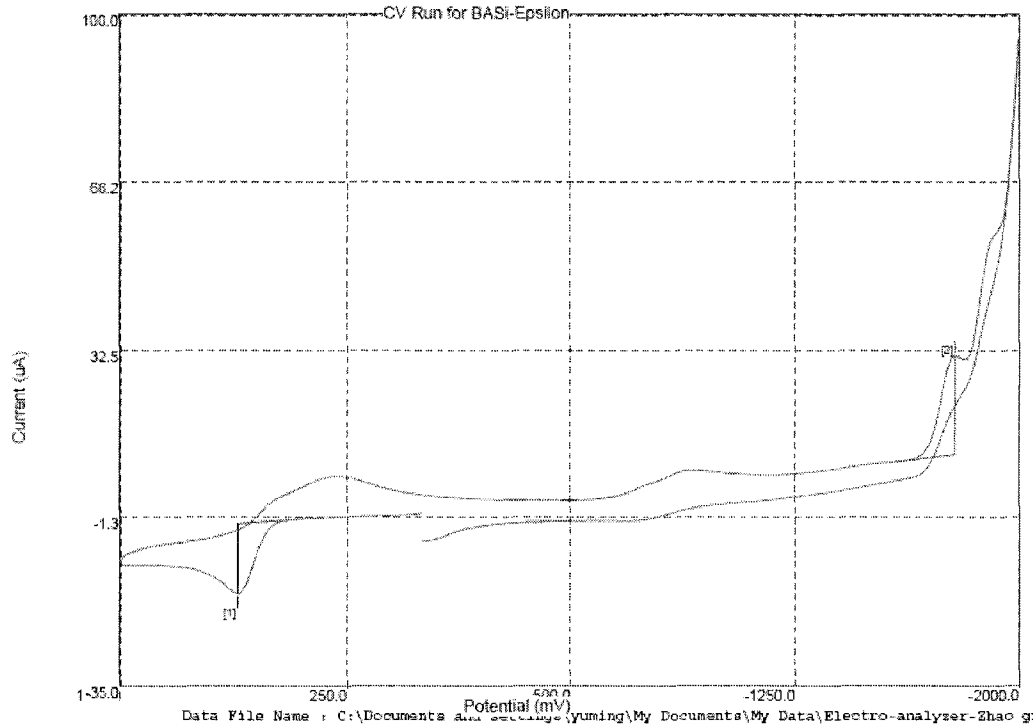

Data File Name : C:\Documents and Settings\yuming\My Documents\My Data\Electro-analyzer-Zhao group\Guang-
Title : CV Run for BASi-Epsilon
Experiment Type : Cyclic Voltammetry (CV)
Printed : 31/12/2006 4:18:23 PM
Date & Time of the run : 2/20/2006 3:25:40 PM
Number of data points : 6000
Display Convention : POLAROGRAPHIC
Initial Potential : 0 (mV)
Switching Potential 1 : 1000 (mV)
Switching Potential 2 : -2000 (mV)
Final Potential : 0 (mV)
Number of segments : 3
Scan rate : 100 (mV/s)
Current Full Scale : 100 uA
Filter : 10 Hz
Quiet Time : 2 (Sec)
Sample Interval : 1 mV

Peak Data:
peak [1] @ 612 [mV], 13.8888 (uA), 8.7535 (uC)
peak [2] @ -1786 [mV], 19.9008 (uA), 11.5181 (uC)

Figure A.46 Cyclic voltammogram of **100**.

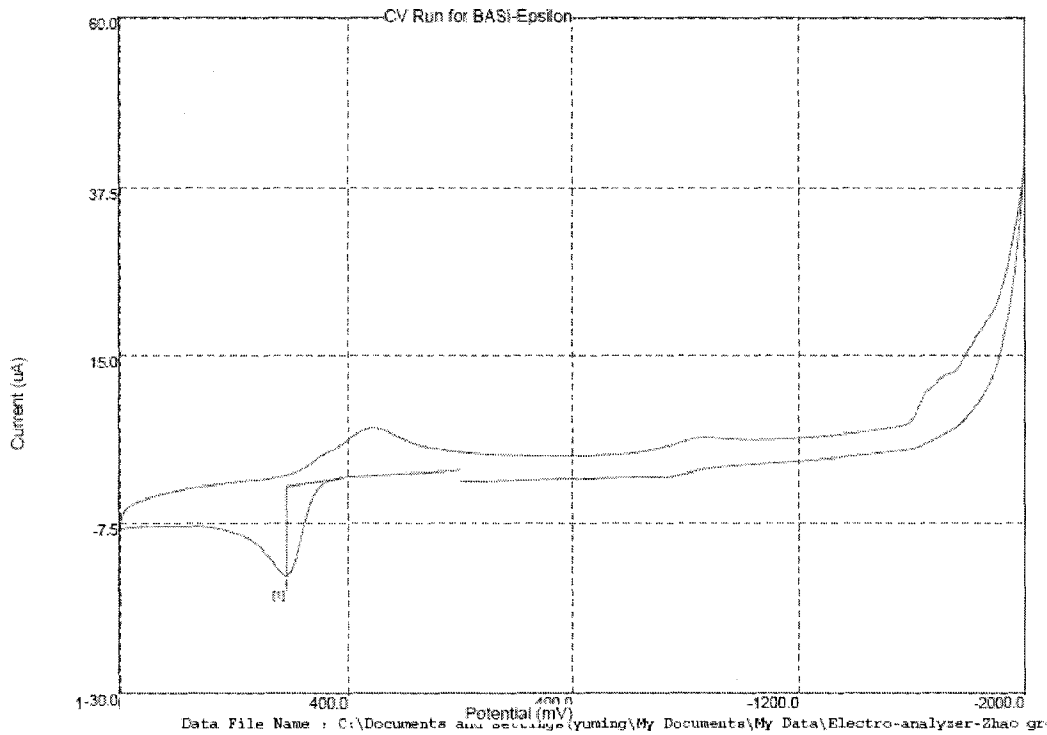

Figure A.47 Cyclic voltammogram of **101**.

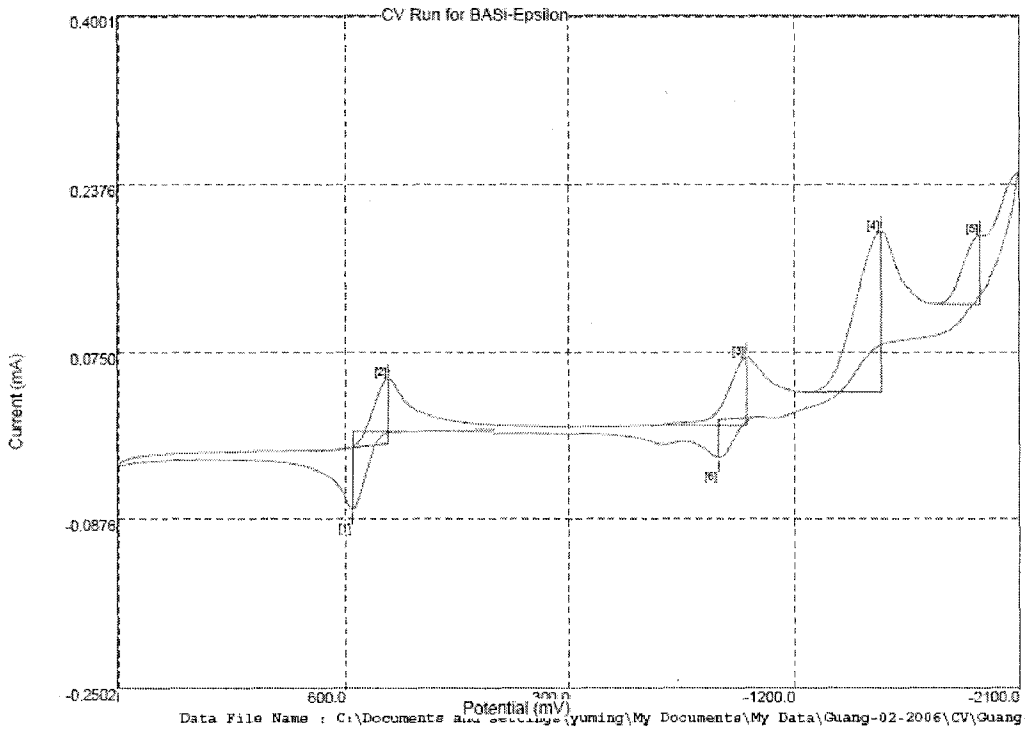

Data File Name : C:\Documents and Settings\yuming\My Documents\My Data\Guang-02-2006\CV\Guang-118-3
Title : CV Run for BASi-Epsilon
Experiment Type : Cyclic Voltammetry (CV)
Printed : 03/01/2007 11:32:16 AM
Date & Time of the run : 10/13/2006 4:24:36 PM
Number of data points : 7200
Display Convention : POLAROGRAPHIC
Initial Potential : 0 (mV)
Switching Potential 1 : 1500 (mV)
Switching Potential 2 : -2100 (mV)
Final Potential : 0 (mV)
Number of segments : 3
Scan rate : 100 (mV/s)
Current Full Scale : 1 mA
Filter : 10 Hz
Quiet Time : 2 (Sec)
Sample Interval : 1 mV

Peak Data:
peak [1] @ 569 [mV], 0.0764 (mA), 0.0469 (mC)
peak [2] @ 426 [mV], 0.0633 (mA), 0.0434 (mC)
peak [3] @ -1011 [mV], 0.0666 (mA), 0.0584 (mC)
peak [4] @ -1546 [mV], 0.1553 (mA), 0.1760 (mC)
peak [5] @ -1945 [mV], 0.0667 (mA), 0.0505 (mC)
peak [6] @ -899 [mV], 0.0376 (mA), 0.0258 (mC)

Figure A.48 Cyclic voltammogram of **103a**.

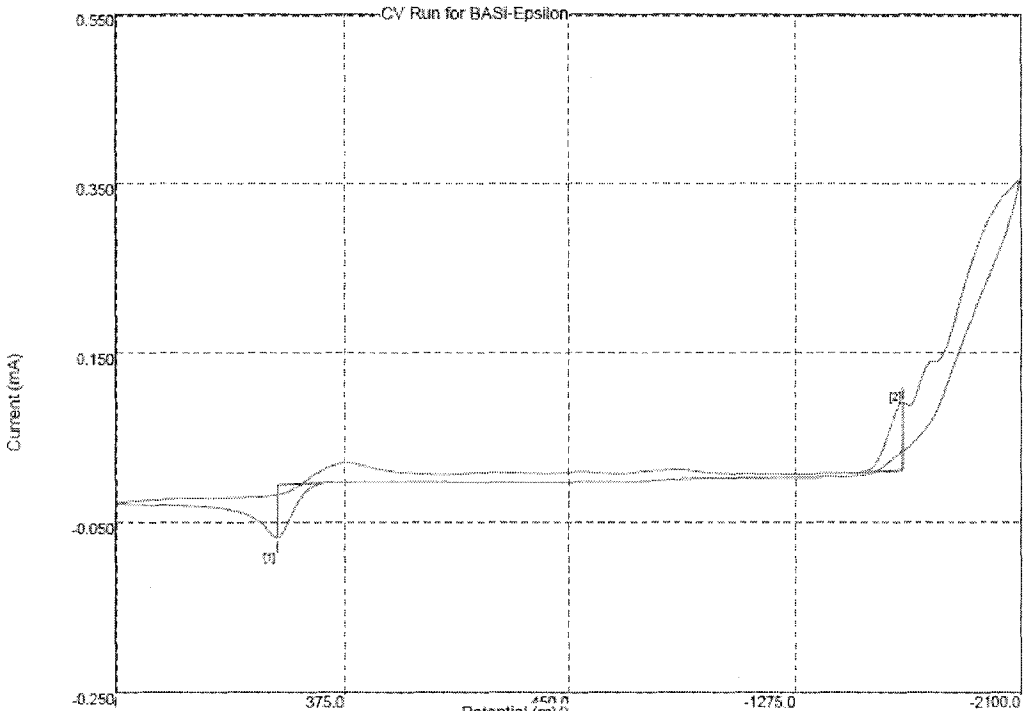

Data File Name : C:\Documents and Settings\yuming\My Documents\My Data\Guang-02-2006\CV\Guang-119-3
Title : CV Run for BASi-Epsilon
Experiment Type : Cyclic Voltammetry (CV)
Printed : 03/01/2007 11:33:40 AM
Date & Time of the run : 10/13/2006 4:47:23 PM
Number of data points : 6600
Display Convention : POLAROGRAPHIC
Initial Potential : 0 (mV)
Switching Potential 1 : 1200 (mV)
Switching Potential 2 : -2100 (mV)
Final Potential : 0 (mV)
Number of segments : 3
Scan rate : 50 (mV/s)
Current Full Scale : 1 mA
Filter : 10 Hz
Quiet Time : 2 (Sec)
Sample Interval : 1 mV

Peak Data:
peak [1] @ 618 [mV], 0.0624 (mA), 0.0822 (mC)
peak [2] @ -1668 [mV], 0.0797 (mA), 0.0995 (mC)

Figure A.49 Cyclic voltammogram of **103b**.

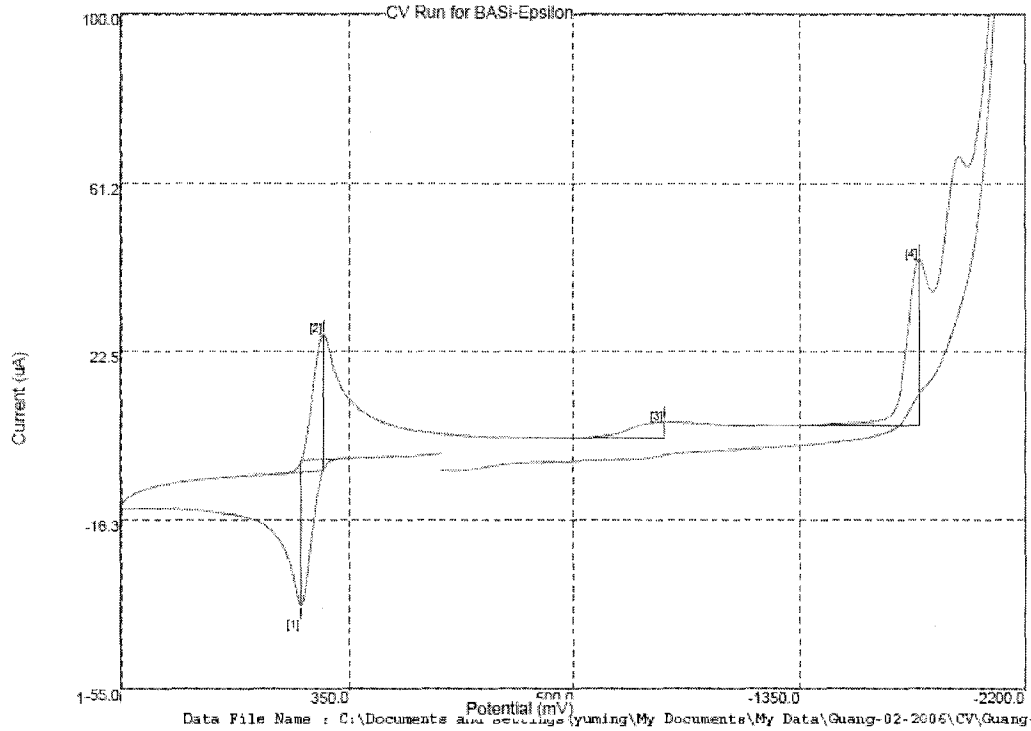

Data File Name : C:\Documents and Settings\yuming\My Documents\My Data\Guang-02-2006\CV\Guang-1-43-2
Title : CV Run for BASi-Epsilon
Experiment Type : Cyclic Voltammetry (CV)
Printed : 03/01/2007 11:30:19 AM
Date & Time of the run : 10/13/2006 3:57:18 PM
Number of data points : 6800
Display Convention : POLAROGRAPHIC
Initial Potential : 0 (mV)
Switching Potential 1 : 1200 (mV)
Switching Potential 2 : -2200 (mV)
Final Potential : 0 (mV)
Number of segments : 3
Scan rate : 100 (mV/s)
Current Full Scale : 100 uA
Filter : 10 Hz
Quiet Time : 2 (Sec)
Sample Interval : 1 mV

Peak Data:
peak [1] @ 529 [mV], 33.5241 (uA), 15.3024 (uC)
peak [2] @ 444 [mV], 31.1223 (uA), 14.9208 (uC)
peak [3] @ -843 [mV], 3.6469 (uA), 5.5295 (uC)
peak [4] @ -1801 [mV], 38.0133 (uA), 21.5474 (uC)

Figure A.50 Cyclic voltammogram of **103c**.